POLITECNICO
MILANO 1863

SCUOLA DI INGEGNERIA INDUSTRIALE
E DELL'INFORMAZIONE

Material characterization of a flax fiber reinforced composite for crashworthiness applications

Tesi di Laurea Magistrale in
Aeronautical Engineering - Ingegneria Aeronautica

Author:

Elia Pinato

Student ID: 944474
Advisor: Prof. Marco Anghileri
Co-advisors: Ing. Ivan Colamartino
Academic Year: 2021-2022

Ringraziamenti

Con queste poche righe vorrei ringraziare tutte le persone che mi hanno sostenuto ed aiutato lungo questo percorso.

Ringrazio il Professor Anghileri per avermi concesso l'opportunità di lavorare su un argomento così innovativo e stimolante. Un grazie speciale va a Impregnatex Compositi, la quale mi ha fornito tutto il materiale e il supporto di cui avevo bisogno. In particolare, sono grato all'Ing. Torno per avermi concesso questa occasione, all'Ing. Cavasin e al Dott. Tagliabue per avermi sostenuto in tutte le fasi del lavoro, fornendomi consigli indispensabili e ottimi spunti. Ringrazio tutto il Laboratorio Prove Sperimentali per avermi fornito gli strumenti per l'esecuzione delle prove, in particolare sono grato all'Ing. Rubini per la sua incredibile disponibilità e pazienza. Ringrazio tutto il personale del laboratorio LaST, grazie all'Ing. Scampini per il supporto tecnico e ringrazio l'Ing. Colamartino per avermi dato sempre ottimi suggerimenti, buonumore e guidandomi nell'ultima fase di questo percorso.

Ci tengo a ringraziare anche tutti i colleghi ingegneri e tesisti del LaST che hanno contribuito ad alleggerire le dure giornate di lavoro e scrittura.

Un grazie enorme va a tutti i miei più cari amici che mi hanno accompagnato in questo percorso universitario, dandomi gioia e serenità anche nei momenti meno felici.

Ultima, ma certamente non per importanza, ringrazio la mia famiglia che mi è sempre stata vicina e mi ha sempre sostenuto in questo lungo percorso.

Grazie di cuore a tutti voi!

Abstract

Natural fiber composites might represent an environmentally sustainable alternative to conventional solutions such as fiberglass and carbon fiber composites. The aim of this work is to perform a material characterization of flax-fiber reinforced composite material, so as to investigate both the static and dynamic mechanical performances for possible future crashworthiness applications.

The specimens employed during experimental tests are composed by ampliTex™ 300 twill 2/2 fibers and IMP 503ZHT BC epoxy resin. Although a fabric material was considered, static tests were performed in order to examine the properties in both warp direction at 0° and weft direction at 90°. In detail, tensile, compressive, flexural and shear properties were achieved from static tests, while indentation, ballistic impact and tensile dynamic responses were analyzed to probe the crashworthiness features.

In order to produce a representative numerical model of flax composite material, numerical activity was performed through the use of LS-DYNA software. The choice of suitable numerical elements and material card was accomplished so as to approximate both the mechanical performances and behaviour of the material.

Eventually, a wide discussion about the results, further improvements and the future development of bio-composites was performed.

Sommario

I materiali compositi costituiti da fibra di origine naturale possono rappresentare una alternativa ecosostenibile rispetto alle soluzioni attualmente offerte dal mercato, come compositi in fibra di vetro e fibra di carbonio. Lo scopo di questa tesi è quello di eseguire una campagna di test su un materiale in fibra di lino, al fine di analizzarne le sue caratteristiche meccaniche, sia a livello statico che dinamico, valutando possibili utilizzi in campo crashworthiness.

I provini in composito utilizzati durante le prove sperimentali sono costituiti da fibre di lino ampliTex™ 300 twill 2/2 e resina epossidica IMP 503ZHT BC. Sebbene il materiale testato sia un tessuto, sono state eseguite prove indagando sia le prestazioni lungo la direzione 0° (ordito) che quelle lungo la direzione 90° (trama). Più in dettaglio, le proprietà di trazione, compressione, flessione e taglio sono state ottenute durante le prove statiche, mentre le proprietà dinamiche di indentazione, trazione e la risposta dinamica ad impatti ad alta velocità sono state analizzate al fine di approfondire le caratteristiche di resistenza agli urti.

Un modello numerico del materiale è stato realizzato mediante l'utilizzo del software LS-DYNA, allo scopo di effettuare una indagine preliminare valutando le scelte di modellazione più idonee. In particolare, la scelta del tipo di elementi numerici, insieme alla scelta della scheda del materiale, sono state eseguite in modo da approssimare al meglio sia le prestazioni meccaniche che il comportamento del materiale durante i fenomeni di deformazione.

I risultati sono stati discussi ampiamente, riportando anche i possibili miglioramenti attuabili al fine di migliorare le procedure di test. Infine, i possibili sviluppi futuri relativi ai materiali bio-compositi sono stati riportati.

Contents

1 | Introduction

This thesis work aims to study innovative composite materials compared to the current solutions offered by the market. Since environmental issue are more and more significant nowadays, an alternative sustainable solution must be found. Green composite materials have great potentiality in this sector, and it would be interesting to examine in depth the mechanical features of these products.

The project here presented will focus on the applicability of these innovative materials in the context of energy absorption applications. Due to the lack of data in literature, material characterization activity is required so as to gather the most relevant mechanical features of flax-fiber reinforced composite, which represents the employed material. Angeloni Group kindly offered his facilities, support and raw materials, such natural fibers and resins, in order to achieve the needed specimens to perform both the material characterization and dynamic tests.

The first stage of this work concerns the literature review, in which a general overview about composite materials will be performed. In detail, composite characteristics and classification will be presented with an in-depth analysis about the most used composite manufacturing techniques. Moreover, an introduction to both experimental and numerical phases will be provided, so as to offer all the information about the procedures and tools employed.

A preliminary study concerning natural composite materials will be conducted. In particular, an overview and classification of these bio-composite materials will be analysed. Advantages and drawbacks are presented as well as the current applications of these products. In addition, in order to fully exploit the potential of natural composite materials, manufacturing processes and chemical treatments will be examined. The latter are fundamental also to select the proper fabrication technique so as to produce the required specimens for test phase. Eventually, the selection of flax composite material will be investigated through the analysis of the most common fibers and resins available on the market.

Material characterization test phase will be performed, In according to the ASTM stan-

dards, so as to gain the characteristics of the material in the most significant loading condition. Numerical simulations will be performed as well, LS-DYNA will be employed to simulate tests and the most representative results will be obtained exploiting a trial and error methodology. Dynamic properties will be investigated throughout experimental tests in order to probe the energy absorption characteristics with respect to the traditional solutions.

In conclusion, the data and the observations gathered in these pages want to be a solid base for further investigations and analyses.

2 | Literature review

In this chapter a definition and classification of composite materials will be presented. Through the dissertation of hypotheses and assumptions, the mathematical tools will be defined, in order to properly describe the behaviour of composites under different loading conditions. Moreover, the most popular fabrication techniques are examined to understand the correlated features. Eventually, an introduction to both experimental and numerical phases will presented to introduce all the required tools.

2.1. General overview composite materials

Composite materials have been always used by humans since ancient times. Civilizations exploit composites characteristics through the centuries, for example, Israelites used straw to reinforce the mud-bricks and the ancient Egyptians rearranged different types of wood in order to produce plywood, a natural material with better thermal expansion resistance and less tendency to swell due to the presence of moisture. Even in the Middle Age composites were used to fabricate swords and armors since they were made with different layers of metals.

Figure 2.1: Straw reinforced mud-brick production

composite materials by definition are two or more materials combined on a macroscopic scale to form a useful third material with specific feature and properties. From a macroscopic point of view the constituents can be identified by the naked eyes and an interface between them can be observed as well [14].

Classification of composite materials can be done and four commonly accepted types are here presented:

1. *Fibrous composite materials* consist in fibers in a matrix. The fiber's section can be very small on the order of micrometer. Thanks to this characteristic the amount of flaws can be reduced to the minimum, increasing the overall mechanical performances. On the other hand the matrix has poor mechanical characteristics but is fundamental to transfer the load inside the material. The most used fibers are E-glass, S-glass, carbon, beryllium, boron and graphite.
2. *Laminated composite materials* consist of layers of at least two different materials that are bonded together. Lamination is used to combine the best aspects of the constituent layers and bonding material in order to achieve better characteristic such as strength, stiffness, corrosion resistance, thermal insulation ect. Both sandwich and honeycomb composites are well known examples of this kind of composite.
3. *Particulate composite materials* are composed of particles of one or more materials suspended in a matrix of another material. The particles can be either metallic or nonmetallic as can the matrix. An example is represented by the solid rocket propellants.
4. Combinations of some or all of the first three types.

Amplitex is the material used in this study, is composed by flax fibers and epoxy resin, which is a polymeric matrix material. It is convenient to focus on fibrous materials since they are the most relevant for our purpose.

2.1.1. Fibrous composite materials

As mentioned before, fibers and matrix compose fibrous composites. Fibers have a length much greater than its diameter, the aspect ratio (length-to-diameter) can be very large. The reinforcing phase provides the strength and stiffness and is harder, stronger, and stiffer than the matrix.

Fibers can be classified in two different typology:

- Continuous fiber has greater aspect ratio and a preferred orientation can be iden-

tified. The mechanical characteristics are greater with respect to the discontinued one but only in the main direction.

- Discontinued fiber exhibits lower aspect ratio and they are organized randomly inside the composite. Strength and stiffness are lower but the cost can be decreased compared to the previous solution.

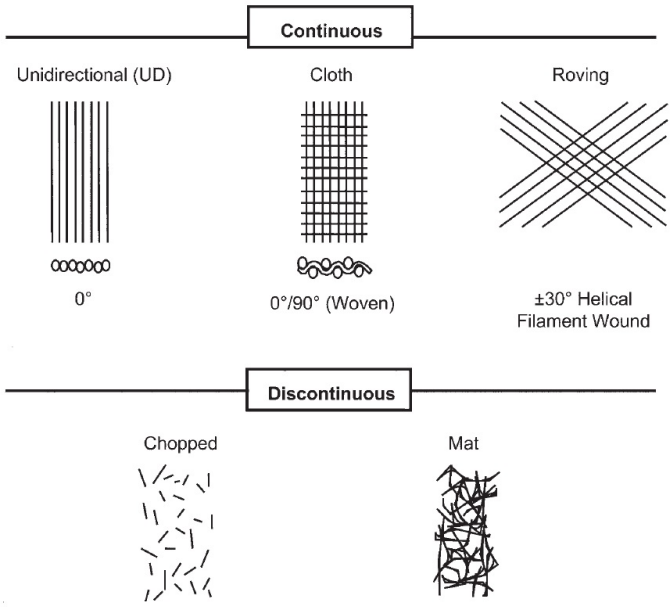

Figure 2.2: Continuous vs discontinuous fibers

Long fibers can be organized in different ways and create different kind of layers. Unidirectional fibers (UD) are formed by fibers aligned in the same direction. This allow to maximize the performances in the main direction while maintain poor characteristics in the others.

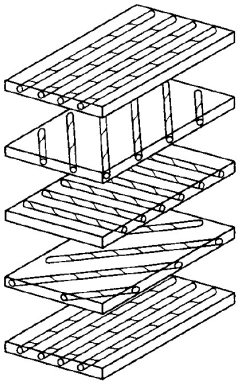

Figure 2.3: Unbounded view of laminate construction

In order to gain isotropy UD layers with different orientations can be used to form laminate so as to gain independence between mechanical properties and orientation of fibers.

Another layout that can be exploited to achieve different mechanical properties is the woven fabric. The latter is produced by the interlacing of wrap (0°) fibers and weft (90°) fibers in a regular pattern or weave style. Complex geometry can be modelled and different fibers can be mixed together (i.e. carbon and kevlar). This material is orthotropic and remarkable mechanical properties can be achieved since the integrity is maintained by the mechanical interlocking of the fibers.

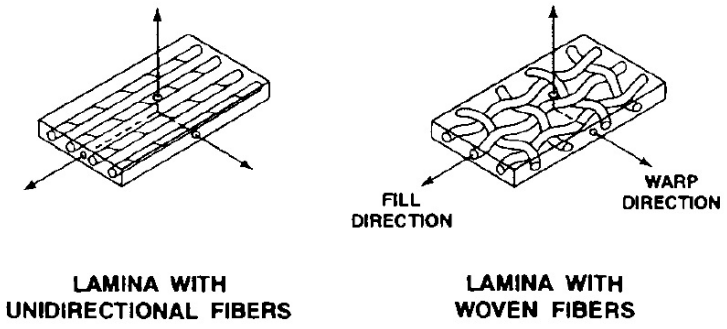

Figure 2.4: Unidirectional and woven laminae

The purpose of the matrix is to bond together all the components and contribute to form a structural element that can carry loads. The mechanical properties of this component are poor compared to the fiber ones but despite this, they cover a vital role. Matrix offers support for fibers, protection against corrosion and mechanical damages, stresses are carry mainly by the fibers but matrix has the capability to transfer loads from fiber to fiber. Even more in case of broken fiber its role is essential, the stress is transferred towards healthy fibers, by preventing the fail of the entire structure.

All the matrices can be classified in three typology:

- Polymeric
- Metallic
- Ceramic

The polymeric matrices are widely used since they allow to achieve components with different size and shape. They can be divided in thermoset and thermoplastic. Metallic matrices are rarely used due to the production issues and the high cost, the most relevant

are aluminium alloy and titanium. Same as above for the ceramic, they are used as thermal insulation and for electrical insulation too.

It is worth noting that composite materials nowadays are generally anisotropic, which means that in different directions are observed different behaviour. Orthotropic is a special case of anisotropy, three mutually perpendicular planes of elastic symmetry have to be identified. By specific manufacturing process is possible to obtain orthotropic composites in order to exploit the best mechanical properties of these materials.

2.1.2. Rule of mixture

Focusing on fibrous composite materials with polymeric matrix we can see clearly that resin and reinforcing fibers exhibit different properties, the resulting composite material will combine these properties, as shows in the figure 2.5.

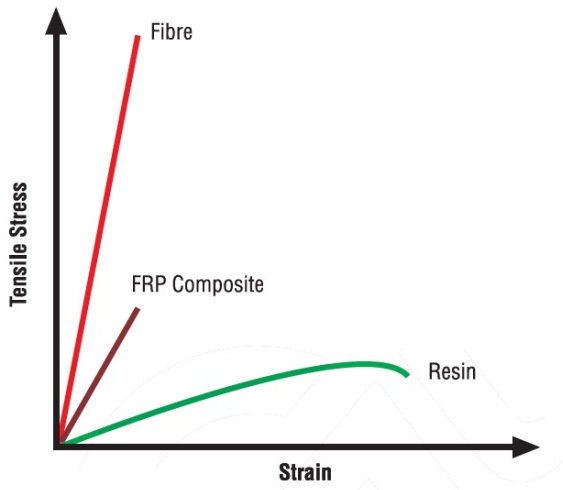

Figure 2.5: Fiber and matrix mechanical properties

Overall, the properties of the resulting composite are determined by [12]:

1. The properties of the fiber
2. The properties of the resin
3. The ratio of fibre to resin in the composite (Fiber Volume Fraction)
4. The geometry and orientation of the fibres in the composite

The ratio of the fiber to resin is related to the manufacturing process and it is also influenced by the type of resin system used, and the form in which the fibres are incorporated.

This is an important aspect since an higher fiber volume fraction improves the mechanical properties of the composite. An upper limit is given by technological issue, the fibers need to be fully coated in resin to be effective and capable to transfer the loads. In most of the case a limit for FVF is approximately 30-40 % but with more sophisticated and precise processes FVF close to 70 % can be successfully obtained.

By approximating the composite as an homogeneous, isotropic material the resulting mechanical properties can be estimated by means of rule of mixture:

$$\rho_{comp} V_{comp} = \rho_{fiber} V_{fiber} + \rho_{matrix} V_{matrix} \tag{2.1}$$

The equation (2.1) is based on the contribution of each part of the composite, in particular it consists in a weighted average over the volume fraction of the starting properties (i.e. Young modulus, Poisson's ratio, density etc.). This equation can be easily understood by considering the analogy of calculating the stiffness of two springs connected in parallel.

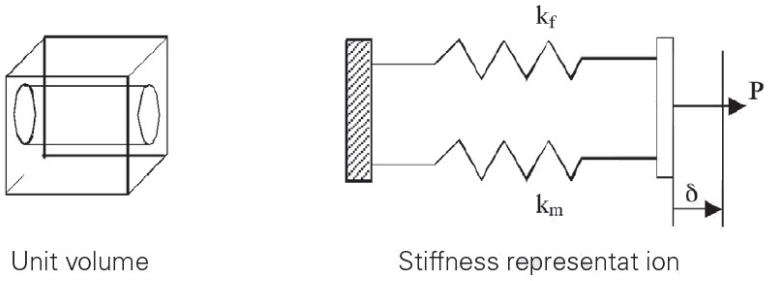

Figure 2.6: RoM model for longitudinal properties

2.1.3. Constitutive law

In order to define constitutive law for orthotropic composite materials it is fundamental to introduce the generalized Hooke's law written in Voigt notation:

$$\sigma_i = C_{ij}\epsilon_j \qquad i,j = 1,...,6 \tag{2.2}$$

Where σ_i are the stress components shown on a three-dimensional cube (see figure 2.7), in x, y, and z coordinates, C_{ij} is the stiffness matrix, and ϵ_j are the strain components.

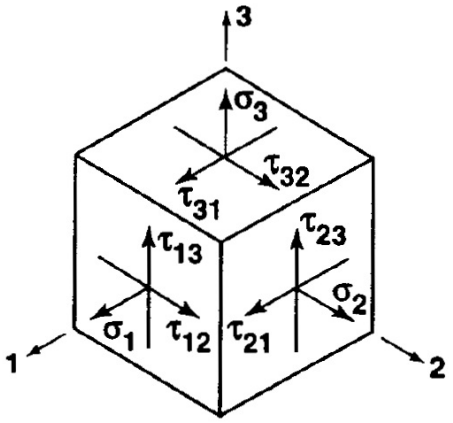

Figure 2.7: Stress state on a element

The stiffness matrix has 36 constants, but they can be reduced if a linear elastic anisotropic material is considered, in this case the matrix become symmetric and only 21 constants have to be evaluated. Moreover, if two orthogonal planes of material property symmetry exist for a material, symmetry will exist with respect to a third mutually orthogonal plane, in this case orthotropic material are considered and the constants to be evaluated in the stiffness matrix reduce to 9.

It is possible to express the constitutive law as a function of the stresses rather than strains, by defining the compliance matrix which is the inverse of the stiffness matrix.

$$\epsilon_i = S_{ij}\sigma_j \qquad i,j = 1,...,6 \tag{2.3}$$

All the simplifications performed on the stiffness matrix can be considered for the compliance matrix as well, and only 9 constants have to be defined.

The composite materials are heterogeneous by their very nature, hence assumptions are needed in order to describe properly their behaviour. Macroscopically the material can be treated as homogeneous since the scale of the reinforcement is small. In addition, composites show a linear elastic behaviour approximately until brittle failure, with these characteristics it is possible to use a Hooke's law to define the relationship between strain and stress.

Here is reported the constitutive law for an orthotropic material in compliant form:

$$\begin{Bmatrix} \epsilon_1 \\ \epsilon_2 \\ \epsilon_3 \\ \gamma_{23} \\ \gamma_{31} \\ \gamma_{12} \end{Bmatrix} = \begin{bmatrix} \frac{1}{E_1} & -\frac{\nu_{21}}{E_2} & -\frac{\nu_{31}}{E_3} & 0 & 0 & 0 \\ -\frac{\nu_{12}}{E_1} & \frac{1}{E_2} & -\frac{\nu_{32}}{E_3} & 0 & 0 & 0 \\ -\frac{\nu_{13}}{E_1} & -\frac{\nu_{23}}{E_2} & \frac{1}{E_3} & 0 & 0 & 0 \\ 0 & 0 & 0 & \frac{1}{G_{23}} & 0 & 0 \\ 0 & 0 & 0 & 0 & \frac{1}{G_{31}} & 0 \\ 0 & 0 & 0 & 0 & 0 & \frac{1}{G_{12}} \end{bmatrix} \begin{Bmatrix} \sigma_1 \\ \sigma_2 \\ \sigma_3 \\ \tau_{23} \\ \tau_{31} \\ \tau_{12} \end{Bmatrix} \tag{2.4}$$

Where:

- ϵ is the normal strain
- γ is the shear strain
- E is the Young's modulus or modulus of elasticity
- ν is the Poisson's ratio, which is defined as $\nu_{ij} = -\epsilon_j/\epsilon_i$
- G is the shear modulus
- σ is the normal stress
- τ is the shear stress

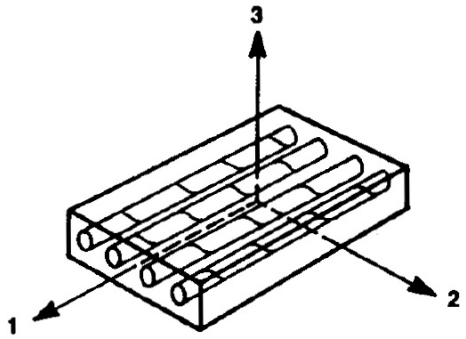

Figure 2.8: Lamina coordinate system

As mentioned above, a three-dimensional Cartesian coordinate system is considered (see figure 2.8) and the subscripts 1,2,3 are respectively refer to the longitudinal direction (parallel to the fibers direction), transverse direction which lie on the plane of the lamina

and it is perpendicular to the longitudinal one, and lastly the third direction is referred to the out-of-plane direction and is defined following the right-hand rule.

It worth noting that the compliance matrix is symmetric and the constants to be determined are 9. As a matter of fact, the following equality must hold:

$$\nu_{21}/E_2 = \nu_{12}/E_1 \tag{2.5}$$
$$\nu_{31}/E_3 = \nu_{13}/E_1 \tag{2.6}$$
$$\nu_{32}/E_3 = \nu_{23}/E_2 \tag{2.7}$$

2.1.4. Plane-stress case

For the purpose of analyzing orthotropic composite materials, the previous constitutive law presented in the section 2.1.3 can be simplified by considering appropriate assumptions. Since the lamina cannot withstand high stresses in any direction other than that of fibers and, usually, in-plane stresses are the only one considered, it is convenient to assume stresses with a component in direction 3 equal to zero.

This observation means that the plane stress state is defined by setting [14]:

$$\sigma_3 = 0 \qquad \tau_{23} = 0 \qquad \tau_{31} = 0 \tag{2.8}$$

so that

$$\sigma_1 \neq 0 \qquad \sigma_2 \neq 0 \qquad \tau_{12} \neq 0 \tag{2.9}$$

This model is particularly suitable for thin materials as laminates, since negligible thickness with respect to the other two dimensions is required to apply it.

The constitutive law become:

$$\begin{Bmatrix} \epsilon_1 \\ \epsilon_2 \\ \gamma_{12} \end{Bmatrix} = \begin{bmatrix} \frac{1}{E_1} & -\frac{\nu_{21}}{E_2} & 0 \\ -\frac{\nu_{12}}{E_1} & \frac{1}{E_2} & 0 \\ 0 & 0 & \frac{1}{G_{12}} \end{bmatrix} \begin{Bmatrix} \sigma_1 \\ \sigma_2 \\ \tau_{12} \end{Bmatrix} \tag{2.10}$$

It worth noting that the equation (2.4) is reduced to (2.10) by considering the zero-stress components. However, is important to highlight that the corresponding strains (ϵ_3, γ_{23} and γ_{31}) are generally different from zero.

2.1.5. Classical Lamination Theory

As mentioned in 2.1.1, the interest of this study is to investigate natural fibrous composite materials. Generally these materials are organized in typical structure called laminate, different layers, or laminae, or plies of material are stacked together in order to obtain the final product. This process allow the designers to optimize the orientation of each lamina with regard to the different behaviour or response needed by the laminate, thus, the feasibility can be maximised in every sectors of interest.

Classical lamination theory (CLT) is here presented to predict the behaviour of the whole laminate starting from the geometry and properties of each lamina. Reasonable and accurate assumptions have to be performed so as to move from a three-dimensional elasticity case towards a two-dimensional solvable one.

Here are presented the assumptions needed to apply the CLT:

- Each ply is considered homogeneous, orthotropic and linear-elastic
- Plane-stress condition is always considered, both for laminate and lamina
- The laminae are perfectly bounded together and the bonds are presumed to be infinitesimally thin as well as non shear-deformable
- Plane section normal to the middle surface, is assumed to remain straight and perpendicular to the middle surface when the laminate is deformed (Kirchhoff hypothesis)

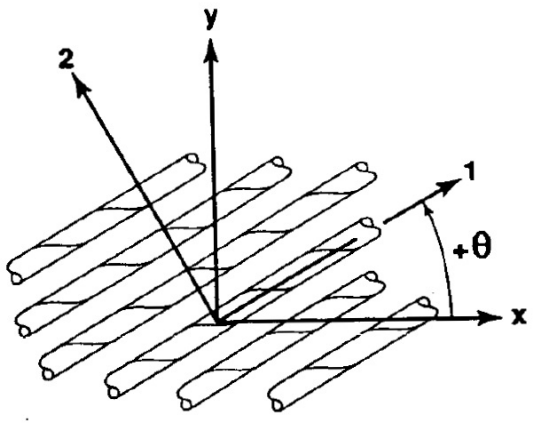

Figure 2.9: Positive rotation of principal material axes

In the section 2.1.3 the constitutive law was presented in principal material coordinates for an orthotropic material. However, in most cases would be useful to describe such a relation in general coordinates, this step is fundamental to properly apply the CLT. In order to describe the lamina properties, which are defined in material axes (1,2), in the laminate coordinate system (x,y), it is convenient to define the transformation matrix $[T]$:

$$[T] = \begin{bmatrix} m^2 & n^2 & 2mn \\ n^2 & m^2 & -2mn \\ -mn & mn & m^2 - n^2 \end{bmatrix} \tag{2.11}$$

With:

$$m = cos\theta \qquad\qquad n = sen\theta \tag{2.12}$$

The purpose of the above mentioned matrix is to perform a rotation between the lamina axes and laminate axes. In particular, as reported in figure 2.9, θ can be defined as the angle from the x-axis (general coordinate system) to the 1-axis (material coordinate system).

Stress can be written as:

$$\begin{Bmatrix} \sigma_x \\ \sigma_y \\ \tau_{xy} \end{Bmatrix} = [T]^{-1} \begin{Bmatrix} \sigma_1 \\ \sigma_2 \\ \tau_{12} \end{Bmatrix} \tag{2.13}$$

as well as strain:

$$\begin{Bmatrix} \epsilon_x \\ \epsilon_y \\ \gamma_{xy}/2 \end{Bmatrix} = [T]^{-1} \begin{Bmatrix} \epsilon_1 \\ \epsilon_2 \\ \gamma_{12}/2 \end{Bmatrix} \tag{2.14}$$

In the equation (2.14) the engineering strain vectors were used for convenience of discussion. Nevertheless, in order to use them is necessary to find the link with the corresponding tensor strain vectors. The Reuter matrix can be used for this purpose and is here presented for completeness:

$$[R] = \begin{bmatrix} 1 & 0 & 0 \\ 0 & 1 & 0 \\ 0 & 0 & 2 \end{bmatrix} \tag{2.15}$$

Eventually, the stress state in the plane of the lamina for a general coordinate system can be obtained:

$$\begin{Bmatrix} \sigma_x \\ \sigma_y \\ \tau_{xy} \end{Bmatrix} = [T]^{-1}[Q] \begin{Bmatrix} \epsilon_1 \\ \epsilon_2 \\ \gamma_{12} \end{Bmatrix} = [T]^{-1}[Q][R][T][R]^{-1} \begin{Bmatrix} \epsilon_x \\ \epsilon_y \\ \gamma_{xy} \end{Bmatrix} \tag{2.16}$$

However, $[R][T][R]^{-1}$ can be shown to be $[T]^{-T}$ and an abbreviation can be introduced:

$$[\overline{Q}] = [T][Q][T]^{-T} \tag{2.17}$$

Hence

$$\begin{Bmatrix} \sigma_x \\ \sigma_y \\ \tau_{xy} \end{Bmatrix} = \begin{bmatrix} \overline{Q}_{11} & \overline{Q}_{12} & \overline{Q}_{16} \\ \overline{Q}_{12} & \overline{Q}_{22} & \overline{Q}_{26} \\ \overline{Q}_{16} & \overline{Q}_{26} & \overline{Q}_{66} \end{bmatrix} \begin{Bmatrix} \epsilon_x \\ \epsilon_y \\ \gamma_{xy} \end{Bmatrix} \tag{2.18}$$

The resultant forces and moments per unit width acting on the laminate can be obtained by integration of the stresses in each layer through the laminate thickness

$$\begin{Bmatrix} N_x \\ N_y \\ N_{xy} \end{Bmatrix} = \sum_{k=1}^{N} \int_{z_{k-1}}^{z_k} \begin{Bmatrix} \sigma_x \\ \sigma_y \\ \tau_{xy} \end{Bmatrix}_k dz \tag{2.19}$$

and

$$\begin{Bmatrix} M_x \\ M_y \\ M_{xy} \end{Bmatrix} = \sum_{k=1}^{N} \int_{z_{k-1}}^{z_k} \begin{Bmatrix} \sigma_x \\ \sigma_y \\ \tau_{xy} \end{Bmatrix}_k z\, dz \tag{2.20}$$

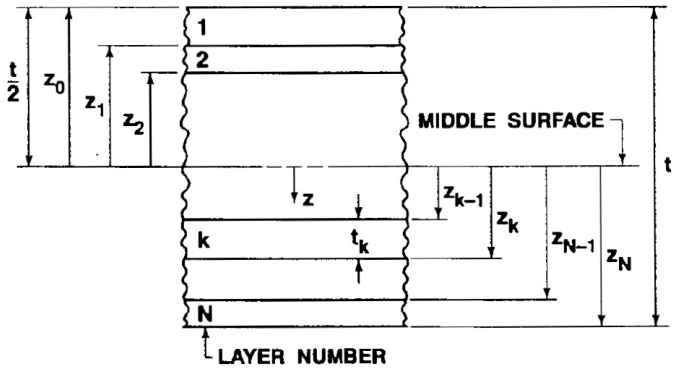

Figure 2.10: Geometry of a N-layered lamina

By substituting the constitutive law (2.18) in both equations (2.19) and (2.20), it is possible to integrate properly the stresses within each layer of the material, so as to obtain from all the plies the contributions to sum, in order to compute the forces and moments per unit width acting on the laminate.

Accordingly, reorganizing all the terms, the laminate constitutive law can be reported in a compact form:

$$\begin{Bmatrix} \{N\} \\ \{M\} \end{Bmatrix} = \begin{bmatrix} [A] & [B] \\ [B] & [D] \end{bmatrix} \begin{Bmatrix} \{\epsilon_0\} \\ \{\kappa\} \end{Bmatrix} \tag{2.21}$$

In the latter equation coupling between forces and moments could be shown. The $[B]$ sub-matrix represents the extension-bending coupling, while the A_{16} and A_{26} are associated with the shear-extension coupling, lastly the bending-torsion coupling is described by the D_{16} and D_{26} terms.
By varying the stacking sequence of the laminae it is feasible to force to zero some of the terms above mentioned. In fact, three different types of layout can be used:

- Symmetric: for each ply located at $+z$ and oriented with an angle θ exists a ply located at -z and oriented with the same angle θ
- Balanced: for each ply located at z and oriented with an angle θ exists a ply oriented with the opposite angle -θ
- Anti-symmetric: for each ply located at $+z$ and oriented with an angle θ exists a ply located at -z and oriented with an opposite angle -θ

The symmetric laminate is capable to return $[B] = 0$, uncoupling stretching-bending behaviour. While balanced layout makes the terms A_{16} and A_{26} null. Eventually, anti-symmetric laminate nullify the terms D_{16} and D_{26}.

2.1.6. Failure modes

Composite materials are composed by different elements and a lot of issues related with them can arise. As a matter of fact, composites can fail in a wide variety of ways, due to their intrinsic nature. By definition, failure of a structural element can be stated to have taken place when it ceases to perform satisfactorily [1]. In wide terms, the definition of failure changes based on the application and the material considered. in some conditions small deformations or even barely visible cracks can define the failure of the component, instead in some others the failure is not declared until the total fracture or separation

of the component. Composites show that internal failure generally initiates well before any appreciable changes in macroscopic appearance or behaviour. Therefore, the material response changes before the material reaches the macroscopic failure. For example, during the tensile test a deviation from the linear stress-strain behaviour can be seen as the initiation of the internal damages in the structural element.

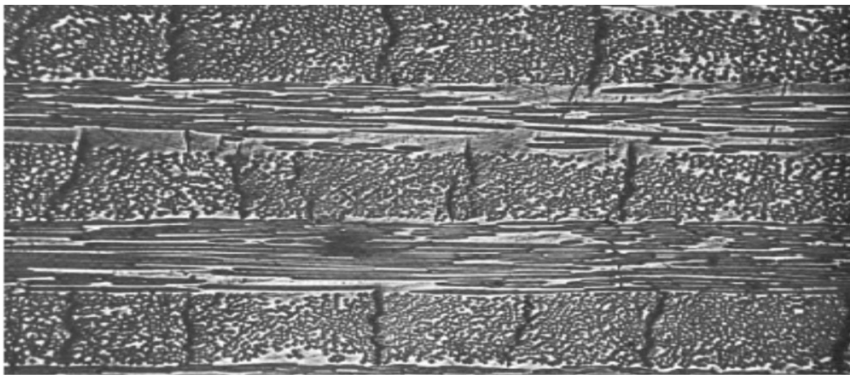

Figure 2.11: Damaged section of $[0/90]_s$ composite

Since polymeric matrices have been used during this project, it is interesting to analyse which kind of issues may be subject to. Matrix microcracking are intra-laminar fractures that traverse the width of the layer and move laterally to the fibers [28]. Considering a $[0/90]_{ns}$ laminate, with a loading applied in the 0° direction, the 90° oriented plies will exceed maximum stress level before than the 0° plies. As a consequence the cracks will develop in the 90° oriented plies, as shown in the figure 2.11.

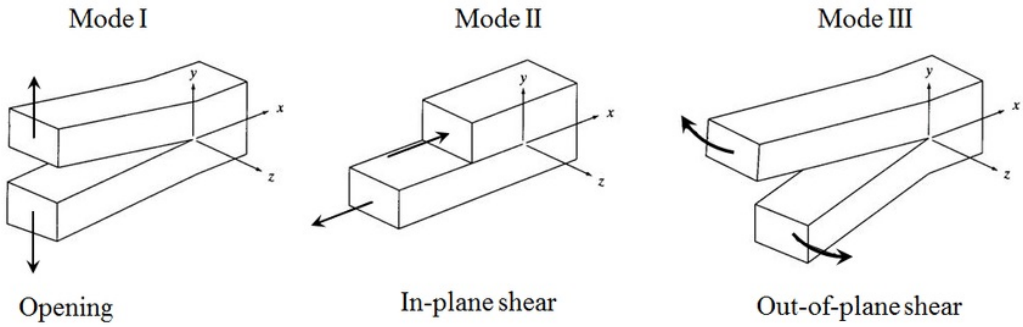

Figure 2.12: Modes of fracture

Fibers can be subjected to tensile failure and compressive failure. The first one happens when the applied tensile load is fiber-oriented, generally the fibers show a brittle breakage and strength depends on defects. The mechanism of compressive failure is very different from tensile failure, the majority of the fibers exhibit instability during the application

of a compressive load and failure of the component is easily reached since the load is no longer sustained.

During the life cycle of a composite component its structural integrity may be affected by loading and environment conditions, here some related issues are presented:

- *Delamination failure mechanism* can be categorized into mode I, mode II, mode III and a mixed-mode (see figure 2.12). This phenomena consists in the interfacial detachment between the plies and is barely visible. It may lead to total failure of the structure if not recognize on time. This mode of failure can be triggered by low-velocity impact, loading condition characterized by great out-of-plane component or even by the microcracking in the matrix due to the shear stresses acting at the interlaminar level.
- *Fibre pull-out and debonding* are mainly related with fibre-matrix interface, they can be caused by weak bonding and high stress level transferred trough interface. The process starts from matrix cracking, while the fibers may still be intact. This means that additional load can be carried, while matrix cracking still opening, until a critical value is reached. At this point, interfacial fibre-matrix debonding will occur and fibers are pulled out gradually. Eventually, breakage of the entire component occurs [19].

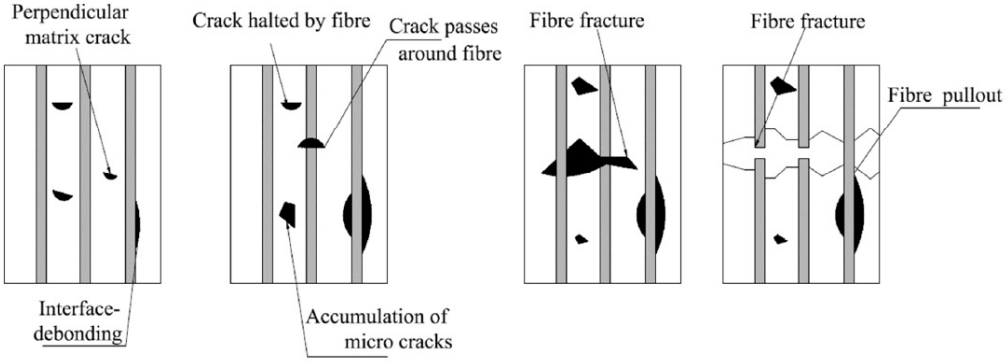

Figure 2.13: Fiber pull-out and debonding

- *Free-edge effect* can influence the failure initiation. When a laminate, characterized by different oriented plies, is subjected to a in-plane load, each ply tends to behave in a different manners. Since the laminae are considered perfectly bonded together, compatibility has to be guaranteed. Because of this, in-plane shear stresses are induced on the edge of the laminate and in order to restore the equilibrium inter-laminar shear stresses are developed as well. The latters are responsible for the edge

dalamination effect. Eventually, it worth noting that CLT is valid only inside the laminate, since out-of-plane stress components are not taken into account.

For completeness failure modes can be presented considering loading conditions. Until now the major issues were presented in general cases, but a more detailed overview is essential to under how the failure could happen. It is important to highlight that the following modes do not act independently and most of the times the stress state is complex.

1. *Failure under longitudinal tensile loads*
   In a UD composite subjected to tensile loading condition failure may initiate by fibers breakage at the weakest cross section. This occurrence happens when 50% of the ultimate load is reached. Fiber pull-out and debonding appear and the broken fibers increase. The weakest cross section tends to reduce until ultimate failure occurs.

2. *Failure under longitudinal compressive load*
   As above mentioned, continuous fibers subjected to compressive loads show instability. This can be exhibited in the form of micro-buckling. In particular, it is possible to have extension mode or shear mode (see figure 2.14). The first one takes place with low volume fraction and extensional strains are predominant, in the second one an higher volume fraction is present and shear strains are prevalent in this case.

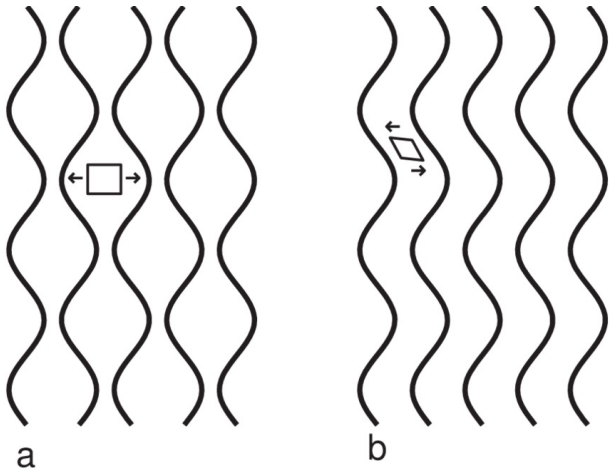

Figure 2.14: Microbuckling

Moreover, transverse splitting may be present as well and appears before compressive failure mechanism occurs. When ultimate transverse tensile load is reached, due to the Poisson effect, cracks at fiber-matrix interface could develop as well.

Eventually, a third failure mode can be described: shear mode. Experimental results

indicates that composites fail with this mechanism at approximately 45° to the loading axis.

3. *Failure under transverse tensile load*
   Fibers perpendicular to the loading direction are accountable for stress concentration at the interface and in the matrix. Failure can be caused by matrix tensile rupture or by constituent dobonding and fiber splitting. It is worth noting that the fracture surface is in part formed by the failure of the matrix-fiber interface.

4. *Failure under transverse compressive load*
   Shear failure of the matrix is the main breakage mechanism in this loading condition. Debonding or fibers crushing are two others mechanism that can come with the main mode. The fracture surface lies on a plane parallel to the fibers. Also in this case fiber-matrix bonding is mainly responsible for the failure and, as expected, the transverse compressive strength is lower with respect to the longitudinal one.

5. *Failure under transverse in-plane shear load*
   In this case the failure may take place by matrix shear failure, with or without constituent debonding. Failure surface could include debonded portions as well.

2.2. Composites manufacturing techniques

As mentioned in section 2.1 composite materials are composed by two or more constituents. Several manufacturing methods are available in order to overcome all the technological issues that may arise. Fibers and matrices are partially responsible for the mechanical features of the final component, also design and production processes can assume a fundamental role. In general, a relevant aspect that must be considered during the manufacturing process is the fiber-matrix interface. It is essential that the matrix adequately wets the fibers so as to fill up any gaps that may be present, this could reduce the number of flaws and the risks related with cracks. Moreover, an appropriate fiber-matrix interface is able to guarantee the continuity inside the component and the correct transfer of stresses. Lastly, the polymeric matrix undergoes the cross-link process [31], which ensures solidification and cohesion of the whole component.

In the following subsections all the most common methods and all their main features will be investigated.

2.2.1. Spray lay-up

Spray-up is a open-mould application technique for composite. In the first step, the mould is prepared with the application of mould release layer covered by gel coat layer. Then, the mould is cured in order to be ready for the process [23]. The fibers and catalysed resin are sprayed into the mould using a hand-held chopper spray gun. In order to apply simultaneously both materials the continuous fiber tow is chopped and the resulting short fibers are directly blown into the sprayed resin stream. Once the spray procedure is completed an operator compact the laminate by hand with a roller so as to remove air and create a smooth surface (see figure 2.15), then the part is left to cure under standard atmospheric conditions.

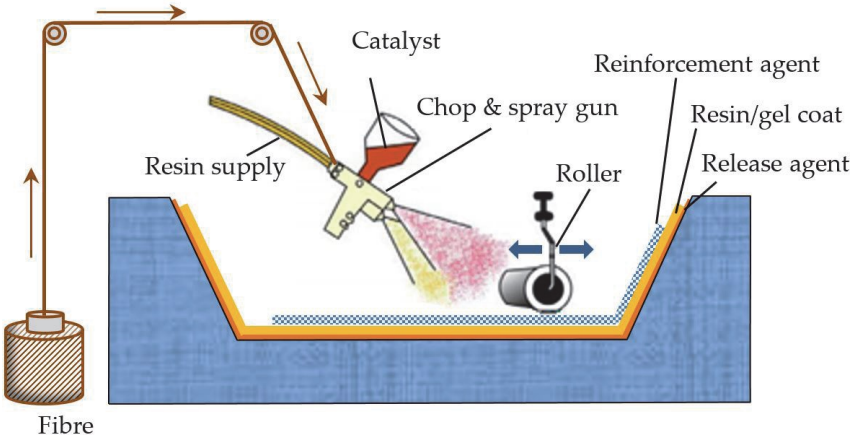

Figure 2.15: Spray lay-up process

It is worth noting that the method ensure design flexibility and low costs, but as a drawbacks relies on operator skill for product quality and only short-fiber component can be obtained, limiting the mechanical properties.

2.2.2. Hand lay-up

Hand lay-up is the most common and widely used open contact moulding technique for fabricating composite materials, is generally suitable for the production of a few large products. Similarly for Spray-up, the mould is prepared with anti-adhesive coat and with gel coat if needed. The consecutive phase consists in laying the dry fibers, in form of woven, knitted, stitched, or bonded fabrics, in the mould. Then, the liquid catalysed resin is poured over the fibers bed. An operator spreads the resin by using brushes or nip-roller-type impregnators in order to compact the material, and force the matrix to wet the fibers so as to remove any entrapped air (see figure 2.16), the process is repeated for

each layer. Eventually, laminates are left to cure under standard atmospheric conditions.

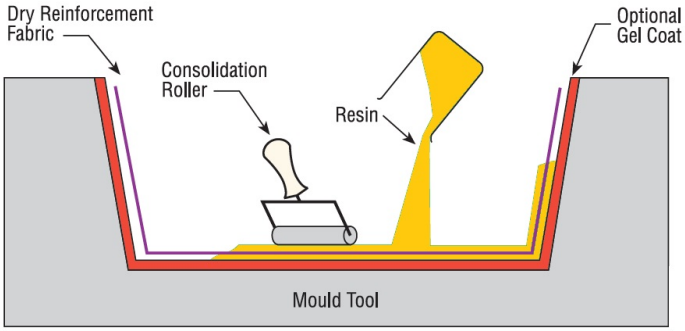

Figure 2.16: Hand lay-up process

Another similar method is called Wet lay-up process. In this case a pressure is applied to the laminate after the lamination process in order to improve the consolidation. A plastic film is sealed over the laid-up laminate and then, through a valve, all the air is extracted by means of a vacuum pump.

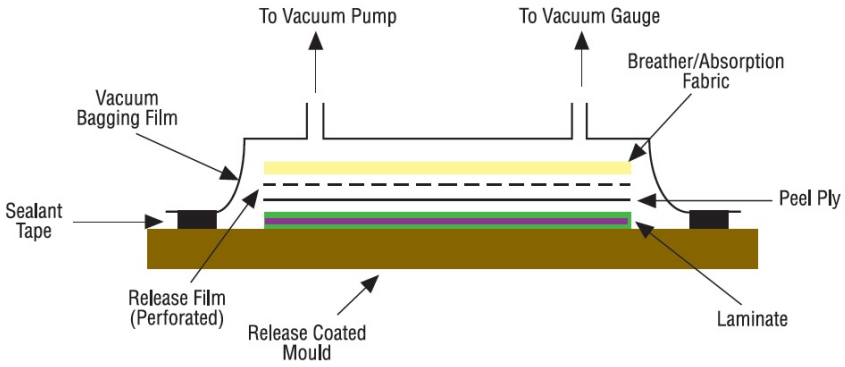

Figure 2.17: Wet lay-up process

Differently by the Spray-up method, both Hand lay-up and Wet lay-up allow the production of long-fiber components, which guarantee an increasing of the mechanical feature.

2.2.3. Filament winding

Filament winding is a continuous process method that can be highly automated, this could lead to an increasing of the repeatability and a reduction of material costs. The fabrication method is useful to create axisymmetric, as well as some non-axissymmetric,

composite products such as pipes, pipe bends and tanks [28]. Continuous prepreg sheets, rovings and continuous dry fibers are driven by several pulleys onto a cylindrical tool called mandrel, which has the final shape of the component. In particular, the dry fibers are made pass through a resin bath so as to be wetted. The nip-roller applies the fibers on the rotating mandrel trough a transverse carriage, which allows to obtain different orientation angles and different layouts. Once the desired thickness is achieved the curing phase takes place at room temperature.

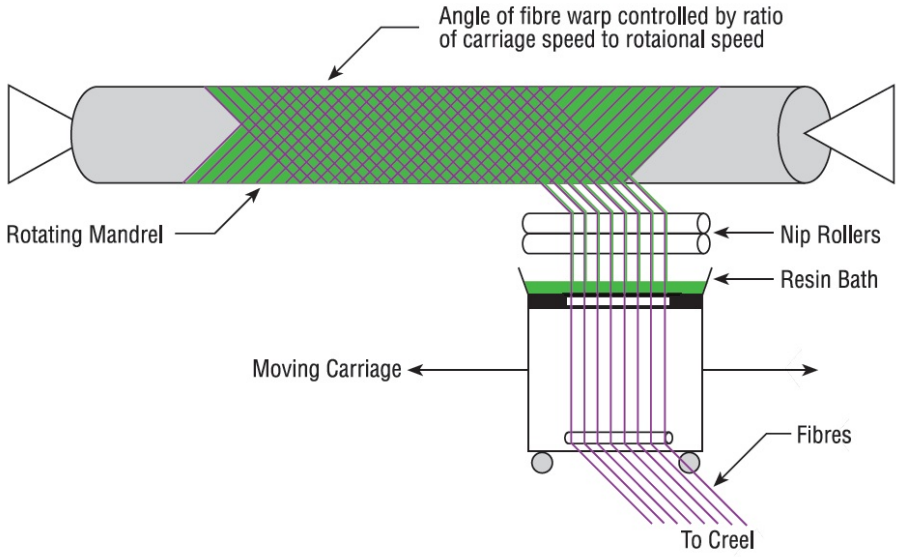

Figure 2.18: Filament winding process

As above mentioned, this fabrication methods has low costs and the entire procedure is fast. Additionally, the final components has execelent structural properties, since straight fibers can be positioned in order to match the loads requirements. As drawback, the obtainable shapes are limited and the external surface is unmoulded, thus the quality is poor. It is interesting to notice that filament winding is one example of aerospace composite material.

2.2.4. Pultrusion

Composite pultrusion is an automated fabrication method for producing continuous length component with constant cross-section. In this process, fibers are pulled from a creel through a heated resin-wetting station, then the wetted fibers are pulled into a heated die so as to obtain the desired cross-sectional shape. In greater detail, the last step complete the impregnation process, by controlling the resin content and curing the material in its final shape. Eventually, parts are made by cutting the long-cured piece. The method can

be very fast and economical, high fiber content can be easily achieved, thus increasing the mechanical feature. On the negative side, the process is able to produce only linear component with a constant coss-section such as beams (e.g. I or T shapes), ladders and mouldings. Fabrics can be used too in order to provide other diretions than 0°.

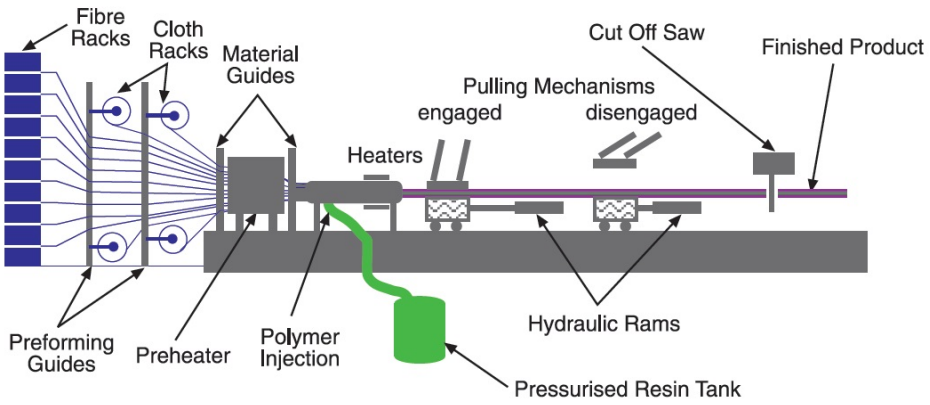

Figure 2.19: Pultrusion process

An alternative variant of the fabrication method is called pulforming, it allows for some variation in the cross-section shape. The wetted fibers are pulled through the die and then clamped in a mould for the curing process. Small changes in the section can be obtained, but the continuity of the method is lost.

2.2.5. Resin Transfer Moulding (RTM)

An alternative fabrication process to replace hand lay-up is the resin transfer moulding (RTM) technique. Firstly, the dry fibers are laid in the mould and then pre-pressed in order to have preformed fiber reinforcements. After, the mould is treated with release agent and the preformed fibers are positioned in the tool. A second mould is then clamped over the first, and pre-heated resin is injected through inlets into the cavity with a low-to-moderate pressure. Generally, the liquid resin has low viscosity and is mixed with catalyst so as to accomplish the polymerization process. When the mould is full and all the trapped air is expelled through the outlets, the resin supply is removed and both mould inlets and outlets are sealed. In the last phase the mould is heated so as to cure the component.

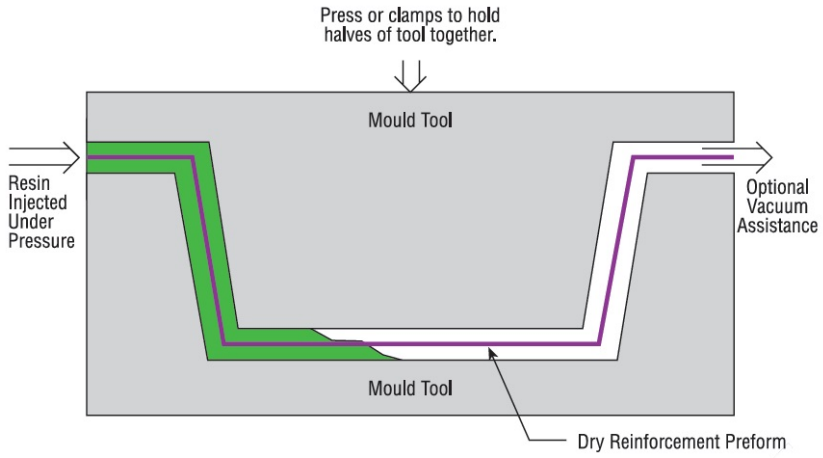

Figure 2.20: Resin Transfer Moulding process

A variation of the RTM process is called vacuum-assisted resin transfer moulding (VARTM). The difference is that in VARTM, vacuum is applied to the outlet of the mold, and the resin is drawn into the mold by vacuum only. Hence, high heat or high pressure are not required to consolidate the laminate structure, and expel completely the air in the cavity.

These simple and effective processes can be employed for making both large and small complex parts within a short cycle time. The costs are low due to the simple tools and the possibility to automate the procedure. A variety of layout of fibers with its orientations can be exploited: continuous-strand mat, woven roving, or even cloth can be used. Thus high-quality and high-strength composite structure with a good quality surface can be achieved. As drawback, extreme large component cannot be obtained with this procedure.

2.2.6. Resin Infusion under Flexible Tool (RIFT)

The RIFT manufacturing method is conceptually similar to VARTM technique. The preformed dry reinforcement is placed onto a mould tool, and a peel-ply is applied in order to spread the resin over the fibers. Then, a flexible plastic polymeric bag, equipped with valves, is positioned over so as to close and seal the component. Through a vacuum pomp, all the entrapped air is evacuated and then the catalysed resin is drawn into the reinforcement [36]. After the curing process the component is extracted and further processes will be performed.

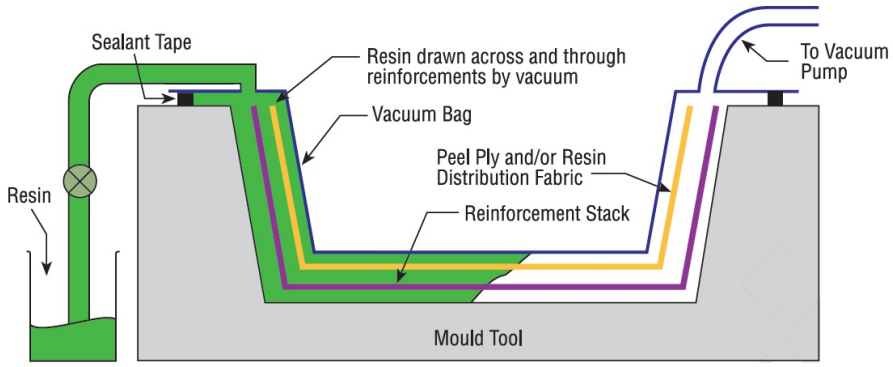

Figure 2.21: Resin Infusion under Flexible Tool process

This technology was developed to reduce the detrimental styrene emissions produced by the polyester resin. However, with respect to both VARTM and RTM, the RIFT process is able to reduce the costs associated with the tools, since half of the conventional rigid mould is replace with a plastic bag. On the other side, there is no direct control over the thickness of the final composite structure, and good quality surface is achieved only on the moulded side. The method is suitable for the production of large components with a low volume production.

2.2.7. Compression moulding

This process is a matched-die moulding fabrication method, which produces a large number of reinforced thermosetting resin products. The process is fast and simple, the preformed moulding compounds or premix with partially catalysed resin are placed in the preheated mould. The mould halves are closed and controlled pressure is applied in the cavity, in this way the resin becomes liquid and the complete polymerization occurs. Once the mould is cooled, the component can be extracted. This method offers an high degree of productivity and automation, high-quality and high-strength components can be produced in a large variety of size and shape in a short cycle time. The most used preformed moulding compounds such as bulk or dough molding compounds (BMC and DMC), sheet moulding compound (SMC) and prepregs are presented below.

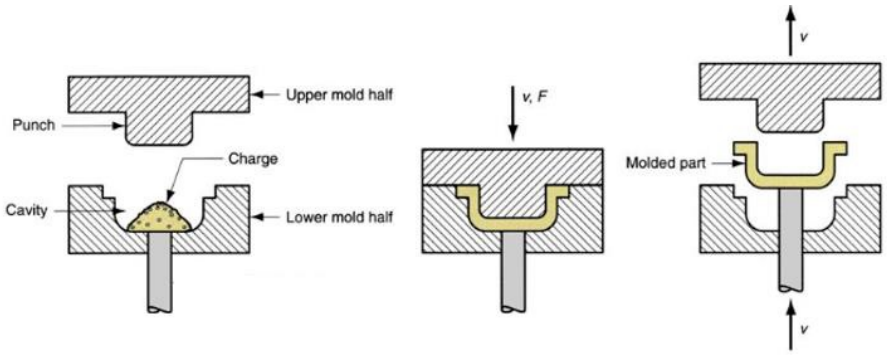

Figure 2.22: Compression moulding process

Bulk or dough moulding compounds (BMC and DMC)

These compounds consist of a dough-like or putty-like mixture of fibers, resin and filler to which pigments and others materials may be added [1]. They are made by mean of an high-shear z-blade mixer, the final compound can be extruded into rope form ready to be used directly in the mould.

Sheet moulding compound (SMC)

To manufacture SMC a continuous polyethylene film is covered with an appropriate polyester resin, then a layer of fiber reinforcement (chopped strand mat or chopped rovings) is deposited. A second layer of polyethylene film coated with resin is placed over the reinforcement, and the sandwich thus formed is forced to pass through a series of rollers so as to properly wet the fibers. Eventually the compound is roll while the resin thickens, the results is a flat and tack-free sheet composed by either glass, carbon or aramid fibers. In order to use the product, both films of polyethylene have to be removed, then the required size of SMC can be placed in the mold, pressed and cured.

Prepreg

Preimpregnated fiber-reinforced plastics are produced in a similar way to sheet moulding compounds, where the reinforcement is sandwiched between two layers of resin system applied to suitable release film. In particular, the first step consists in wetting the fiber reinforcement into a resin bath, then through a metering roller assembly the picked resin is controlled. The wetted fibers are forced to pass through an heating zone to evaporate the solvent and partially cure the resin. Then, two release films are applied on both sides of the prepreg so as to form the sandwich shape, heated rollers may be used to ensure and adequate wetting of the fibers. Eventually, the final sheet is rolled up and the curing

process proceeds until a tack-free product is obtained, the product can be stock for several weeks to months in an appropriate environment. Different types of fiber reinforcements can be use: continuous unidirectional, woven fabric or random chopped-fiber sheets, while the epoxy resin is the most employed. The difference with SMC is that thickening agents, fillers, pigments, and additives are rarely used in the resin system. Lastly, the prepregs can be use in the compression moulding method similarly to SMC.

Figure 2.23: Sample of prepreg lamina

2.2.8. Prepreg - Autoclave

This bag moulding process is one of the oldest and most versatile manufacturing composite parts. In the first step the mould is prepared, release coating is applied and a peel-ply is used so as to protect the mould surface. Optionally, an extra release film can be used to facilitate the final stage of the process. At this stage, the pre-impregnated material with semi-catalysed resin (see 2.2.7) is positioned in the mould, and then breather layer is applied externally to the whole sandwich structure. The latter layer allows to absorb excess resin and promotes the evacuation of the entrapped air and volatile substances. All the above-mentioned elements are placed inside a vacuum bag, equipped with valves, and sealant tape is used to ensure no air leakage. Once the air is pumped out, the sandwich structure is laid in the autoclave (see figure 2.24). In the chamber the curing process takes place, the temperature is raised up to 180° and the pressure applied can reach up to 5 atmospheres. This allows the resin to to reflow and cure, while the entrapped air is completely evacuated due to the applied high external pressure. Eventually, after the curing cycle and the cooling phase, the prepreg can be extracted from the mould.

Figure 2.24: Autoclave production process

This fabrication method offers composites with high mechanical features and good quality surface. Since inexpensive tooling are required, the cost are limited. On the other side, the laying-up and bagging steps are crucial for obtaining high quality products. Consequently, the workers skill and know-how are essential to properly perform every step of the procedure. Eventually, the method is time-consuming and it is suitable for low production volume.

2.2.9. Additive manufacturing

Additive manufacturing (AM) is a tree-dimensional (3D) printing technique. The process starts from 3D CAD model, then several thin layers of material can be successively printed, by means of a specif 3D printing machine, in order to obtain the final component. Generally, AM guarantees high level of geometrical complexity, and provides a wide range over the selection of fiber volume, orientation and type. Since the requirement of moulds is eliminated, cost, cycle time and material wasting can be considerably reduced. Hence, the method is particularly suitable for the design-to-prototype phase of product development [27]. As drawbacks, low mechanical features are achieved and poor quality surface is obtained as well.

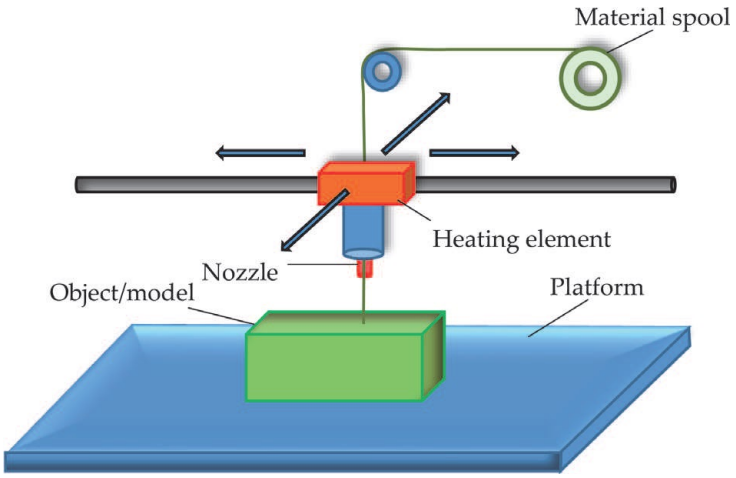

Figure 2.25: Additive manufacturing process

2.3. Experimental testing phase

Material characterization needs an experimental testing campaign in order to achieve all the relevant mechanical features of the material. Different approaches are available, but the most effective is the building block approach (BBA), which is is used during airworthiness certification process of an aircraft. The aim is to conduct numerical analysis and related tests at various levels of structural complexity so as to fulfil all the safety requirements. The BBA can be seen with a pyramidal organization and, in the lowest level, a large amount of tests on simple, cheap and standard specimens are performed.

The focus of this work concerns the lowest level of the BBA. In detail, the material characterization of composites needs reliable method to obtain information such as: stress-strain relationship, elastic constant and damage mechanism. Unfortunately, different elements could affect the results of the tests, especially: orthotropy, non-homogeneity, inelasticity and stacking sequence. Even production problems must be taken into consideration, since composite materials are produced in batches. Quality of the raw materials and human work play a major role on the final product, thus a quality check is needed to ensure adequate mechanical features. Therefore, non-destructive inspection (NDI) techniques must be used on proper samples, the most used are ultrasound and radiography. High-resolution experimental methods are able to offer a comprehensive overview of the material response, based on the study of the micromechanics a detailed stress-strain relationship can be obtained and an understanding of material damage process can be acquired as well. In order to achieve a complete analytical material model the damage effects have to be considered, the reason is related with the dependency between damage mechanism and loading condition. In this way a long-term response can be reached, since composites

can be subjected to a large variety of loading conditions during their life cycle.

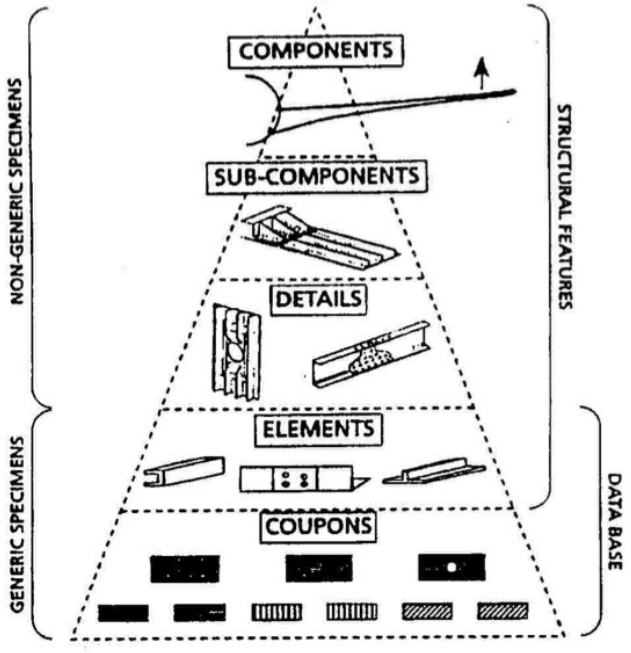

Figure 2.26: Schematic of a building block approach

For this thesis work the American Society for Testing and Materials (ASTM) standards have been considered so as to perform the characterization tests. Eventually, by applying well known analytical models the damage evolution have been predicted from the experimental results.

2.4. Numerical modeling phase

Numerical simulation is largely used nowadays in order to achieve more precise solutions in a short amount of time. Generally, this tool is implemented when dealing with complex, non-linear mathematical problems is required. In the field of structural engineering, the Finite Element Method (FEM) is the most employed approach, from this, thanks to his functionality and adaptability, different commercial codes have been developed through the years. Composite materials behaviour is very complex and in order to capture such a response many materials models were developed. Especially, damages and failure modes are the most challenging parts to be modelled, since a trade off between computational costs and accuracy have to be found in order to obtain a valuable solution in the shortest amount of time. Indeed, the development process is still ongoing nowadays and phenomena such as delamination and microscopic behaviour are being investigated.

LS-DYNA is a commercial software used to solve highly non-linear transient dynamic finite element analysis (FEA) problems exploiting explicit time integration. Green composite materials are a new and innovative solution recently on market, due to the relevance of numerical simulations it is essential to replicate their behaviour so as to develop increasingly accurate and efficient material models. LS-DYNA was selected to start this process due to its huge variety of material cards already present in the software library. Parameters will be found in order to predict and simulate both the static and dynamic behaviour. It worth noting that the selected solver is the most suited in the context of dynamic impacts.

As well known, composite materials are made by layers stacked together and are mostly used in aeronautical and automotive fields. The manufactured components are panels usually joined together, which can be seen as thin-wall structures. For this reason plane-stress condition and CLT (see sections 2.1.4 and 2.1.5) were presented so as to approximate the behaviour of these structures. Different mesh element can be chosen in order to numerically simulate composites. Two-dimensional (2D) shells and three-dimensional (3D) thick shells are the most suitable for this purpose, by exploiting through-the-thickness integration points each ply can be considered in the numerical procedure and the stacking sequence of the composite material can be thus easily modeled within one element [8]. In order to evaluate out-of-plane shear resistance the 3D thick shell elements can be used, since Kirchhoff hypothesis is discarded. Overall, shells are very efficient since good results can be achieved with a limited computational effort. By exploiting solid (brick) elements a more accurate solution can be obtained as well, but is essential to highlight that bricks are not suitable for this purpose, as the plies stacking sequence cannot be explicitly defined within one element, thus increasing exponentially the computational cost. Eventually, stacked-shell approach can be introduced: each layer is numerically modelled by a single shell and then the constraints between the plies are properly imposed. This model allows to take into account delamination phenomena, but the drawbacks are an increasing of the computational cost and additional experimental tests for the calibration phase.

In conclusion, even if 2D shell elements are not capable to capture interlaminar behaviour, they are the most suitable for representing numerically natural composite materials behaviour.

2.4.1. Material cards overview

The first material models were very simple, generally elastic behaviour until failure was preferred. Over the years development led to more advanced models in which post-failure

evolution and damage parameters were taken into account. In doing so the LS-DYNA material library has been expanded, offering a wide choice in terms of orthotropic material models.

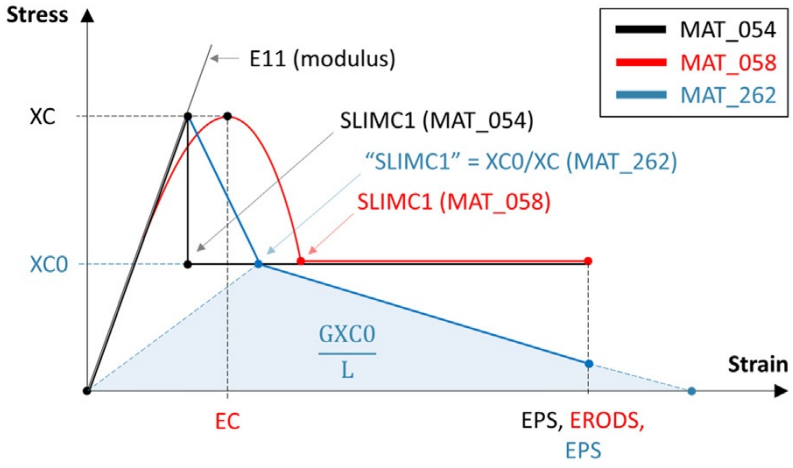

Figure 2.27: Comparison of MAT054, MAT058 and MAT262

In the LS-DYNA database the first composite material card is *MAT_022, which is based on the Chang-Chang failure criteria. A linear elastic law until failure is used, but neither failure in longitudinal compression nor post-failure behaviour are exhibited. The *MAT_054/055 models are the most used in crash simulations [7], are based respectively on Chang-Chang and Tsai-Wu failure criteria. with respect to the previous material, a post-failure phase is introduced, in detail a pseudo-elastic response is exploited while a strain-based failure criterion defines the ultimate failure. The *MAT_058 is based on Matzenmiller work [18] and the first improved version, based on *MAT_054, was presented in [32]. Non-linear behaviour until failure can be defined by setting appropriate damage parameters, and post-failure phenomena can be described as well as in *MAT_054. Failure in the three directions can be completely uncoupled and a bi-linear stress-strain relationship can be achieved in the shear direction. Because of these features the model is able to simulate complex forms such as woven fabric. The material models *MAT_261 and *MAT_262 were respectively developed by Pinho and Camanho. A linear behaviour until failure is chosen, while the post-failure damages are represented by a linear or bi-linear degradation formulation. Additional fracture toughness tests are needed in order to achieve the parameters useful to calibrate the material models.

Eventually, a trade-off among results accuracy, computational cost and number of executable tests must be found in order to select the best material model. The *MAT_058 fits all the requirements to accomplish the numerical characterization phase.

2.4.2. *MAT_058 material model

The material card 58 relies on an anisotropic elastic damage model, where micro-cracks and voids development is taken into consideration during the deformation process. This assumption leads to degradation of stiffness and other elastic properties, as well as to plastic deformation. In this way, the typical brittle-elastic behaviour of natural composite material can be assessed.

In the context of homogenized continuum (see 2.1.3), for each lamina of the composite structure four failure criteria can be defined following the Hashin methodology (1980). In particular, fiber failure mode and matrix failure mode are divided, as well as compressive and tensile stress conditions.

Here the quadratic parameters:

- Tensile fiber mode ($\sigma_{11} \geq 0$):

$$e_m^2 = \left(\frac{\sigma_{11}}{X_t}\right)^2 - 1 \quad \begin{cases} \geq 0 & failed \\ < 0 & elastic \end{cases} \tag{2.22}$$

- Compressive fiber mode ($\sigma_{11} < 0$):

$$e_c^2 = \left(\frac{\sigma_{11}}{X_c}\right)^2 - 1 \quad \begin{cases} \geq 0 & failed \\ < 0 & elastic \end{cases} \tag{2.23}$$

- Tensile matrix mode ($\sigma_{22} \geq 0$):

$$e_m^2 = \left(\frac{\sigma_{22}}{Y_t}\right)^2 + \left(\frac{\tau}{S_c}\right)^2 - 1 \quad \begin{cases} \geq 0 & failed \\ < 0 & elastic \end{cases} \tag{2.24}$$

- Compressive matrix mode ($\sigma_{22} < 0$):

$$e_d^2 = \left(\frac{\sigma_{22}}{Y_c}\right)^2 + \left(\frac{\tau}{S_c}\right)^2 - 1 \quad \begin{cases} \geq 0 & failed \\ < 0 & elastic \end{cases} \tag{2.25}$$

Where strength coefficients X_t, X_c, Y_t, Y_c, S_c can be obtained from uniaxial loading tests.

The effective stresses must be considered in the equations above since only the undamaged part of a cross section can carry load. In order to obtain this stress definition the net area

is considered. Besides, it is possible to specify the relationship between effective stresses and nominal (true) stresses:

$$\begin{Bmatrix} \hat{\sigma}_{11} \\ \hat{\sigma}_{22} \\ \hat{\sigma}_{12} \end{Bmatrix} = \begin{bmatrix} \frac{1}{1-\omega_{11}} & 0 & 0 \\ 0 & \frac{1}{1-\omega_{22}} & 0 \\ 0 & 0 & \frac{1}{1-\omega_{12}} \end{bmatrix} \begin{Bmatrix} \sigma_{11} \\ \sigma_{22} \\ \sigma_{12} \end{Bmatrix} \tag{2.26}$$

Where ω_{ij} is called damage parameter and must lower than one ($\omega_{ij} < 1$).

It must be noted that ω_{11} and ω_{22} assume different values for tension (ω_{11t} and ω_{22t}) and compression (ω_{11c} and ω_{22c}) so as to account for the on-sidedness of the phenomenon, typical for many materials. The parameter ω_{12} is assumed to be independent from the sign of the shear stress τ.

The constitutive law for plane-stress condition and orthtropic material can be now written as function of the damage parameters:

$$\begin{Bmatrix} \sigma_1 \\ \sigma_2 \\ \tau \end{Bmatrix} = \frac{1}{D} \begin{bmatrix} (1-\omega_{11})E_1 & (1-\omega_{11})(1-\omega_{22})\nu_{21}E_2 & 0 \\ (1-\omega_{11})(1-\omega_{22})\nu_{12}E_1 & (1-\omega_{22})E_2 & 0 \\ 0 & 0 & D(1-\omega_{12})G \end{bmatrix} \begin{Bmatrix} \epsilon_1 \\ \epsilon_2 \\ \gamma \end{Bmatrix} \tag{2.27}$$

With

$$D = 1 - (1-\omega_{11})(1-\omega_{22})\nu_{12}\nu_{21} > 0 \tag{2.28}$$

The state of damage is uncharged in the elastic range, which is bounded by the failure surfaces. The threshold values described by the failure criteria can be defined by substituting the nominal stresses with the effective stresses:

$$f_{\parallel} = \frac{\sigma_{11}^2}{(1-\omega_{11c,t})^2 X_{c,t}^2} - r_{\parallel c,t} = 0 \tag{2.29}$$

$$f_{\perp} = \frac{\sigma_{22}^2}{(1-\omega_{22c,t})^2 Y_{c,t}^2} + \frac{\tau^2}{(1-\omega_{12})^2 S_c^2} - r_{\perp} = 0 \tag{2.30}$$

Where the size of the elastic region is defined by the damage threshold r.

In order to obtain all the failure criteria independent from each other a partial uncoupling of the failures can be performed. Here the general solution with non-smooth failure surfaces is presented:

$$f_{\parallel} = \frac{\sigma_{11}^2}{(1-\omega_{11c,t})^2 X_{c,t}^2} - r_{\parallel c,t} = 0 \tag{2.31}$$

$$f_{\perp} = \frac{\sigma_{22}^2}{(1-\omega_{22c,t})^2 Y_{c,t}^2} - r_{\perp} = 0 \tag{2.32}$$

$$f_s = \frac{\tau^2}{(1-\omega_{12})^2 S_c^2} - r_s = 0 \tag{2.33}$$

The state of damage changes once the state of stress is outside of the failure criteria. In particular, for the damage parameters many evolution laws are possible. with respect to material model 54 a smooth increasing of damage is described and the material response gradually changes. In this way the *MAT_058 proves to be more accurate and physically more correct.

$$\omega_i = 1 - \exp\left[\frac{1}{m_i e}\left(\frac{\epsilon_i}{\epsilon_f}\right)^{m_i}\right] \tag{2.34}$$

With ϵ_f is the nominal failure strain:

$$\epsilon_{f\parallel} = \frac{X_{t,c}}{E_{\parallel}} \qquad ; \qquad \epsilon_{f\perp} = \frac{Y_{t,c}}{E_{\perp}} \tag{2.35}$$

The parameter m_i describes the development of the different failure modes in the different directions. When the damage parameter is equal to 1, complete failure is reached.

The application of strain softening damage models can bring the localization effect. When, in the loaded element, the stress level exceeds the maximum stress value, strain softening starts and due to minor numerical differences some elements are further deformed, whereas other elements are unloaded. This problem introduce the mesh size dependencies into any FE model and it must be considered. To avoid the localization effect a modification to the damage evolution law is introduced. The idea consists in not letting the stress fall below a threshold value, the yield-stress. After the reaching of this limit value the damage parameter ω becomes:

$$\omega = 1 - \frac{\alpha X_{t,c}}{E\epsilon} \tag{2.36}$$

In order to relate the yield stress with the strength value α is defined. In particular, the value can be $0 \leq \alpha \leq 1$. For $\alpha = 1$ (without softening) the strains grow in all the elements in a similar manner, whereas for value of α lower than 1 localization effect is still present and the damage growth is only in the first affected elements.

The implementation of the material model can be now reported by highlighting the most significant parameters. The table below shows the card structure [17].

MID	RO	EA	EB	EC	PRBA	TAU1	GAMMA1
GAB	GBC	GCA	SLIMT1	SLIMC1	SLIMT2	SLIMC2	SLIMS
AOPT	TSIZE	ERODS	SOFT	FS	EPSF	EPSR	TSMD
XP	YP	ZP	A1	A2	A3	PRCA	PRCB
V1	V2	V3	D1	D2	D3	BETA	LCDFAIL
E11C	E11T	E22C	E22T	GMS			
XC	XT	YC	YT	SC			

Table 2.1: *MAT_058 card overview

In the table 2.1 there are elastic constant, strength-related terms and some non-physical parameters. The latter can considerably change the material behaviour. It is worth introducing the most relevant [9]:

- SLIMxx: it represents the constant α in the equation (2.36). It can be defined both in tension and compression for each material direction. It should not be set to zero.
- ERODS: it is the maximum effective strain for an element layer. It control the element failure determining the complete failure (complete deletion). It is define as: $\epsilon_{eff} = \sqrt{\frac{2}{3}\epsilon_{ij}\epsilon_{ij}}$
- FS: Failure surface type, see equations from (2.29) to (2.33)
- SOFT: This factor is related to the material strength in crashfront. In order to simulate crack propagation, the elements adjacent to the deleted ones are subjected to a stress reduction during the softening phase.
- Non-linear (bi-linear) stress-strain curve for shear part: if failure surface definition (2.33) is considered, non-linear shear behaviour can be set through parameters: GAMMA1, TAU1, GMS, SC. For a better understanding the figure 2.28 is reported.

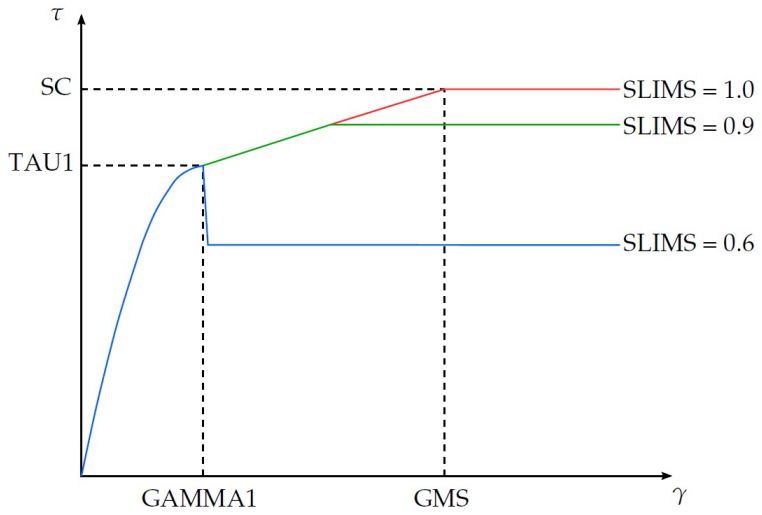

Figure 2.28: Non-linear stress-strain relationship for shear

3 | Natural composite materials

As already mentioned in the section 2.1, composite materials have been used the first time more than 3000 years ago. In particular, natural fibers and natural matrices represented the only available sources to achieved composites. Over the last centuries, the technological progress led to the development of synthetic composite materials with increasingly better mechanical performances and remarkable reliability. Nowadays, the environmental issues are more and more relevant and the need to develop new materials, that are entirely based on renewable resources, is only the first step to reduce the consumption of fossil fuel and the consequently production of CO_2 emissions. Natural composite materials can represent a valid alternative to the petroleum-based composites [29]. Through the last years, the studies and researches on these materials exhibit significant mechanical features and competitiveness with respect to the traditional solutions. Although there is still a lot of work to be completed, these results show the opportunity to employ these new products in a sustainable and responsible way [25]. Bio-based composite materials advantages have been already exploited in recent years in different industrial sectors, such as: transportation (automobiles, railway coaches, aerospace), building and construction industries (ceiling paneling, partition boards), packaging, consumer products, etc. In addition, their mechanical features and dynamic behaviour have attracted their use in many crashworthiness applications. Natural composite materials can be defined as the combination of fibers and matrix where at least one component has a natural source. If in the composites both the constituents are obtained from renewable resources, the product can be called green composite material. On the other side, a partially eco-friendly composite is obtained. Natural fibers can be either plant or animal sourced. The latter are composed by proteins, whereas the first typology are comprised of cellulose. For the sake of simplicity, in composite industry and in this work, natural fibers are referred to vegetables fibers. It is worth noting that most of the natural composites are composed by natural fibers with polymeric matrix, due to technological limitations in obtaining a suitable natural matrix.

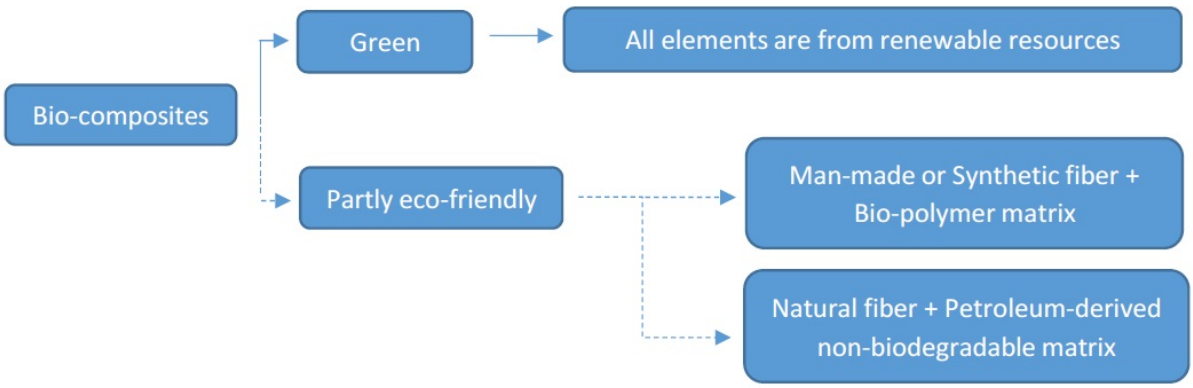

Figure 3.1: Classification of bio-composites

Natural composite materials can be divided in three different type [21]:

- Synthetic polymers matrix reinforced with natural fibers, they are the most used due to their mechanical characteristics and production ease.
- Bio-polymers reinforced with synthetic fibers such as glass or carbon, they are the least used due to their disposal issue at the end of their life cycle.
- Green composite materials are composed by natural fibers and natural matrix. They are the most interesting, as acceptable mechanical properties can be achieved while preserving biodegradability.

Bio-base fibers can be vegetable, animal or mineral origin, excluding the plant fibers, the remaining fibers are the least used due to the lack of applications or even because are banned by the law. Indeed, animal fibres are not commonly used and asbestos was banned due to risks of exposure and risks associated with human health. Hence, plant fibers are the most commonly used in industry and the most analysed by the research community, thanks to their renewability, wider availability and short growth period. These fibers can be divided in six basic types:

1. Bast fibers (jute, flax and hemp)
2. Leaf fibers (abaca, sisal and pineapple)
3. Seed fibers (coir, cotton and kapok)
4. Core fibers (kenaf, hemp and jute)
5. Grass and reed fibers (wheat, corn and rice)
6. All other types (wood and roots)

Natural fibers may offer a large variety of properties depending on the plant species employed. Cellulose, hemicellulose and lignin compose a generic plant structure, and each of these constituents have an influence on the fiber features, such as: strength, thermal degradation, biological degradation, moisture absorption and UV degradation. It is worth noting that linear cellulosic macromolecules are linked by hydrogen bonds and are closely associated with hemicelluloses and lignin, which confer stiffness to fibres. Additionally, the latter are responsible for the cellulose containment within the fibre cell wall and hold the fibres together [5].

The properties of a bio-composite materials depend on the polymeric matrix chosen. To produce this constituent can be exploited either bio-based sources (plant or animal) or synthetic (oil-base product). The natural polymer or bio-polymer are biodegradable and to produce them starch or proteins can be used. Nowadays, poor mechanical performances are offered by this product due to the lack of interfacial adhesion between matrix and fibers, however development is just begun and a wide room of improvement is still available. Synthetic fillers can be divide in thermoset and thermoplastic. The latter can be melted over a certain temperature, the van der Waals and hydrogen bonds are temporarily broken allowing molecular manoeuvrability. Due to its behaviour, this matrix type can be reused, but the mechanical features can fulfil non-structural requirements. The thermosets have a wide range of applications thanks to their good adhesion, high thermal and chemical resistance and excellent mechanical properties. Their are the most used in composite industry since good mechanical features such as: strength, stiffness, toughness and transverse fracture stress can be obtained in the final composites. Also the matrix-fiber interfacial properties fulfil all the structural mechanical requirements. Unfortunately, thermoset matrices are difficult to recycle and reuse.

3.1. Reasons to study them

As well known, traditional composite materials have several advantages with respect to the metals, and they were capable of satisfying the market demand for several decades. However, the requests changed over the past few years and new needs must be satisfied. For this reason, natural composite materials become more and more attractive in composites industry, due to their numerous advantages and the possibility to develop and improve considerably their main features.

In table 3.1 the most important benefit and drawbacks are reported. In particular, the low density of these materials must be taken into account in the context of the mechanical properties. When the specific modulus is considered, the natural fibers show data

comparable or even better than those of glass fibers [21]. In table 3.2, the specific gravity is evaluated to obtain the specific quantities, in detail it can be defined as the ratio of the fiber's density over the water's density. These higher specific properties can be exploited in applications where, besides the request of good mechanical feature, the weight aspect plays a major role. In the context of crashworthiness, due to the elongation property, high energy absorption capability can be reached as well as high specific energy absorption, thanks to the low density values [24].

Advantages	**Disadvantages**
• Good thermal insulation • High acoustic damping • Vibrations damping • Low cost materials • High specific mechanical properties • Environmentally friendly • Light weight/low density • Less health hazard • Ease in fabrication • Availability • Morphological flexibility • Corrosion resistance • Electrical insulation	• High hygroscopicity • Low thermal resistance • Low durability • Poor fiber-matrix adhesion

Table 3.1: Pros and cons of natural composite materials

During crash tests on ramie epoxy composites, a ductile behaviour was exhibited and there was no debris split after crushing, this can be attributed to the high elongation property of ramie fibers [11]. Several studies pointing out the lower cost of natural fibers comparing with synthetic fibers, for example were demonstrated that plain weave jute fabric combined with epoxy resin is considerably cheaper than the synthetic counterpart such as glass/epoxy or carbon/epoxy [4]. However, in order to perform a correct evaluation it is essential to consider the applications, the production process and the life cycle costs. In general, raw natural fibers are cheap and require low energy processes to be manufactured, this leads to a reduction of the overall costs with respect to traditional reinforcing fibers (see table 3.3).

Fiber	Specific Gravity	Tensile Strength (MPa)	Modulus (GPa)	Specific Modulus
Jute	1.3	393	55	38
Sisal	1.3	510	28	22
Flax	1.5	344	27	50
Hemp	1.07	389	35	32
Glass fiber	2.5	3400	72	28

Table 3.2: Specific mechanical properties

At the actual rate of consumption, the world petroleum resources are estimated to last for the next 50 years or so [33]. Moreover, several environmental issues are rising throughout the last years. Hence, pollution laws are getting stricter leading to an increasing of the disposal costs of synthetic composite materials. Natural composite materials are able to meet these needs by exploiting their most relevant benefit: biodegradability. The production process starts from the plantation, which is a labor-intensive activity. Nowadays, plants are cultivated extensively but most of their abundant wastes do not have any usefulness. Since natural fibers are extracted manually, the human resources prove to be fundamental to complete such task. Hence, the natural composites can represent an economic interest for agricultural entrepreneurs while creating new employment opportunities, especially in developing countries, where the primary sector is predominant [29]. During the plantation phase, a huge benefit is given by the consumption of CO_2 in favor of the emission of O_2 back to the environment. Additionally, the manufacturing process for natural composites requires less amount of energy with respect to the traditional solutions, leading to a further reduction of emitted CO_2. Eventually, at the end of their life cycle, natural composites can be reuse for other application. Otherwise, if not recycled, they will not represent a threat for the environment, thanks to their biodegradable feature.

Fiber	Cost (US$/ton)	Energy (GJ/ton)
Natural fiber	200-1000	4
Glass fiber	1200-1800	30
Carbon fiber	12500	130

Table 3.3: Energy and cost of different fibres

As reported in table 3.1 the drawbacks are mostly related with degradable nature of these materials. A major problem is represented by the thermal resistance, due to the

presence of cellulose inside the natural fibers, the product is not suitable either for high temperature treatments or applications. When fibers are exposed to such conditions can easily catch fire. To effectively address this problem, a flame retardant substance can be add during the production process, so as to minimize fire hazards [13]. Another important issue to be considered is associated with the higher variability of the raw materials, several aspects such as soil composition and morphology can influence the quality of the fibers, thus the mechanical properties of the final product. Green fibers are rich of cellulose, hemicelluloses, lignin, and pectin, all these components are usually hydrophilic sources [22]. This cause the fibers to be highly hygroscopic and prone to absorb water, especially when exposed to moisture. This feature is in contrast with the hydrophobic nature of polymeric matrices, thus interface adhesion issue between fiber and matrix can arise. As well known, mechanical properties are related with this aspect, so a reduction of strength can happen if a proper adhesion is not performed. Eventually, in the context of crashworthiness studies, in order to reduce the moisture content of the composite materials a pre-production treatment on fibers is performed, this consists in adding an appropriate amount of nanoparticles so as to reduce adhesion uncertainties.

3.2. How they are manufactured

The manufacturing techniques employed to fabricate natural composite materials are similar to those used for the traditional synthetic composites. However, due to their innovative nature, researches and experiments are still going on. Hence, various and new manufacturing methods are investigated so as to improve and develop the natural composites features, reducing the costs and increasing the overall efficiency.

The first stage of the manufacturing process starts from the extraction of the raw materials, as mentioned in the previous section (see section 3.1), this operation relies mainly on human labor. Many extraction techniques can be exploited such as mechanical, chemical or a combination of both, some of them are rudimentary processes and there is no scientific consensus or standards capable of allowing a robust comparison. These techniques can produce crops with good quality, but a long and laborious work is required. It is worth noting that bast fibers are the most widely used due to their ease of extraction and remarkable mechanical properties. As well known, natural fibers are affected by high level of water absorption index, and adhesion problems related with the fiber-matrix interface may arise. In order to address these issues several techniques have been studied through the years such as water-repellent chemicals, coupling agents and physical treatment. Those are able to improve the final mechanical properties by modifying the surface

morphology and the roughness of the fibers. Physical treatments are most economical and practical, since they do not involve the use of detrimental chemical product. Four methods can be presented as the most popular: corona treatment, plasma treatment, steam treatment and heat treatment [21]. Corona and plasma rely on two different technologies, but the aim is similar: forming an ionized region so as to induce a surface modification of the fibers, this can promote the wettability of the reinforcement. Steam treatment is exploited to give permanent deformation to fibers, high temperature and moisture are used to achieved such a result. Eventually, heat treatment is the most widely and valid accepted techniques to dry natural fibers, different tools can be employed such as hot air jets, rotating driers, ventilated ovens, in order to reduce the humidity level below 3%. Another solution employed to improve matrix-fiber interfacial adhesion and fiber dispersion, and to reduce the formation of voids inside the material, consists in the addition of small amounts of a "third component", which acts as an adhesion promoter between polymer matrix and cellulosic fiber. The latter is called coupling agent, in detail its molecules are characterized by a hydrophilic part, able to create the bonds with the polar groups typically present on cellulosic fibers, and a hydrophobic part, which shows higher affinity to the macromolecular chains. Generally, coupling agents are identified as suitable polymer and the most used are methyl methacrylate, acrylamide, acrylonitrile and maleic anhydride polyethylene. An example of the improvements that a maleated adhesion promoter can assure to a green composite based on polypropylene matrix and 30 wt.% wood flour is reported in table 3.4 [16].

Property	**Standard GC**	**GC with 3%MAPP**
Elastic modulus (MPa)	954	1035
Tensile strength (MPa)	19.5	27.2
Elongation at break (%)	4.2	4.6
Impact strength (J/m)	83	98

Table 3.4: Mechanical features green composite (GC) without and with the use of a maleated adhesion promoter (MAPP)

More invasive chemical treatment are available in the market, these are based on the utilization of reactive functional groups which are able to interact with the fiber structures and changing their composition. The objective is to make fibers hydrophobic and improve the interfacial adhesion, thus enhancing the overall final performance. The most employed chemical treatments and their effects are reported in the table 3.5 [2, 15, 37].

Treatment	Effect
Alkali	Reduce the lignin content. Improve fibre-matrix adhesion, thermal stability and heat resistivity
Acetylation	Improve tensile and flexural strength
Benzoylation	Improve hydrophobicity
Enzyme	Reduce the lignin content
Grafting	Improve UV-protective properties, hydrophobicity and mechanical properties
Isocyanate	Surface modification
Mercerization	Reduce the moisture regain and improve the mechanical properties
Methacrylate	Improve tensile and flexural strength
Ozone	Affect surface energy and contact angle
Peroxide	Reduce the moisture regain
Silane	Improve hydrophobic and mechanical properties
Sodium chlorite	Improve tensile strength, young's modulus and elongation at break

Table 3.5: Chemical treatments on natural fibers and their effects on functional properties

Figure 3.2: Illustration of hand lay-up of natural kenaf fiber/epoxy composite

Once that all the materials are prepared, the manufacturing process can take place. In the section 2.2 the most popular fabrication techniques were presented, among those the most suitable were selected to produce natural composite materials, so as to obtain the best mechanical features possible. The most used method is hand lay-up due to their low cost and ease of use, it can be applied for many types of fibers and resins. Especially for

natural fibers, voids can represent a relevant issue, in order to prevent their occurrence in the hand lay-up process an intensive use of the rollers is performed to facilitate uniform resin distribution and the removal of air pocket. In addition, this procedure can be used with compression bladder to improve the mechanical feature. In the field of energy absorption composite structures (EACS) an intensive use of the VARTM techniques is employed. One of the biggest advantages of this method is that 70% of fiber volume fraction (FVF) content can be achieved. This aspect allows for increasing the SEA value and performing possible modification in the composite composition so as to fulfill all the needed requirements.

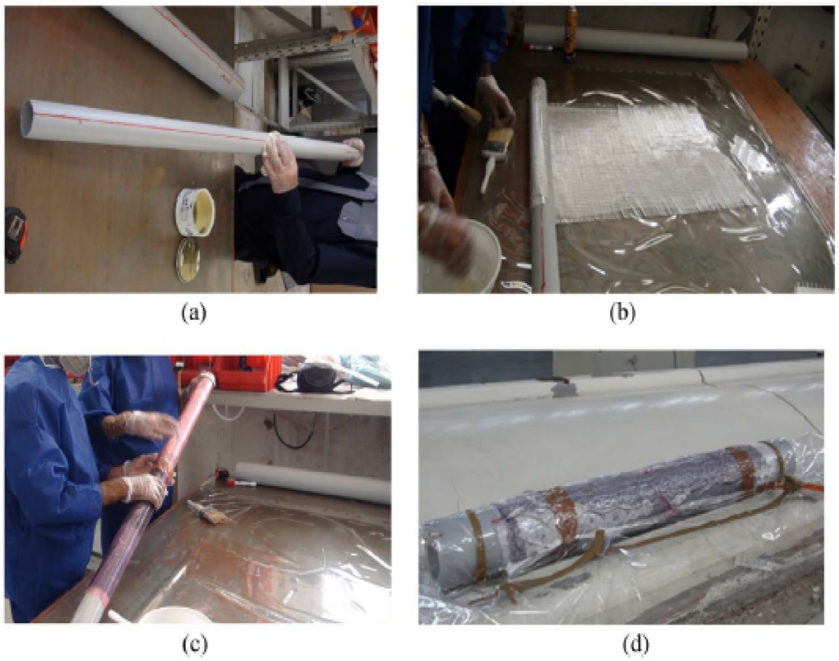

Figure 3.3: Illustration of vacuum bagging manufacturing of GFRP and CFRP composite cylindrical shell

Another suitable technique for the production of EACS is the filament winding, it can be used to fabricate cylindrical structures. The materials most commonly employed are continuous fibers such as yarn and liquid resin such as epoxy, polyester and vinyl ester. Some studies have been conducted on compression molding techniques with good results, however the low thermal resistance of natural components affects the processing temperature, which should be kept below 200°. Eventually, natural fibers can be organized in the form of prepreg, this allows for the employment of the autoclave, as reported in section 2.2.8. The method is economical and good mechanical properties can be easily achieved. As a drawback, the processing temperature is a critical aspect and should be properly set. It should be pointed out that small amount of humidity is not always detrimental

for natural composites, on the contrary water can help to "soften" the fibers allowing for an easier manipulation of the material, especially during the placement phase of the manufacturing process.

Innovative methods are still investigating to guarantee even more effective and more economical procedures. For example, electromagnetic induction properties are exploited in compression molding technique in order to gain an instantaneous heating of the mold surface. In this way the production cycle time is reduced as well as the related cost. To maximize the benefits of this method thermoplastic matrix must be employed [35]. Stirring technique has been investigated so as to prepared a green composite based on dispersion-type biodegradable resin and cellulose nanofibers. A relevant increase in flexural modulus and strength have been found with respect to traditional molding methodology [34]. Moreover, improvement of mechanical properties can be obtained by adding semi-synthetic cellulose fiber (Lyocell) to hemp fiber-reinforced PLA composites. The results show that combining hemp and Lyocell in a composite can improve the impact properties by 160% compared to hemp fiber reinforced composites [21].

3.3. Applications

Since composite materials have been created, their applicability has been exploited in many different sectors. Natural composite materials make no exception, and their numerous advantages are already used in several applications. As reported in section 3.1, characteristics such as low specific weight, relatively high strength, resistance to corrosion and fatigue, relatively low production cost and biodegradability may allow for an increasingly employment of these materials. Another important aspect that allows for this widespread application is given by the huge amount of natural fiber types available. Each fibers type has unique features that can fulfil different market needs.

Natural composite materials are particularly suited for automotive and transportation industry due to low density and satisfactorily high specific properties. Body parts such as engine hood, dashboards, storage tanks, bumpers and so forth can be manufactured by using reinforcements of natural fibers such as flax, hemp, jute, sisal, and ramie. Numerous car companies invested in the research and development of this technology, in order to assure the good quality of manufactured natural products. In addition, from these analyses emerged that the use of natural composites leads to an overall vehicle weight reduction, thus reducing the amount of carbon dioxide released to the environment. Some of the above-mentioned car components fall under the energy absorption structures, their purpose is to absorb the majority of the impact energy so as to guarantee protection of

passengers from severe impact injuries or death. The aim is to substitute the current traditional solutions with natural composite materials. In particular, their mechanical features can be exploited in order to improve important characteristics such as energy absorption, average load, peak load and crash force efficiency [3]. In this regard, investigative studies with promising results have been conducted in recent years. For example, crashworthiness characteristics have been studied on natural silk-epoxy rectangular tubes [10], or on carbon-jute-glass-epoxy composite circular tubes [4], or even a comparison among hemp-epoxy, flax-epoxy and jute-epoxy composite cones has been conducted [20]. Since 90s, natural materials were already employed for the production of non-structural car components. Especially, car interior parts such as seat backs, parcel shelves, front and rear door coating, trunk coating, and door-trim panels were fabricated with plant reinforced composites (for furthers details, see [22]). In this case, mechanical resistance was neglected in favor of low purchasing and maintenance costs, which are the drivers chosen by car companies to select most suitable material.

Figure 3.4: Abt Cupra XE body sheel made of flax composite materials

Natural material composites show to be promising for acoustic energy absorption applications. Their use can be extended to include vibration control and noise reduction. This behavior was noticed during crashworthiness studies, in fact the use of these materials in low and mid-frequency region event can damp both mechanical and acoustic vibrations during crash scenario [13]. Moreover, composite structures with bamboo, cotton, and flax fibers with PLA showed to be great solutions for the improvement of the sound

absorption coefficient in automobile door panels [27]. Natural fiber-reinforced thermoset and thermoplastic composites fulfil the properties required for aircraft interior panels such as resistance to heat and flame, serving easy recycling, and disposal of materials being cheaper and lightweight over conventional sandwich panels. Although traditional composites show to be suitable for aerospace applications, they exhibit some difficulty in recycling. Bio-composites can overcome this issue by taking advantage of their low cost and biodegradable features. Some attempts to fabricate structural parts has been performed: aircraft wing boxes made of ramie fiber composites revealed a 12–14% decrease in weight. In addition, hybrid kenaf/glass fiber-reinforced polymer composites showed increased resistance to rain erosion, which is suitable aspect for aircraft application [27].

Figure 3.5: Door panel made of hemp fiber

The new green buildings generation must be ecologically mindful, suitable and healthy place to live and work, for these reasons natural composites can be considered one of the major used materials in the construction phase. With respect to their applications, bio-composites can be classified in two main products: structural bio-composites and non-structural bio-composites. The latter include window, exterior construction, composites panels, and door frame, while the first can comprehend bridge as well as roof structure. Thin-walled elements made by sisal fiber reinforced composites exhibit good mechanical properties such as both high strength in tension and compression, this can allow for a wide area of application in the structural field. Additionally, bamboo fibers can be used in structural concrete elements as reinforcement, while both sisal fiber and coir fiber composites have been used in roofing components in order to replace asbestos [22].

3.4. Material selection

For the purpose of performing experimental analyses so as to confirm the good quality of natural composite materials, the most appropriate fiber and matrix must be chosen among the numerous. This section aims to investigate the most popular solutions in order to determine the most suitable natural composite materials for this thesis work.

Fiber	Density (g/cm^3)	Diameter (μm)	Length (mm)	Moisture Content(%)
Abaca	1.5	10–30 (20)	4.6–5.2 (4.9)	14
Bamboo	0.6–1.1 (0.85)	25–88 (56.5)	1.5–4 (2.75)	11–17 (14)
Banana	1.35	12–30 (21)	0.4–0.9 (0.65)	10–11 (10.5)
Coir	1.2	7–30 (18.5)	0.3–3 (1.65)	10
Cotton	1.21	12–35 (23.5)	15–56 (35.5)	33–34 (33.5)
Flax	1.38	5–38 (21.5)	10–65 (37.5)	7
Hemp	1.47	10–51 (30.5)	5–55 (30)	8
Jute	1.23	5–25 (15)	0.8–6 (3.4)	12
Kenaf	1.2	12–36 (24)	1.4–11 (6.2)	6.2–12 (9.1)
Pineapple	1.5	8–41 (24.5)	3–8 (5.5)	14
Ramie	1.44	18–80 (49)	40–250 (145)	12–17 (14.5)
Silk	1.32	-	-	-
Sisal	1.2	7–47 (27)	0.8–8 (4.4)	11

Table 3.6: Physical properties of natural fibres (average value between parenthesis)

Because of their natural origin several factors may influence the fibers properties such as the type of soil, growing conditions, harvesting conditions, weather and post-treatment as well as damage during processing [25]. Due to this relevant variability in the final characteristics, it must be taken into consideration that there is not one type of fiber better than the others. Indeed, the suitable fiber selection process depends by several aspects such as type of application requirements, type of composites to be manufactured, fibers availability and the possibility to guarantee properties levelling among different crops or batches. The fiber length is the first issue to be addressed, many studies show the existence of a critical fiber length value, which is required to develop a complete stresses condition in the material. In general, fiber lengths shorter than the critical one can lead to premature failure due to the debonding at the fiber-matrix interface. However, fiber lengths greater than the critical length can represent a threat as well, since an increase in fiber length corresponds to an increase in defects, which can compromise the final

mechanical performances. Hence, a compromise must be found in order to maximize the final performances of the composite. In detail, in crashworthiness application were found that longer fibers are suitable for this purpose, as the energy absorbing features results to be superior with respect to the shorter fiber-reinforced composites [21].

Fiber	Tensile Strength (MPa)	Young's Modulus (GPa)	Elongation at Break (%)
Abaca	430–813 (621.5)	31.1–33.6 (32.35)	2.9
Bamboo	270–862 (566)	17–89 (53)	1.3–8 (4.65)
Banana	529–914 (721.5)	27–32 (29.5)	5–6 (5.5)
Coir	175	6	15–25 (20)
Cotton	287–597 (442)	6–10 (8)	2–10 (6)
Flax	343–1035 (689)	50–70 (60)	1.2–3 (2.1)
Hemp	580–1110 (845)	30–60 (45)	1.6–4.5 (3.05)
Jute	187–773 (480)	20–55 (37.5)	1.5–3.1 (2.3)
Kenaf	295–930 (612.5)	22–60 (41)	2.7–6.9 (4.8)
Pineapple	170–1627 (898.5)	60–82 (71)	1–3 (2)
Ramie	400–938 (669)	61.4–128 (94.7)	2–4 (3)
Silk	500–1300 (900)	5.22	15.4
Sisal	507–855 (681)	9–22 (15.5)	1.9–3 (2.45)

Table 3.7: Mechanical properties of natural fibres (average value between parenthesis)

As show in the tables 3.6 and 3.7, the most relevant properties of natural fibers are gathered to give an overall overview of the main available products on the market. Starting from the density values it shows that bamboo has lowest value, while abaca, pineapple, hemp and ramie have the highest values among the bio-fibers. Diameter can be another important aspect for the mechanical resistance, jute and coir exhibit the lowest average values, while ramie and bamboo have the thickest fibers. Regarding the tensile strength the best results are exhibited by flax, hemp, ramie, pineapple, sisal and banana. Moreover, ramie, pineapple and flax confirm their good mechanical properties with higher Young's modulus values, on the other side fibers such as coir and cotton exhibit low stiffness values. Another important aspect to be addressed is the elongation at break, in this case coir shows the best value with respect to all the others fibers. As already explained, moisture represents one of the major threats for the stability of the mechanical properties, fibers such as sisal, coir, banana, flax and hemp are able to achieve remarkable results, while cotton does not reach adequate results.

It becomes obvious that from these analyses the promising fibers can be identified as bamboo, banana, hemp, flax, jute and ramie. Although the good mechanical features, both banana and bamboo fibers are not suitable for energy absorbing application due to their poor fiber length, which unlikely will be higher than the critical fiber length value. Ramie can represent a valid solution, but due to the limited regions of production an adequate availability cannot be offered, in addition expensive pre-treatments are required with respect to the other bast fibers. Hence, flax, hemp and jute are the most interesting products available on the market.

Flax fiber is one of the oldest fiber crops in the world, an increasing interest about this plant has grown through the last years due to their mechanical features such as low density, relatively high toughness, high strength and stiffness. It is worth noting that flax has specific tensile properties greater than E-glass fiber. Hemp fiber is another interesting solution, it belongs to the cannabis family and it is an annual plant that grows in many areas of the world. It is characterized by excellent mechanical features and the availability is guaranteed by an advanced supply chain due to their current use in the textile industry. Jute fiber is obtained from plants of the genus Corchorus, which includes about 100 species. Jute has remarkable features such as high aspect ratio, high strength to weight ratio and good insulation properties. Fabric and fiber forms can be easily produced, which establish this plant as a valid solution for several applications [29].

Figure 3.6: Macroscopic detail for each fiber type

Eventually, the crashworthiness features of these fibers have been investigated, unwoven hemp exhibits an SEA value of 54.3 J/g comparable with carbon fiber (55.7 J/g). While woven flax had a SEA of 48.5 J/g and woven jute 32.6 J/g [20]. However, a fundamental aspect should be considered: the fiber volume fraction (VF) content. It must be highlighted that hemp samples exhibit the highest fiber VF (43.51–52.52%), while flax and jute have lower values. In detail, jute has the lowest one with a VF content of 30.27–31.6%. From this study is emerged that an increasing of VF in the composite leads to highest

values of SEA. Hence, it appears reasonable to expect better performance both from flax composite and jute composite materials.

Figure 3.7: Polylactic acid (PLA) in raw material form

Alternative solution to synthetic matrices were found in bio-polymer matrices, which are mostly renewable and biodegradable. Some of the natural matrices are obtained in form either of polysaccharides such as gelatine and starch or as protein such as collagen and soy protein. Other formulations include polyester such as polyvinyl acetate, polyvinyl alcohols, polybutylene succinate (PBS), polyhydroxybutyrate-co-valerate (PHBV), polyhydroxybutyrate (PHB) and polylactic acid (PLA). PHBV are produced by a wide range of microorganisms, their appeal is due to their good mechanical properties comparable to those of traditional thermoplastics such as polyethylene and polypropylene [21]. Although the good features their high costs hinder the growth of their popularity in the market. PLA is one of the most popular bio-based polyester employed in the market. It is a thermoplastic matrix and its basic component is lactic acid which derives from the fermentation of corn starch. In general, it is used for non-structural applications such as casings of electronic products, interior parts of automobiles. Additionally, several tests show that PLA is suitable for embedding fibers in composites. Soy protein is obtained from soybean and represent the least expensive and one of the most widely available material in the world. The matrix obtained from these proteins has many befits such fire retardant, vibration damping, remarkable impact strength, gas barrier, water resistance. Moreover, bending, torsional and tensile deformations can be tolerated without visible damages, thanks to their ductile behavior. Eventually, Protein-based matrix contains

polar groups which allow for the strong bonding between matrix and fibers, thus good adhesion can be achieved. As drawbacks, only non-structural applications can be performed with protein-based matrices.

In conclusion, in order to perform the experimental tests phase the most suitable materials for crashworthiness application must be chosen. As reported, either hemp, jute or flax are valid solutions, but the most encouraging and easily achievable appears to be flax fiber solution. Regarding the filler matrix, the natural solutions presented are unable to guarantee the required mechanical features. As a consequence, a thermoset matrix is needed to obtain remarkable results. In particular, epoxy resin is selected due to its low density, low viscosity, high strength, good mechanical characteristics and chemical stability [10].

4 | Material Characterization

In this chapter all the required activities to perform a complete material characterization will be analyzed. In detail, the first section will be presented so as to provide as much information as possible about the used material and the manufacturing procedure to which it was subjected. Then, the experimental activities will be subdivided in two major sections: static tests and dynamic tests. The latter aim to analyze the dynamic features of the materials, while the first activities are performed to obtain the material characteristics in terms of elastic constants and strength-related parameters.

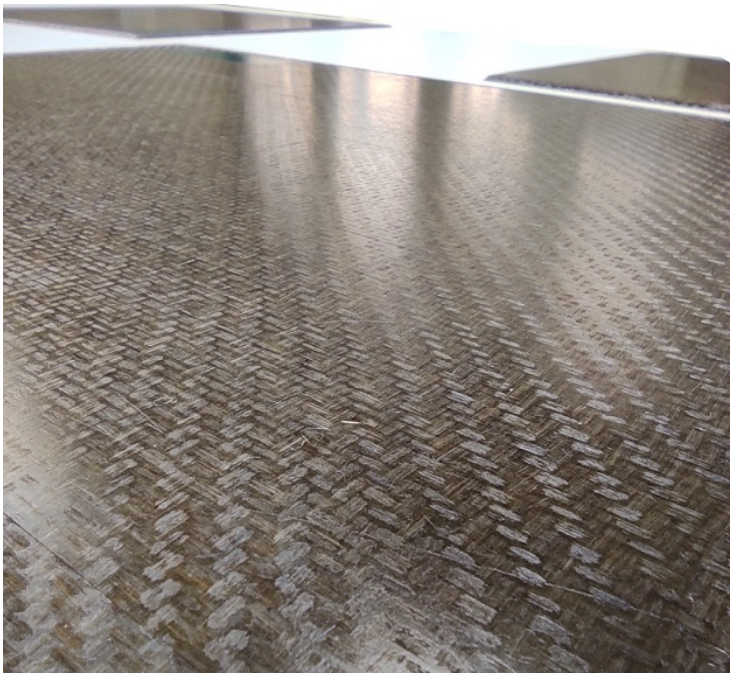

Figure 4.1: Detail of an ampliTex™ 300 laminate

4.1. Samples manufacturing

The selected natural composite material is a flax-based fiber product called ampliTex™ obtained through the collaboration between Bcomp and Angeloni Group.

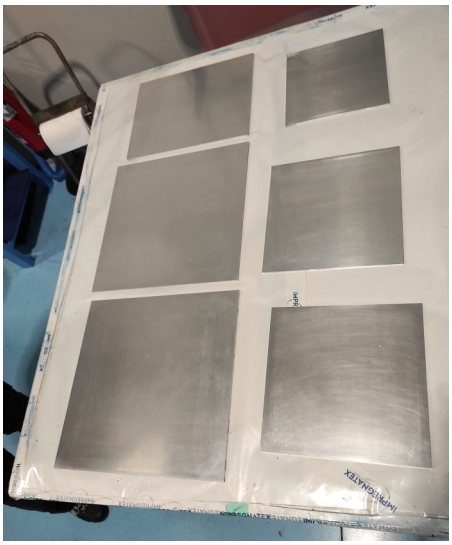

(a) Mold plates

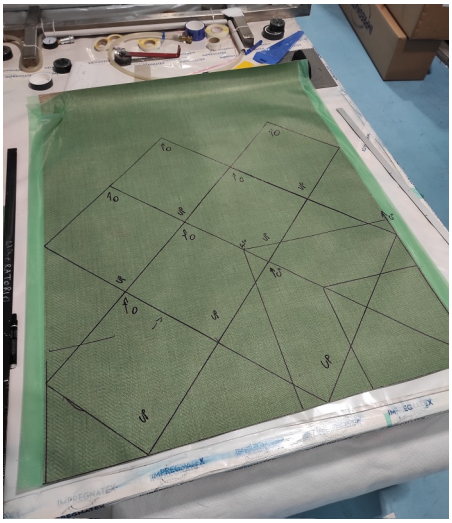

(b) Drawing phase

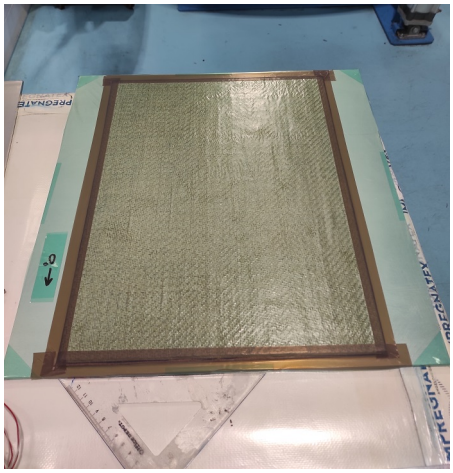

(c) Prepregs on mold

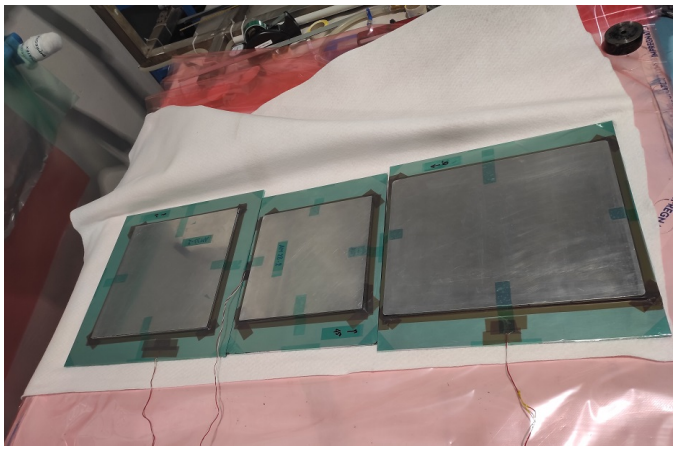

(d) Molds laid on breather

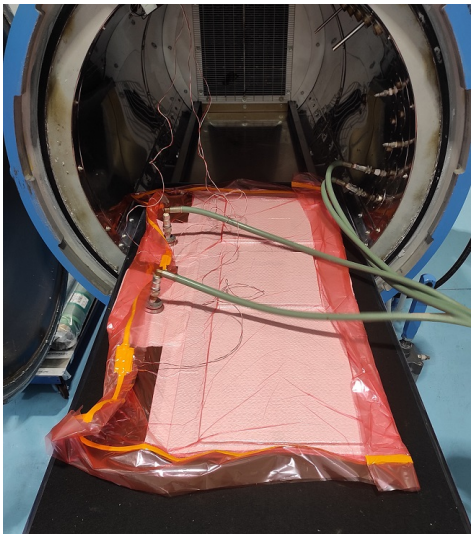

(e) Vacuum bag placed in autoclave

Figure 4.2: Production phases of flax composite laminates

In particular, ampliTex™ 300 twill 2/2 prepreg was employed to fabricate the required samples. The fabric is bidirectional with fibers oriented at 0° and 90° with a density of 1.33 g/cm^3. In order to obtain the prepreg product the dry fibers are chemically treated to increase the compatibility with both epoxy and polyester resins. In order to achieve the best mechanical performances epoxy-based prepreg was employed. in particular the used epoxy resin was IMP 503ZHT BC, which is particularly suitable for composite natural materials.

To produce the flax composite specimens the manufacturing procedure presented in section 2.2.8 was accomplished. As show in figure 4.2b, the first step consists in drawing the lamina shape on the prepreg sheet and for each sketched layer both the upper side and zero direction must be marked in order to prevent any mistakes. As shown in figure 4.2a, the employed molds were simple metal plates, both molds and counter-molds were required to achieved an high-quality surface. At this stage, the realise film were applied only on molds in order to protect the surface. Then, the adequate sized prepreg layers were carefully laid on the release film, following the proper stacking lamination sequence. Another important purpose of the micro-perforated film is to ensure that all trapped air can be properly removed, so as to ensure perfect adhesion between the plies (see figure 4.2c). To guarantee the temperature control during the autoclave cycle a thermocouple is installed on the mould. Thereafter, the structure is positioned in between a breather layer which has the function to absorb all the excess resin and promotes the air transfer from the prepreg towards the outlet valves. Eventually, the prepreg is laid in a sealed vacuum bag equipped with valves (see figure 4.2e).

The following step consists in pumping out all the air from the vacuum bag, to assure this is essential to minimize the amount of wrinkles present on the bag, hence an high competence is required to fulfill such task. At least 10 minutes are required to guarantee the complete debulking procedure. After this phase the prepreg can be placed inside the autoclave where not only the vacuum condition is maintained, but also a controlled increasing both in temperature and pressure are applied inside the chamber. In detail, the employed autoclave is produced by Maroso, the latter is characterized by a capacity of 3315 l, a maximum pressure of 12 bar and a maximum temperature of 250 °C. As show in the graph 4.3 the pressure and temperature are reported over the time. In the first phase the temperature is increased up to 80 °C in about 30 minutes. In the second stage the temperature is maintained constant while the pressure is set to ambient pressure. As shown by the thermocouples measurements, almost 2 hours are need to reach the set temperature and guarantee a complete temperature homogenization of the prepregs. During the third phase, an increasing both of pressure and temperature is performed,

especially the temperature value is raised to 130 °C, while the pressure is set to 6 bar, the time required to reach such condition is 30 minutes. In the last phase both value of pressure and temperature are maintained constant so as to allow the resin to reflow and cure, guaranteeing a complete expulsion of the air from the laminates and homogenization of the prepreg temperature. After 60 minutes the temperature is gradually reduced, whereas the pressure value is kept at operating value for at least 90 minutes in order to assure the complete polymerization of the epoxy resin.

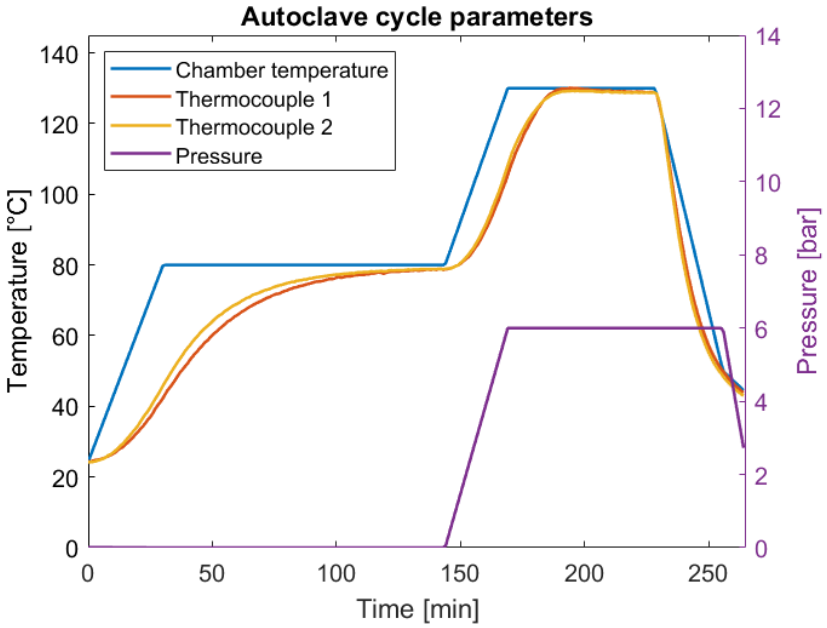

Figure 4.3: Autoclave cycle parameters

At the end of the procedure three different laminates were obtained, two of them were characterized by a 6 plies layout, whereas the third laminate has a greater thickness due to the 8 plies layout. The latter will be employed for the realization of the shear test samples. The cutting procedure is the last phase, in order to accomplish such task the ProtoMAX abrasive waterjet cutter was employed. This technology offers the possibility to achieve precise cut, on the other hand the usage of water can be an issue for natural composites as explained in section 3.1. For this reason, the achieved specimens must be dried by means of a industrial oven. The set heating temperature must be limited to 60 °C so as to stay well below the glass transition temperature (T_g) and avoiding the damage of the fibers.

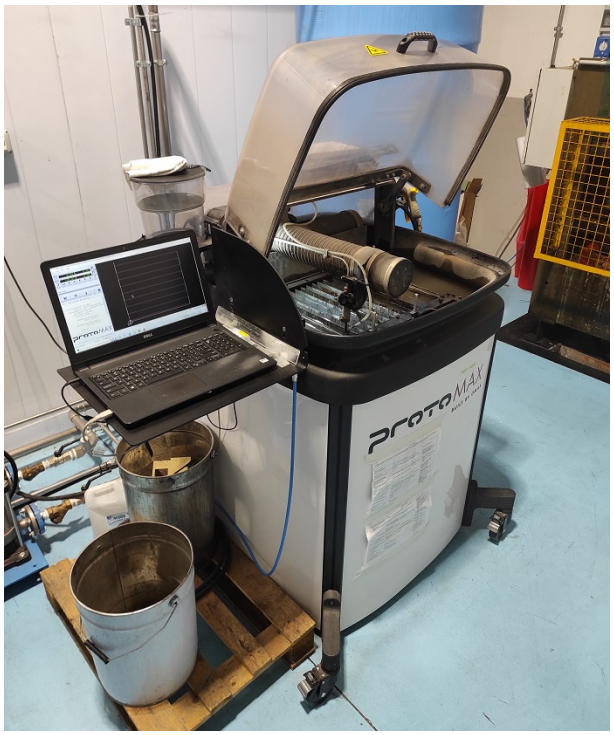

Figure 4.4: ProtoMAX abrasive waterjet cutter

It is worth noting that the T_g of the flax composite laminates was determined through the dynamic mechanical analysis (DMA) performed in the Impregnatex (Angeloni Gruop) laboratories.

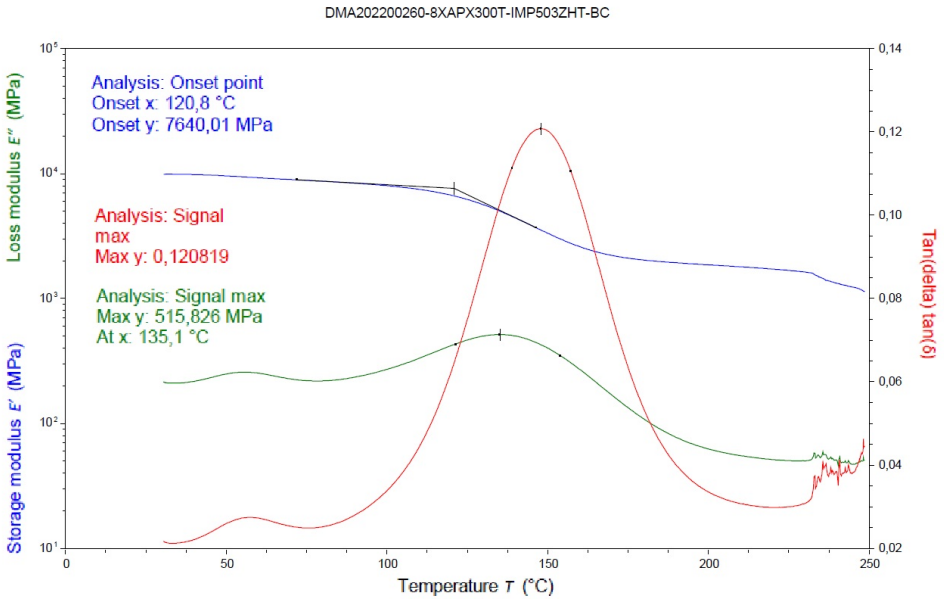

Figure 4.5: Dynamic mechanical analysis of 8-layered composite

As shown in the graph 4.5, the DMA results of the least thick laminate are reported. In detail, storage modulus (E') represents the elastic portion, loss modulus (E'') represents the viscous part and δ represents the phase lag between stress and strain and can be defined as: $\delta = \arctan(E''/E')$. From the storage modulus is possible define the T_g value that appears to be 120.8 °C. However, it must be noted that changes in the physical features are exhibited from about 75 °C, as shown by the small changes in the slope of E''. Hence, a precautionary limit heating temperature is set at 60 °C.

4.2. Static tests

Static tests are performed in a condition where all the dynamic effect are minimized, especially inertia forces. Since a small velocity component will be always present in this test typology, it is unfeasible to apply forces at a zero-velocity condition. For this reason, the tests are defined as "quasi-static". This does not represent a threat for the consistency of the results, on the condition that the loads are applied in order to be sufficiently slow to neglect the inertia forces. American Society for Testing and Materials (ASTM) standards are considered so as to define aspects such as the size specimens, testing procedures and calculus procedures. In this way, repeatability and consistency of the results can be assured, providing reliable test.

The static tests selected to conduct the material characterization are:

- ASTM D3039 Tensile test
- ASTM D6641 Compression test
- ASTM D3518 Shear test
- ASTM D790 Three-point bending test

As reported in section 2.3, these tests represent the lowest level of the building block approach. In order to achieve an all-round knowledge of natural composite materials a strict procedure must be followed so as to provide an adequate level of characterization. The latter requirement is essential to move towards the upper level: the lamina/laminate level testing phase. It is worth noting that thermo-physical features of the material can be very important to determine the behaviour of a component in different working conditions, testing activities such as moisture absorption, void volume, etc. can represent a basic step in the testing campaign.

However, this thesis work aims to characterize the mechanical features of the material and thus the testing will be limited to such activities. ASTM standards assure the statistical

validity of the tests, since at least five samples must be tested for each type of test. However, an increase number of specimens, derived from at least three different batches, can be used in order to obtain even more consistent results. Although the good outcomes, the latter methodology may increase the general costs related with the manufacturing process, as a consequence the minimum number of required specimens was employed to perform the tests of this project. Lastly, environmental conditions and sample conditions may represent a relevant source of uncertainties. In order to increase repeatability, an industrial oven was employed before each test. Samples were heated up to 60 °C for at least 2 hours so as to dry them and guarantee the least amount of moisture content. In this way specimens can be tested under the same conditions regardless of environmental conditions.

4.2.1. Testing equipment

In order to perform static tests two different machines were employed: MTS 858 Table Top System for bending test and MTS 370.10 Elastomer System for all the remaining type of tests (see figure 4.6).

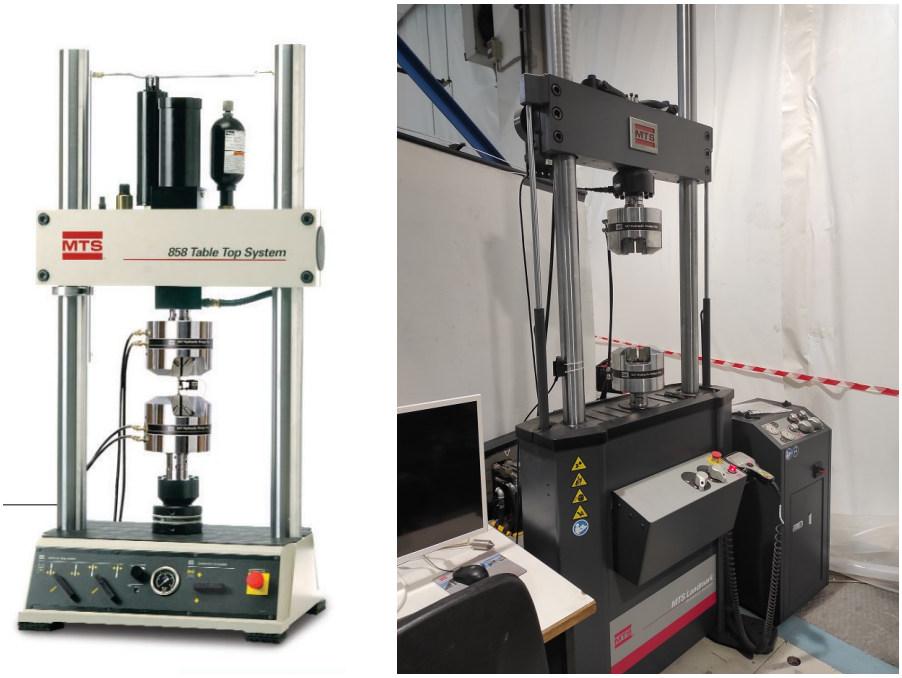

(a) MTS 858 (b) MTS 370.10

Figure 4.6: Employed material testing system

The data were collected directly from the machines, both of them are able to return

applied load and crosshead displacement. The latter does not allow for an accurate measurement of the strain value, hence some of the specimens were equipped with strain gages. In particular, two models were used: the biaxial KYOWA KFGS-3-350-D16-11 and the uniaxial KYOWA KFGS-3-350-C1-11. The former was used to perform tensile and shear tests, whereas the latter was employed for compression test. In addition, the axial extensometer MTS 634.31F-24 was used to guarantee the results consistency.

4.2.2. Tensile test D3039

This test method is designed to produce in-plane tensile properties of polymer matrix, fiber-reinforced composite materials. Thin flat specimens of material with a constant rectangular cross-section are mounted in the grips of a mechanical testing machine and axially loaded in tension until failure, as proscribed by the ASTM D3039 rule. The recorded data are used to determine the stress-strain response of the material and others fundamental information such as:

- Ultimate tensile strength
- Ultimate tensile strain
- Tensile chord modulus of elasticity
- Poisson's ratio
- Transition strain

The employed specimens and their sizes are reported in table 4.1. A digital caliper with a resolution of 0.01 mm and an accuracy of 0.03 mm were used to take all the measures. Samples were measured in three different points, then the average values were obtained for each dimension. The specimens names are reported as: "material name_fibers orientation_specimen number", for example, "APX300_0_1" identifies sample number 1, made of ampliTex 300 with 0-degrees fiber orientation. This nomenclature can be used even with woven fabric composites, ideally warp and weft directions should exhibit the same mechanical features. However, due to manufacturing process, the warp direction (0°) tends to show slightly better performance than weft direction (90°). Hence, fibers orientation must be considered during test procedure.

The test setup is presented in figure 4.7. As shown the sample is characterized by both the presence of the biaxial strain gage and the extensometer. The specimen is directly clamped in at both ends by the wedge grips. The load can be properly transferred due to the presence of coarse emery cloth, thus the presence of tabs is not required to perform

such test.

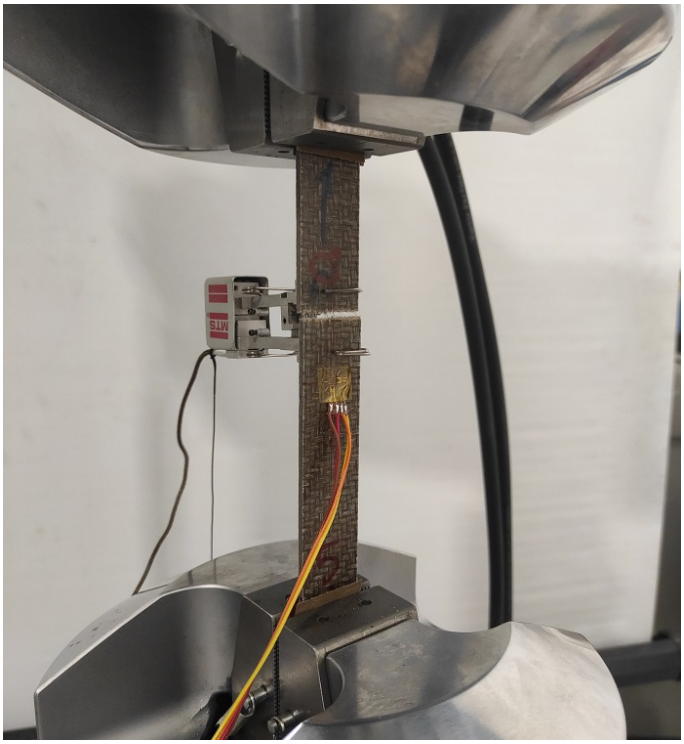

Figure 4.7: Tensile test set-up

Specimen ID	Length (mm)	Width (mm)	thickness (mm)
APX300_0_1	251.07	24.97	2.34
APX300_0_2	250.18	24.98	2.36
APX300_0_3	250.12	25.01	2.32
APX300_0_4	251.21	25.03	2.32
APX300_0_5	250.06	25.02	2.36
APX300_0_6	249.93	25.02	2.36
APX300_0_7	249.73	25.01	2.33
APX300_0_8	250.14	25.06	2.32
APX300_90_1	251.15	25.00	2.36
APX300_90_2	249.91	24.99	2.32
APX300_90_3	250.88	25.01	2.35
APX300_90_4	250.04	24.97	2.36
APX300_90_5	250.03	25.01	2.34
APX300_90_6	251.22	24.99	2.36

Table 4.1: Tensile test specimens sizes

Once the tests are completed the data are organized so as to obtain the stress-strain curve, the latter represents a fundamental outcome from which many observations and parameters can be extrapolated. The ultimate tensile strength is one of them, it can be easily achieved from the expression:

$$\sigma_{max} = F_{max}/A \tag{4.1}$$

Where σ_{max} represents the ultimate tensile strength, F_{max} the maximum applied forced recorded by the machine and A is the cross-sectional area of the specimen. The value of the strain can be performed considering three different measurements:

1. Crosshead displacement measure
2. Extensometer measure
3. Strain gage measure

The strain measure from the crosshead displacement require some manipulation to be obtained. The acquired data from the machine is in form of displacement, whereas the required result is in the form of a strain. In order to achieve such value the definition of strain can be applied:

$$\epsilon = \Delta l/l_0 \tag{4.2}$$

Where ϵ is the strain, l_0 represents the gage section length and Δl is the crosshead displacement that comes directly from the acquired data. The gage section describe the part of the specimen between the wedge grip of the machine. However, by considering this definition an important assumption is made: no slippage condition inside the grips. From the graph 4.8 it can be seen that the crosshead strain, for the same value of stress, is higher with respect to the others strain measures. From this observation, it can be deduced that the approximation of no-slip condition is not valid in most of the cases, as a consequence, this strain value may be used for qualitative evaluations. In addition, from the graph a discrepancy between the strain measures obtained from strain gage and extensometer can be seen. In particular, the extensometer strain value is overestimated, the reason is related with two aspects. Firstly, the device is not rigidly connected to the specimen and, additionally, the possible presence of human errors during the setup phase can be a source of uncertainties as well. Hence, the strain gage measure represents the most accurate value of the strain.

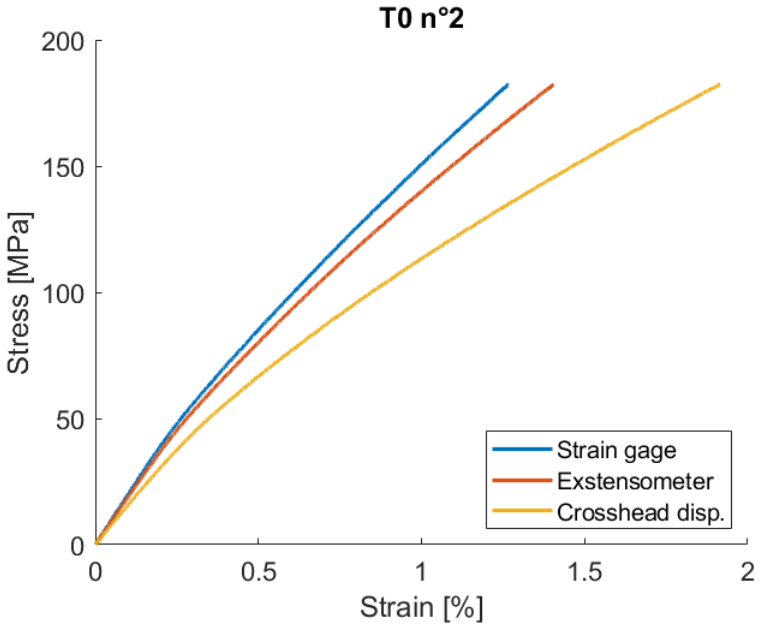

(a) Stress-strain curve APX300_0_2

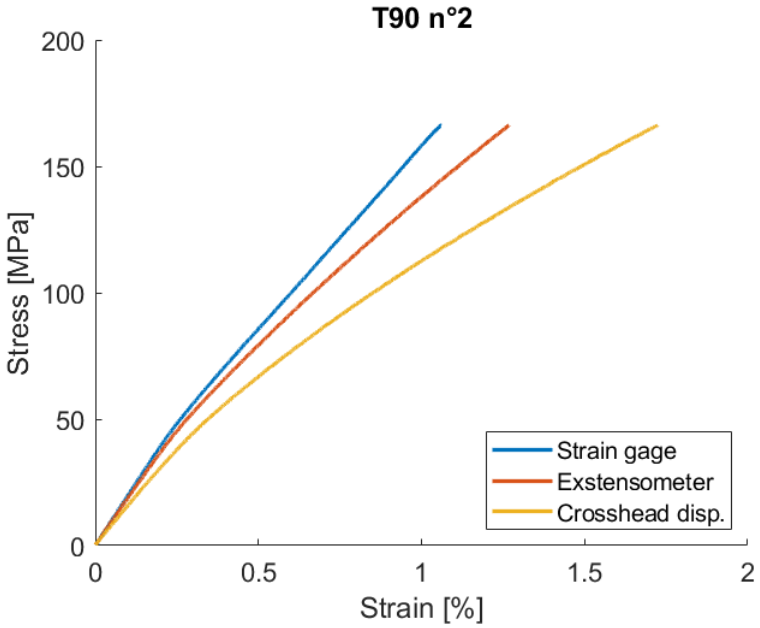

(b) Stress-strain curve APX300_90_2

Figure 4.8: Stress-strain curve comparison

The results of the tensile test are reported for both the 0° oriented samples and 90° oriented samples in the table 4.2 and figure 4.9. The tested material is a woven fabric, but it worth noting that a difference in the mechanical performances between the two fibers directions can be observed. In particular, the the 0° oriented samples show better ultimate tensile stress. The reason for such behaviour can be associated with the manufacturing process

to produce prepregs, the fibers in the warp direction are maintained straight and pulled during the process, whereas the fiber in the weft direction are bent, thus lower mechanical performance are generally achieved.

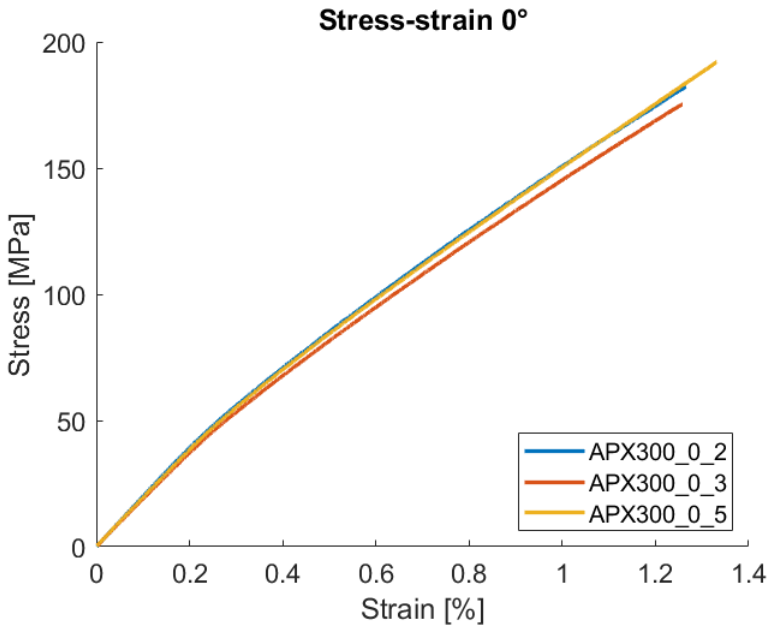

(a) Stress-strain curve APX300_0_x

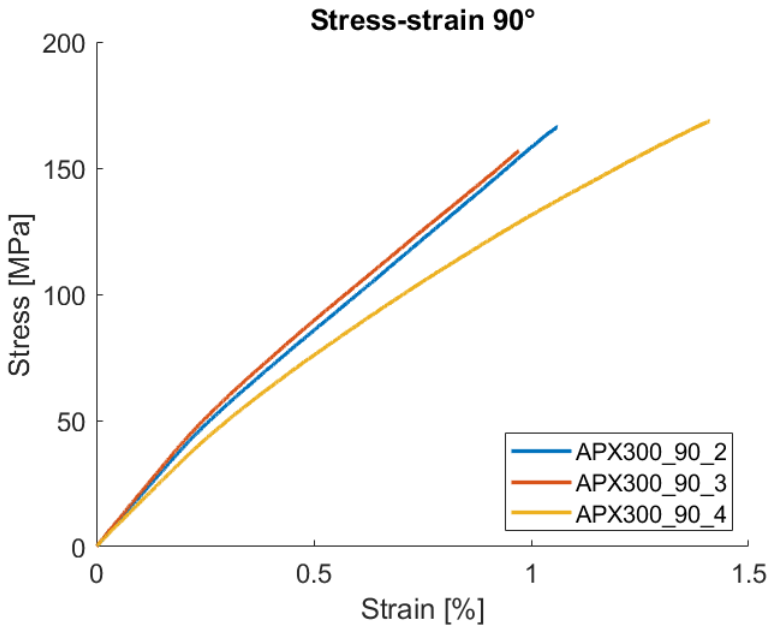

(b) Stress-strain curve APX300_90_x

Figure 4.9: Stress-strain curve for tensile test

The Poisson's ratio is calculated from the measure of the axial strain and transverse strain acquired by the strain gage sensor, the interval for the calculation is in between 1000$\mu\epsilon$

and $3000\mu\epsilon$, as prescribed by the standard. The expression use is:

$$\nu = -\epsilon_{\perp}/\epsilon_{||} \tag{4.3}$$

As expected for fabric composites, the results obtained for both fibers orientations are similar, but it must be highlighted that the result for 0° oriented samples has a high variance value. In order to verify the outcome, the relationship $\frac{\nu_{12}}{E_{11}} = \frac{\nu_{21}}{E_{22}}$ can be used, thus the calculated Poisson's coefficient ν_{12C} results equal to 0.15. This consideration confirms the less accuracy of the ν_{12} experimental outcome, which should be closer to calculated coefficient. So as to justify such high variance value, the sample APX300_0_5 should be considered due to its low Poisson's ratio equal to 0.08. In fact, if the latter sample is not assessed a drop in standard deviation larger than 12% is show and a Poisson's ratio closer to 0.15 value is reached. The elastic modulus outcomes show consistent data with low value of variance. In this case the formula to obtain this parameter is:

$$E = \Delta\sigma/\Delta\epsilon \tag{4.4}$$

As with the Poisson's ratio, the interval for the calculation is provided by the standard and is always in between $1000\mu\epsilon$ and $3000\mu\epsilon$.

	Avarage value	**Std. Dev.**	**Coeff. of variation (%)**
APX300_0			
σ_{1_max} (MPa)	181.39	5.84	3.22
E_1 (GPa)	17.73	0.46	2.62
ϵ_{1_max} (%)	1.28	0.04	3.14
ν_{12}	0.13	0.06	45.62
$\epsilon_{1\_trasition}$ (%)	0.35	0.004	1.01
APX300_90			
σ_{2_max} (MPa)	161.69	7.30	4.52
E_2 (GPa)	17.87	1.45	8.11
ϵ_{2_max} (%)	1.15	0.23	20.23
ν_{21}	0.15	0.01	7.57
$\epsilon_{2\_trasition}$ (%)	0.31	0.08	26.25

Table 4.2: Tensile mechanical properties

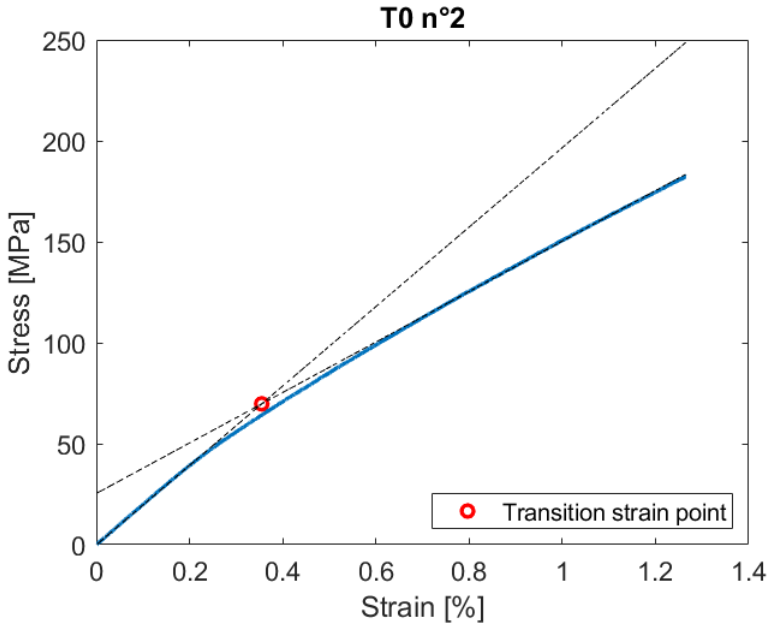

(a) Transition strain point for APX300_0_2

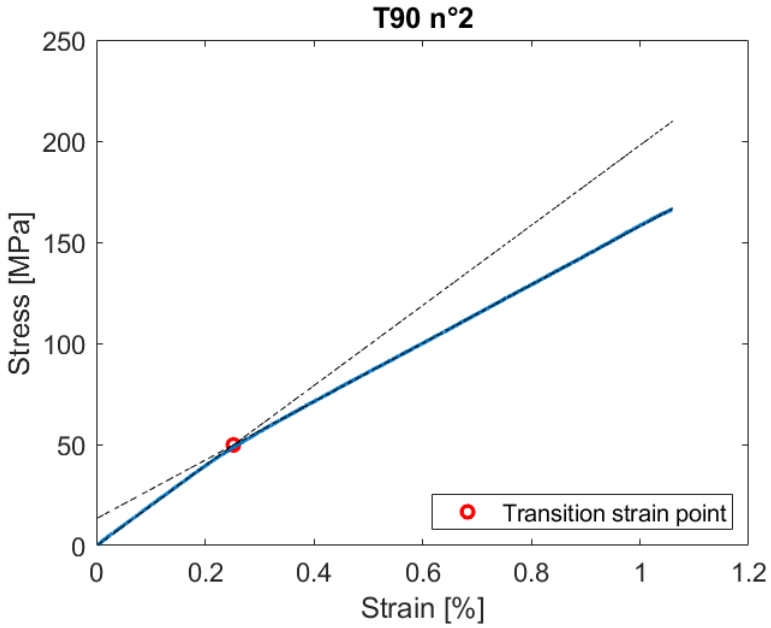

(b) Transition strain point for APX300_90_2

Figure 4.10: Transition strain points

So as to determine the transition strain point two linear stress functions were generated starting from the longitudinal stress function. As show in the figure 4.10, the linear functions are tangent to the two ends of the longitudinal stress function. In order to determine the left end linear function a strain range between $100\mu\epsilon$ and $2000\mu\epsilon$ was taken, the starting point was selected other than zero so as to obtain a more consistent

result. The right end linear function was generated considering an interval in between $8000\mu\epsilon$ and $11000\mu\epsilon$, if the fail occurs before $11000\mu\epsilon$, the ultimate strain value is selected as maximum limit of the range.

Eventually, failure mode examination is the last step to obtain a whole evaluation of the experimental test. So as to validate the test an understanding of location and type of failure must be performed. In this case, the APX300_0_x samples shown homogeneous results and the failures always occurred within the gage section. On the other side, the samples with weft oriented fibers did not always exhibit compliant failure. For example, althogh the specimen APX300_90_2 shows results consistent with the others, the failure occurs inside the wedge grip. In addition, sample APX300_90_5 shows lower mechanical performances, presumably due to the presence of flaws inside the material. Further details of failures are shown in appendix A.

4.2.3. Shear test D3518

The in-plane shear response of polymer matrix composite materials is ruled by ASTM D3518 standard. The set-up procedure is similar to test method D3039 applied for tensile tests, the differences are both in samples stacking sequence and sizes. In detail, a $\pm 45^{\circ}$ balanced and symmetric laminate, characterized by greater thickness, is employed to investigate mechanical response. During the evaluation of the final results must be taken into consideration the free-edge effect. As mentioned in 2.1.6, the in-plane normal stress component, combined with the $\pm 45^{\circ}$ oriented plies layout, lead to a complex stress field near the free-edges. In particular, a three-dimensional stress field is achieved and CLT cannot be employed to predict such behaviour, since out-of-plane component is not considered. Considering the complexity in investigating such test outcomes, through the years many procedures were developed. The first version of the shear test method was presented by Petit [26], then Rosen [30] improved it obtaining the current test methodology.

Specimen ID	Length (mm)	Width (mm)	thickness (mm)
APX300_45_1	249.96	25.03	3.12
APX300_45_2	249.59	25.02	3.15
APX300_45_3	250.03	25.02	3.17
APX300_45_4	250.97	25.03	3.17
APX300_45_5	250.03	25.07	3.17
APX300_45_6	249.66	25.01	3.17

Table 4.3: Shear test specimens sizes

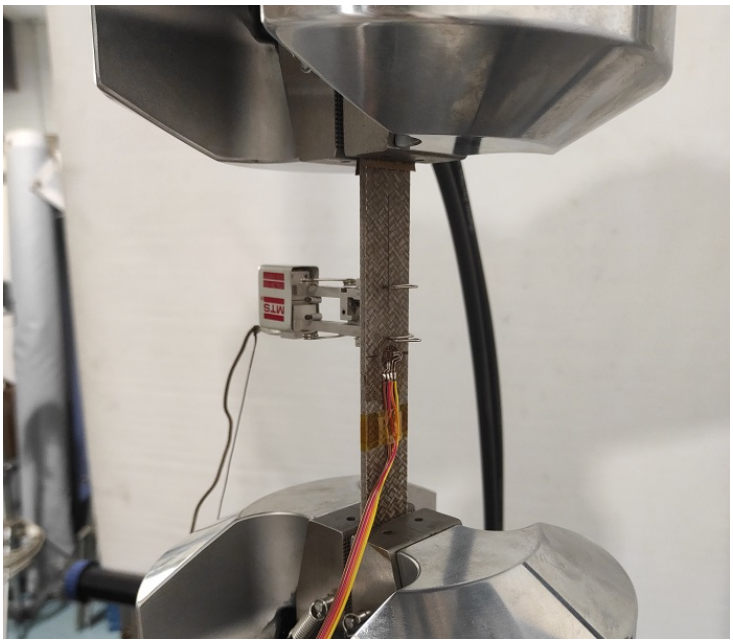

Figure 4.11: Shear test set-up

From the in-plane shear stress versus shear strain chart, information such as shear modulus, maximum shear stress and maximum shear strain can be achieved. In order to draw such graph, in-plane shear stress can be defined as $\tau_{12} = F_x/2A$, where F is the applied force and A is the section area. While, the shear strain can be described as $\gamma_{12} = \epsilon_x - \epsilon_y$, where ϵ_x and ϵ_y are respectively the longitudinal and transverse strains measured by the biaxial strain gage sensor applied on the specimen. It must be noted that the subscripts 1,2 represent the lamina directions, whereas x,y are referred to laminate directions.

In order to calculate the shear modulus of elasticity the following equation can be used:

$$G_{12} = \frac{\sigma_x}{2(\epsilon_x - \epsilon_y)} \tag{4.5}$$

With σ_x is the longitudinal stress term calculated as the ratio of applied force to the cross-section of the sample. The shear strain range of 2000 to 6000 $\mu\epsilon$ is selected to perform the calculus. This interval is obtained considering the normal strain range used for tensile test D3039, if $\pm 45°$ sample is employed a Poisson's ratio near to 1 can be assumed, thus the selected range for shear test corresponds approximately to the normal strain range of 1000 to 3000 $\mu\epsilon$ used for tensile test. The ultimate in-plane shear stress is achieved considering the maximum load at or below 5% shear strain. If a maximum stress value is recorded with a corresponding strain value greater than 5%, the maximum shear stress is taken at 5% of the shear strain. The specimen APX300_45_3 shown this behaviour and

its maximum stress value was discarded because at 5.5% of shear strain. So as to obtain the ultimate shear strain, the value at the corresponding ultimate shear stress, within 5% of shear deformation, was considered. The outcomes are presented in table 4.4.

	Avarage value	**Std. Dev.**	**Coeff. of variation (%)**
APX300_45			
τ_{12_max} (MPa)	46.21	0.46	0.99
γ_{12_max} (%)	4.71	0.25	5.29
G_{12} (GPa)	1.96	0.06	2.89

Table 4.4: Shear mechanical properties

It is worth noting that the upper limit of the engineering shear strain defined at 5% is not accidental. The above mentioned issues, in addition with large deformation effect (fibers rotation or scissoring) and the total thickness effect can alter the measurements, hence producing non-compliant results. Eventually, though failures occur always within the gage section, the specimen APX300_45_3 shown lower mechanical performances. Such behaviour can be explained considering the presence of defects and voids inside the material or due to an incorrect application of the strain gage sensor.

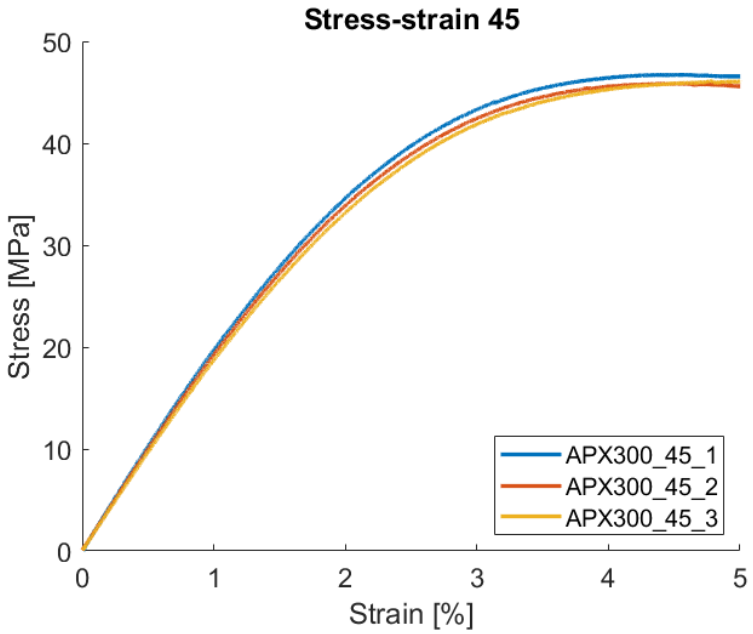

Figure 4.12: Stress-strain curve for shear test

4.2.4. Bending test D790

Out-of-plane properties can be defined through bending test method in according with ASTM D790 standard. The test is performed through a 3-point-bending machine, in detail the setup is presented in figure 4.13. The specimen is simply supported by two steel cylinders with a diameter of 15 mm and is loaded by means of a third cylindrical loading nose midway between the supports.

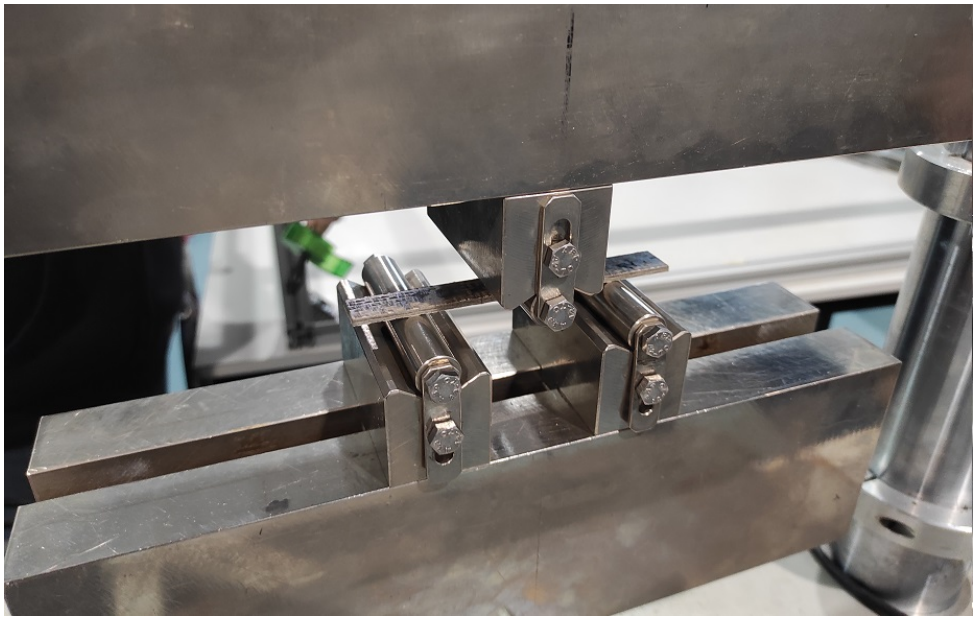

Figure 4.13: Bending test set-up

Specimen ID	Length (mm)	Width (mm)	thickness (mm)
APX300_0_1	120.02	14.93	2.33
APX300_0_2	120.02	14.95	2.28
APX300_0_3	119.92	15.34	2.34
APX300_0_4	119.16	14.97	2.30
APX300_0_5	119.13	14.97	2.34
APX300_0_6	119.17	14.96	2.32
APX300_0_7	119.95	14.93	2.31
APX300_0_8	119.15	14.98	2.34

Table 4.5: Bending test specimens sizes

In order to guarantee a failure in the outer surface of the specimen, a support span-to-depth ratio of 32:1 was chosen to perform the test. In detail, the average thickness of the

specimens is 2.35 mm, thus the obtained span value is 75 mm. The first flexural feature that can be achieved is the flexural stress, below the general equation is reported:

$$\sigma_f = (3FL/2bt^2)[1 + 6(D/L)^2 - 4(t/L)(D/L)] \tag{4.6}$$

Where:

- F is the applied force
- L is the span distance
- b is the specimen width
- t is the specimen thickness
- D is the loading nose vertical displacement

The equation 4.6 was employed due to the high span-to-depth ratio selected. Significant end forces are developed at the supports when relatively large deflection occurs, this can affect the moment in a simple supported beam. In the latter equation these terms are considered through correction factors. Due to the orthotropic nature of flax composite fabric, shear deflection may seriously reduce the apparent modulus of elasticity, hence tangent modulus was considered. The following formula was considered:

$$E_B = L^3 m/4bd^3 \tag{4.7}$$

The parameter m represents the slope of the tangent to the initial portion of the load-deflection curve. As in tensile test, a range in between $1000\mu\epsilon$ and $3000\mu\epsilon$ was defined to perform the calculus. In table 4.6 the most relevant results are reported.

	Avarage value	**Std. Dev.**	**Coeff. of variation (%)**
APX300_0			
σ_{f_max} (MPa)	199.80	12.40	6.21
ϵ_{f_max} (%)	1.86	0.12	6.58
E_B (GPa)	15.95	0.44	2.74

Table 4.6: Flexural mechanical properties

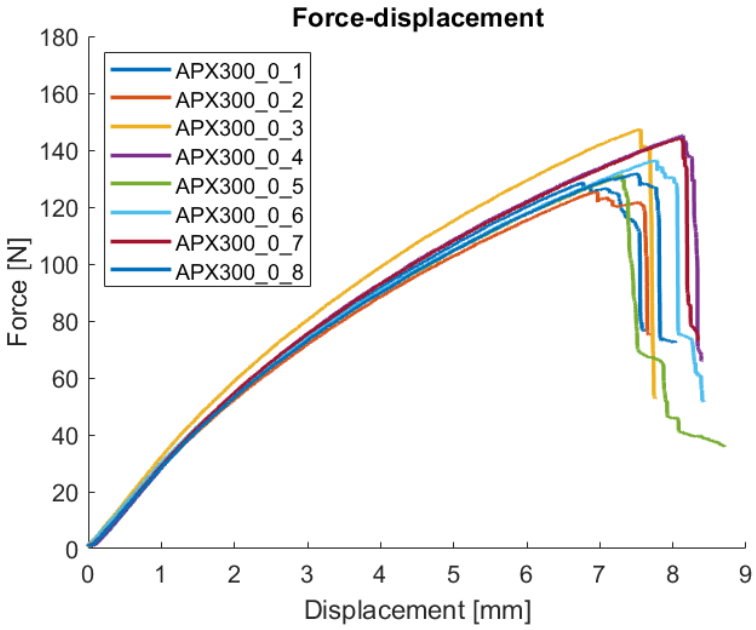

Figure 4.14: Force-displacement curve for bending test

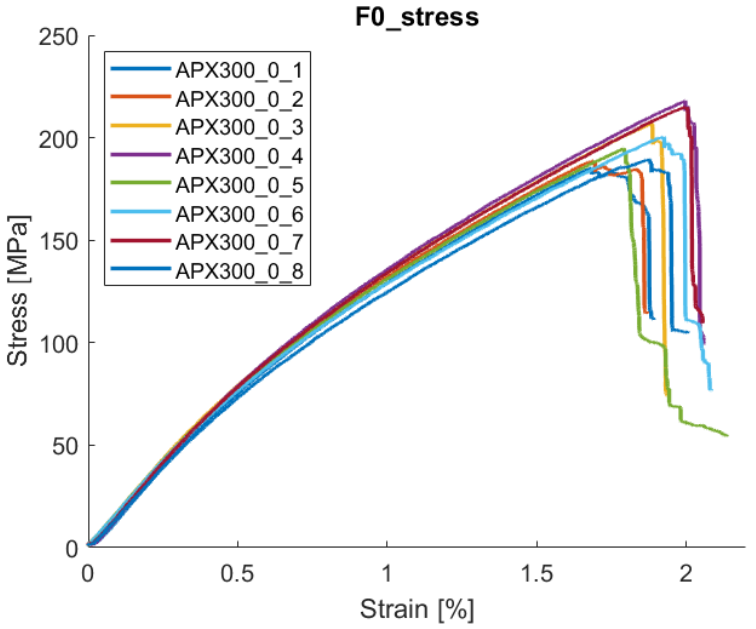

Figure 4.15: Stress-strain curve for bending test

It is worth noting that the specimen was able to carry a portion of the load even after reaching the maximum stress peak, thanks to the undamaged plies in the laminate. Eventually, a step descending trend can be observed in figure 4.15. Lastly, all the tested samples were able to fail in compliance with the standard. As a verification a low value of variance can be noted from the results.

4.2.5. Compression test D6641

This test method determines the in-plane compressive properties of natural composite materials by means of a combined loading compression test fixture. The used ASTM D6641 standard applies the compressive load on the specimen through a combination of shear and axial forces. In this way instability is prevented, with respect to test method D3410 where a pure shear-loading is used. The most relevant compressive features of the material are ultimate compressive strength and compressive modulus of elasticity. The test method setup is similar to tensile test method, but with a loading acting in compression. The specimen geometry reported in table 4.7 are in compliance with the standard, but a larger value of thickness could have been employed so as to minimize instability phenomena (or Euler column buckling) during the test. However, the latter phenomena was taken into consideration during the selection of a suitable gage section value. Thanks to this, the provided samples were able to give consistent results while avoiding the instability phenomena.

Specimen ID	Length (mm)	Width (mm)	thickness (mm)
APX300_0_1	140.01	16.09	2.34
APX300_0_2	139.75	16.09	2.31
APX300_0_3	139.88	16.07	2.31
APX300_0_4	139.76	16.06	2.31
APX300_0_5	139.99	16.10	2.36
APX300_0_6	140.00	16.10	2.36
APX300_0_7	139.95	16.04	2.34
APX300_90_1	140.06	16.06	2.36
APX300_90_2	140.06	16.07	2.36
APX300_90_3	140.08	16.07	2.34
APX300_90_4	140.05	16.12	2.35
APX300_90_5	140.00	16.07	2.33
APX300_90_6	140.02	16.08	2.29
APX300_90_7	140.06	16.10	2.35
APX300_90_8	140.02	16.10	2.34

Table 4.7: Compression test specimens sizes

In table 4.8 the outcomes are presented. In particular, the compressive modulus of elasticity was obtained through the equation 4.4, used for tensile, and a range in between 1000 $\mu\epsilon$ and 3000 $\mu\epsilon$ were used. In order to evaluate the strain value and guarantee the control of the induced bending, two axial strain gages were employed on both the surfaces of the specimen. In detail, the following percent bending equation were used:

$$B_y = \frac{\epsilon_1 - \epsilon_2}{\epsilon_1 + \epsilon_2} \times 100 \tag{4.8}$$

This parameter can be affected by imperfections in test specimen, test fixture, or even testing procedure. During the evaluation of the modulus, values no greater than 5% were reached, this result allows the test to be considered valid, as the maximum admissible value is 10%. Eventually, the evaluation of the strain consists in an average between the measurements given by the two sensors applied on both sides. By means of equation 4.1 the ultimate compressive stress value can be evaluated, comparable results were achieved both for 0° and 90° oriented samples.

(a) Front view of compressive sample (b) Side view of compressive sample

Figure 4.16: Strain gages layout of compressive specimen

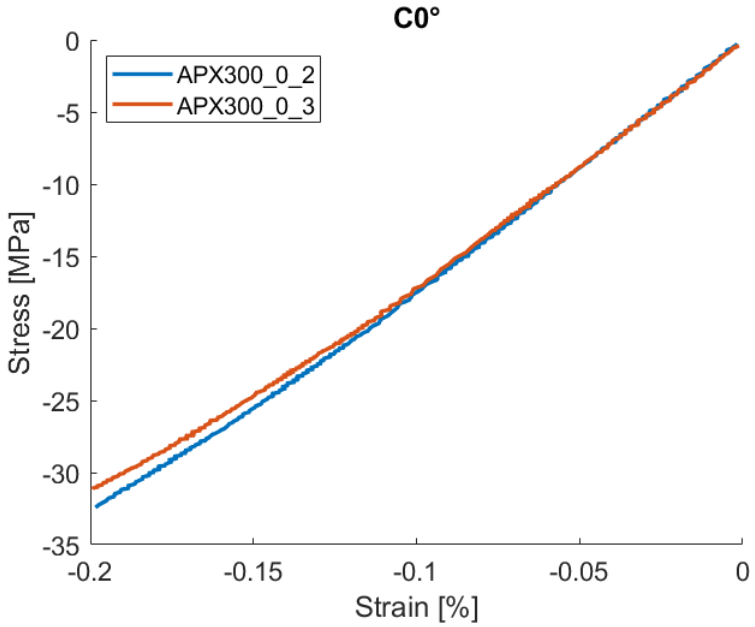

(a) Elastic modulus APX300_0_x

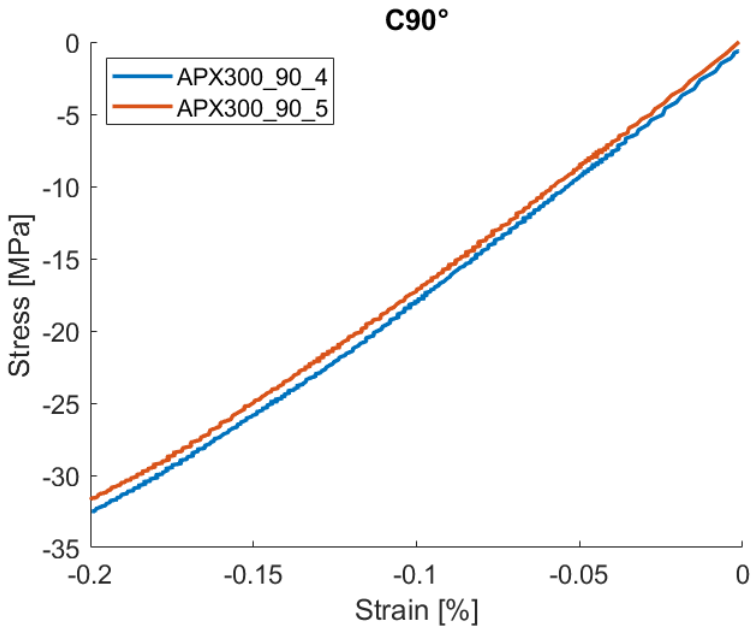

(b) Elastic modulus APX300_90_x

Figure 4.17: Graphical representation of elastic compressive modulus

This test method is very sensitive to specimen geometry, manufacturing defects, fiber orientation and improper alignment. From failure mode analysis it is possible to understand if some of these aspects have altered the in-plane compressive features. From appendix A, the samples show through-thickness failures limited to gage section , which means that compliant test have been performed. Lastly, it is worth noting that no explosive failure

were observed, which is an essential aspect in the context of crashworthiness applications.

	Avarage value	Std. Dev.	Coeff. of variation (%)
APX300_0			
σ_{1_max} (MPa)	141.57	5.10	3.61
E_1 (GPa)	15.04	0.69	4.60
APX300_90			
σ_{2_max} (MPa)	141.53	0.85	1.00
E_2 (GPa)	15.02	0.10	0.69

Table 4.8: Compressive mechanical properties

4.3. Dynamic tests

During design procedures the mechanical performance obtained from static tests are assessed in order to properly sizing structural components for the harshest loading conditions. However, during design phase dynamic properties may be important as well. Aspects such as weight reduction can be optimized and crash phenomena (e.g. bird strike) can be properly evaluated during this stage so as to minimize structural failure. In order to evaluate the dynamic response of flax composite material three tests were performed:

- Strain rate sensitivity test
- ASTM D7136 Indentation test
- High-velocity impact test

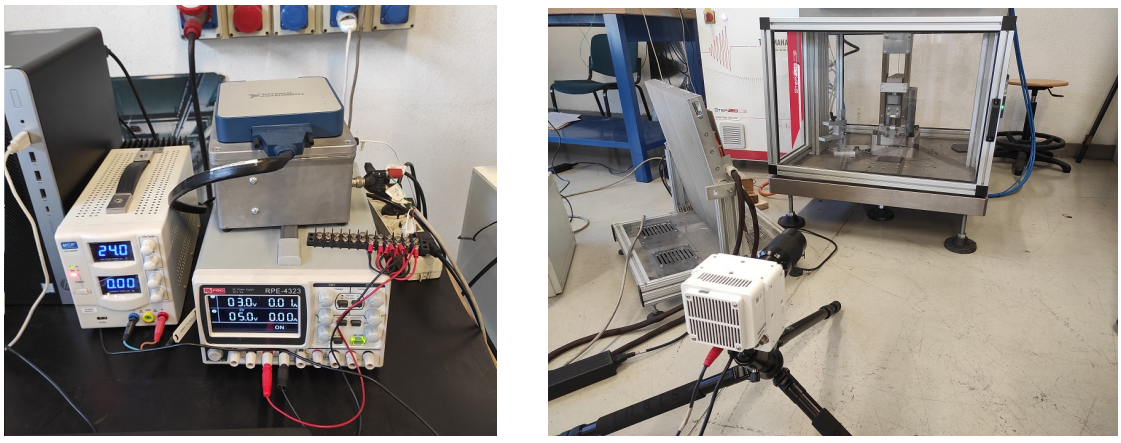

(a) Data acquisition system (b) High-speed camera layout

Figure 4.18: Data acquisition devices

In order to measure strain rate, the standard ISO 8256:2004 recommendations were considered, but not fully implemented. In particular, the specimens geometry was modified so as to maximize the number of tests and analyse the response with different cross sections. This choice has allowed to maintain low manufacturing costs, while ensuring the consistency of the test. Low-velocity impact test was conducted, in according to the ASTM D7136 standard, so as to verify the impact resistance of flax laminates. For the same reason high-velocity impact test were performed as well, in this case no standard were applied. Eventually, the failure modes and behaviour of natural composites was investigated.

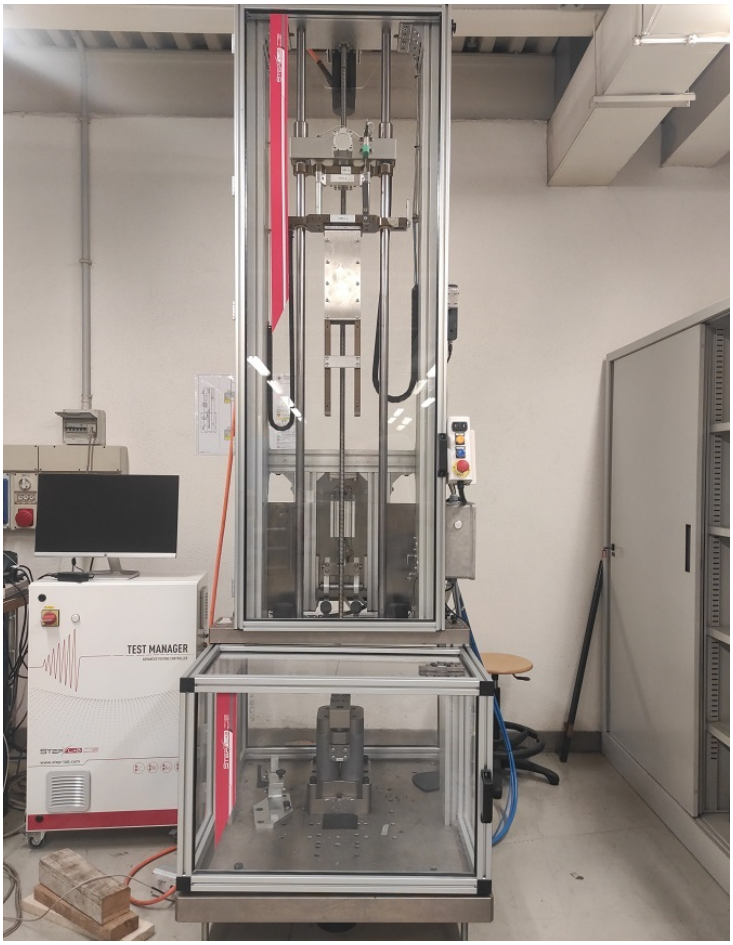

Figure 4.19: Step Lab DW1000 system

Both the indentation and strain rate tests were performed exploiting the Step Lab DW1000 drop weight tower functionalities (see figure 4.19). Information such as impact load, velocity and energy were provided directly from the machine. All the data are acquired with a sampling frequency of 3MHz and then a filter of 50 kHz is applied. Additionally, some specimens of the strain rate test were equipped with uniaxial strain gages, in order to

accurately compare stress-strain dynamic behaviour with static results. So as to perform the ballistic test the gas gun reported in figure 4.20 was employed. Lastly, high-speed Phantom VEO-E 310L cameras were used, for both strain rate and ballistic tests, in order to measure the input and output velocities, capture the details during the failure stages and validate the tests.

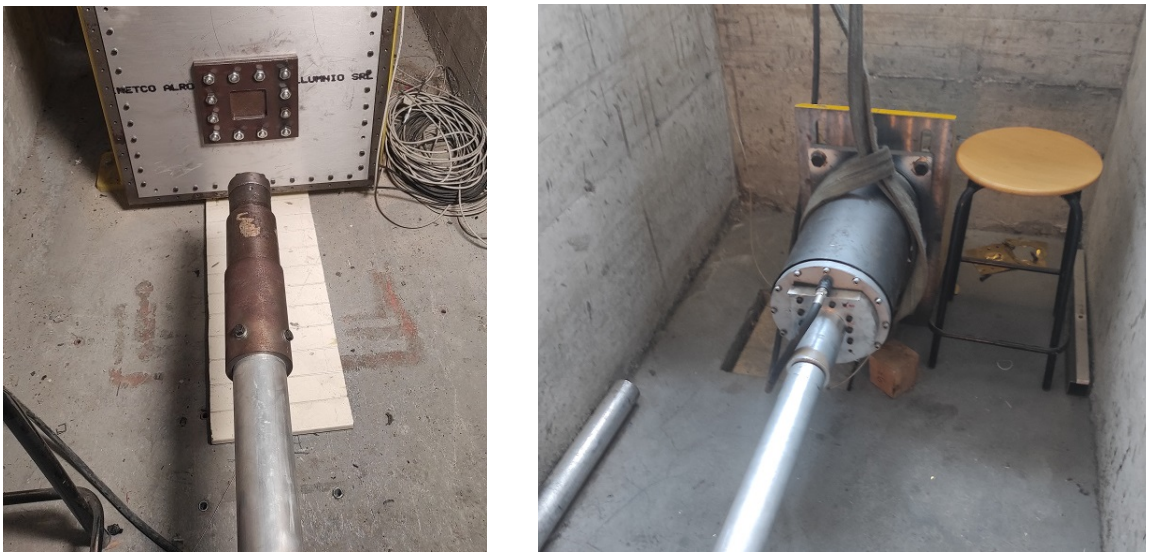

(a) Barrel tip with sabot stopper (b) Barrel base attached to pressure vessel

Figure 4.20: Gas gun set-up

4.3.1. Strain rate sensitivity test

This test aims to investigate strain rate dependency of flax fiber composite material. In order to execute the test the specimen is clamped in the lower grip, which is free to move, then the upper part is clamped to the machine-integrated grips. It is important to highlight that specimens are devoid of tabs, however, to guarantee a correct distribution of the load over the clamped area, both emery cloth and aluminium plates were applied between the sample and the grip, as shown in figure 4.22. So as to provide the tensile dynamic load a weight of 12.85Kg is applied on a sled, the latter is released from a certain height in order to impact the lower end of the specimen. The maximum impact velocity depends on the maximum height reachable by the machinery, while the maximum energy is bounded with the used weight. Although these limits, both suitable value of energy and velocity have been obtained during the test. In fact, due to the relatively small cross-sectional area the failure of the samples have always been guaranteed.

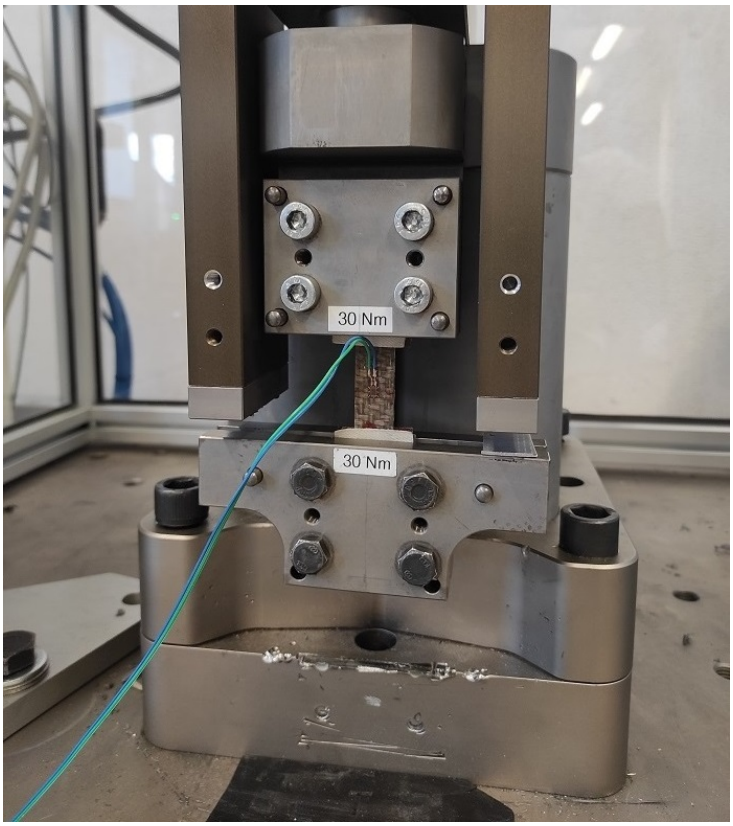

Figure 4.21: Strain rate test set-up

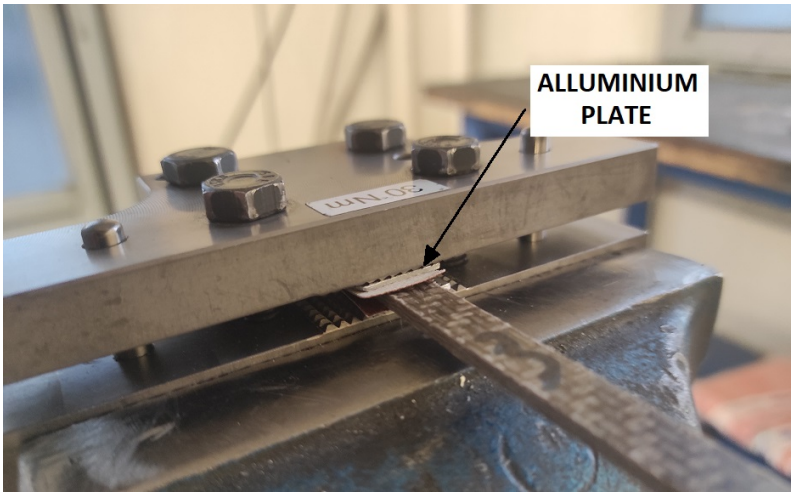

Figure 4.22: Lower grip set-up

The geometry of the employed samples is reported in table 4.9, the specimens are fabricated using woven fabric prepreg with 0° oriented fibers (warp direction), in order to inspect the greatest mechanical performances.

Strain rate is defined as the variation of strain over the time, it represents the sensitivity of material characteristics with respect to the deformation velocity. In general, the materials tends to exhibit an increase of mechanical properties such as ultimate stress, ultimate strain and Young's modulus. This aspect can be taken into consideration during design phase so as to optimize the mass distribution. In order to obtain strain rate values the following equation was used:

$$\dot{\epsilon} = \frac{d\epsilon}{dt} = \frac{1}{L_0}\frac{dL}{dt} = \frac{v}{L_0} \tag{4.9}$$

Where v is the impact velocity of the sled and L_0 is the gage section of the specimen. By means of these parameters a wide strain rate range can be considered to perform the tests. This dynamic evaluation aims to verify whether the flax composite material shows an increasing of mechanical performances with an increasing of strain rate.

Specimen ID	**Length (mm)**	**Width (mm)**	**thickness (mm)**
APX300_0_1	164.93	9.41	2.35
APX300_0_2	164.94	9.41	2.37
APX300_0_3	164.92	9.40	2.37
APX300_0_4	165.00	9.39	2.33
APX300_0_5	164.89	9.38	2.33
APX300_0_6	164.77	9.39	2.33
APX300_0_7	165.15	9.38	2.34
APX300_0_8	165.05	9.39	2.35
APX300_0_9	164.88	9.43	2.37
APX300_0_1_SG	165.04	15.13	2.37
APX300_0_2_SG	165.00	15.16	2.36
APX300_0_3_SG	165.05	15.10	2.35
APX300_0_4_SG	165.03	15.11	2.33
APX300_0_5_SG	165.07	15.14	2.34
APX300_0_6_SG	165.05	15.12	2.33

Table 4.9: Strain rate sensitivity test specimens sizes

At first, the specimens were tested with a gage section of 40 mm, and the drop height was continuously modified so as to obtain different strain rate values. From the graph 4.23 the relationship between stress and strain rate is reported. In particular, the material exhibits an increasing of more than 22% in stress value for higher strain rate, and a positive trend is depicted as well. The latter represents a significant aspect, since it is possible to assume

that similar behaviour may be exhibited for even higher strain rate values.

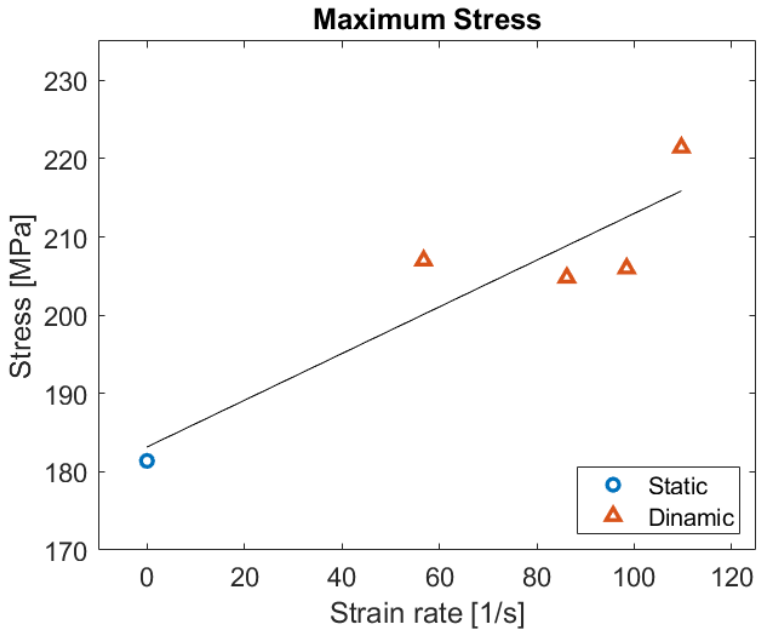

Figure 4.23: Strain rate effect on ultimate stress

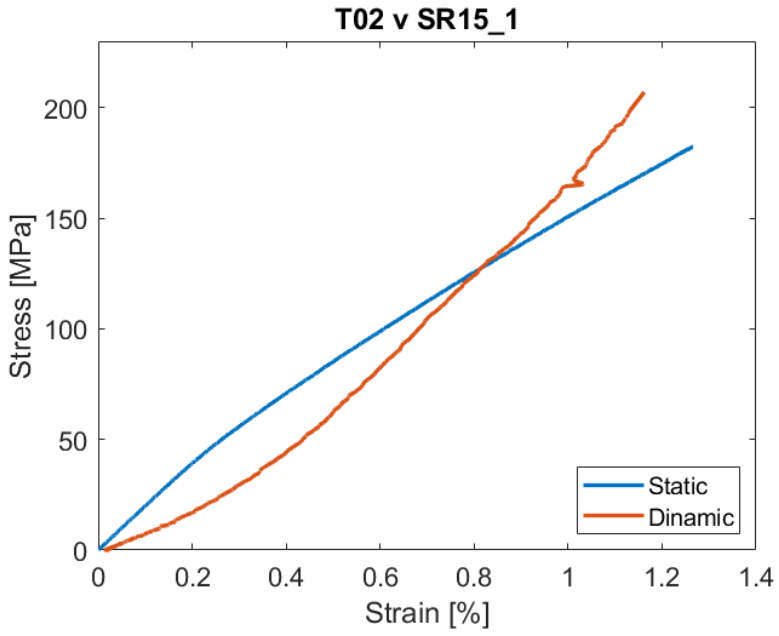

Figure 4.24: Comparison between static and dynamic tensile response

Modulus of elasticity is another important parameter to verify the strain rate sensitivity of the material. In the figure 4.24 the stress-strain relationship is reported, this result was obtained by exploiting the strain gage sensor installed on some samples. A comparison

between static result and dynamic is made, in the first half of the graph less steep trend is shown by the dynamic outcome, on the contrary in the second half the increase of elastic modulus it is obvious. In detail, The maximum value of the modulus is 21.77 GPa, which represents an increase of 23% with respect to the static result. The poor results obtained in the first half can be attributed to slippage phenomena at grips level.

An analysis about the specific absorbed energy (SEA) can be conducted as well. This parameter can be obtained either as the integral of the force with respect to the displacement or as the difference between the kinetic energy before and after impact. The results reported in graph 4.25 show an increasing of the energy parameter with higher strain rate. In detail, the best result achieved value twice as high as in the static case and a positive trend was identified as well. Although acceptable results were achieved, the use of tabs may lead to better outcomes with more accurate behaviour.

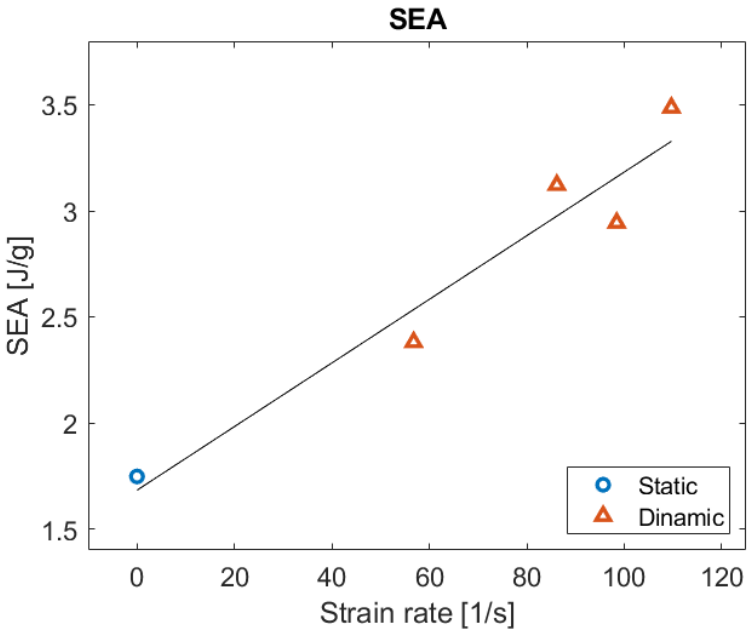

Figure 4.25: Strain rate effect on tensile SEA

Overall, the analysed parameters have exhibited sensitivity to strain rate variation. Lastly, it is worth noting that the increasing in the mechanical performances is comparable both for the ultimate stress and Young's modulus parameters, while for specific absorbed energy the best improvement was found. This proves the consistency of the achieved results.

4.3.2. Indentation test D7136

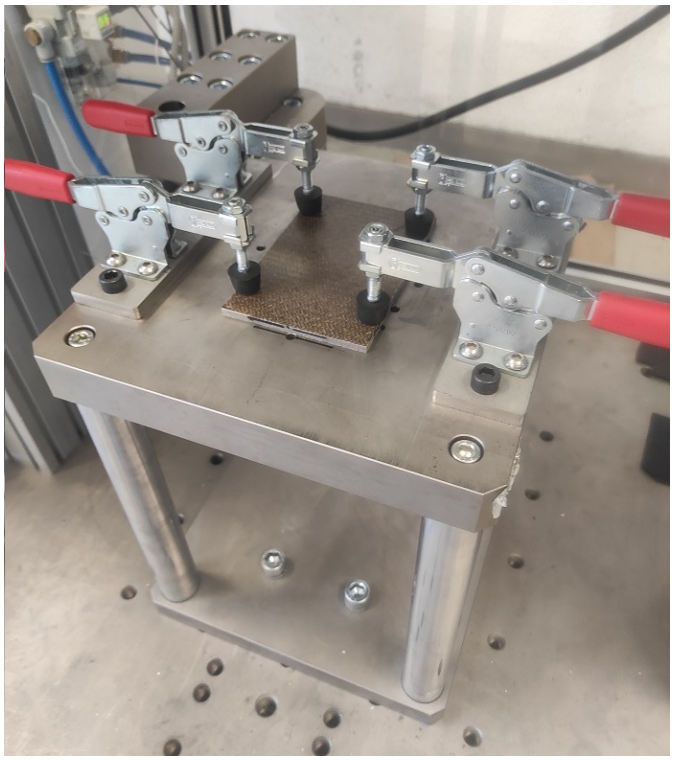

Figure 4.26: Indentation test setup

Damage resistance of multi-directional natural composite materials is investigated through the application of ASTM D7136 standard. In order to perform such test a drop tower is employed with the use of a suitable impact support fixture installed on a rigid base (see figure 4.26). Toggle clamps with rubber tips are employed to ensure a proper fixation while avoiding damage to the plate. The test execution is very similar to the strain rate sensitivity test, but in this case tree different hemispherical striker tips are used as impactors, so as to ensure low-velocity indentation damage. The weight applied on the drop tower sled can be seen as the sum of two different parts: a fixed weight of 10.260 Kg and the weight associated with the selected tip. In detail, in table 4.10 the characteristics of the hemispherical tips are reported:

Tip ID	Diameter (mm)	Mass (g)	Impactor mass (Kg)
D127	12.7	171.0	10.4305
D16	16.0	242.0	10.5015
D20	20.0	227.6	10.4870

Table 4.10: Hemispherical striker tips characteristics

Thus, depending on the utilized tip, the proper value of total weight must be considered to provide the desired amount of impact energy.

Figure 4.27: D20 hemispherical striker tip

Specimen ID	Length (mm)	Width (mm)	thickness (mm)
APX300_mix_3	150.31	100.43	4.96
APX300_mix_4	150.34	100.86	4.94
APX300_mix_5	150.35	100.79	4.95
APX300_mix_7	150.42	99.82	4.93
APX300_mix_14	150.28	100.55	4.93
APX300_mix_15	150.34	100.32	4.96
APX300_mix_16	150.40	100.46	4.97
APX300_mix_17	150.40	100.42	4.96
APX300_mix_18	150.19	100.54	4.96
APX300_mix_19	150.22	100.36	4.96
APX300_mix_20	149.35	100.33	4.96
APX300_mix_21	151.30	100.19	4.93

Table 4.11: Indentation test specimens sizes

In table 4.11 the specimens geometry are reported in compliance with the D7136 standards. A thickness value in between 4mm and 6mm is required to guarantee proper failure mode. To ensure this requirement the specimens are composed by 12 plies with a stacking sequence of $[(+45/-45)/(0/90)]_{3S}$, as a consequence a thickness value close to 5mm can be achieved.

The damage resistance properties generated by this test method are highly dependent upon several factors such as impactor geometry, impactor mass and impact energy. For this reasons, for each impactor tip at least three value of impact energy are evaluated. In table 4.12 the parameters of each test are presented.

Specimen ID	**Peak force (N)**	**Impact velocity (m/s)**	**Deflection (mm)**	**Absorbed energy (J)**
D127				
19	2654.27	1.39	5.35	9.98
21	3081.99	1.73	7.23	15.52
15	2957.65	2.27	15.18	23.62
D16				
20	-	1.10	-	-
3	2723.22	1.32	4.89	9.11
17	-	1.91	-	-
14	2937.74	2.25	12.16	22.00
18	2825.29	2.46	17.80	28.42
D20				
4	2731.78	1.43	5.41	10.63
7	2976.23	1.80	7.32	16.98
16	3322.66	2.27	10.71	26.47
5	3370.28	2.65	14.94	34.90

Table 4.12: Parameters and results of indentation test

Both force value and the initial impact velocity are directly collected from the machine. In particular, these are used to calculate the other parameters such as velocity trend, energy evolution and displacement. The latter cannot be assumed as an accurate value, since obtained from the integral of velocity over time, which could be affected by some errors. However, it is worth considering this outcome to perform relative evaluation among the tested samples and verify the consistency of the results. Although a wide range of impact velocity is used, the variation of peak force between the higher value and the lower one is

within 15%. On the other side, the increasing in terms of absorbed energy is more than 60% for D20 tests, which is in accordance with the increasing of the impact velocity, as reasonably expected.

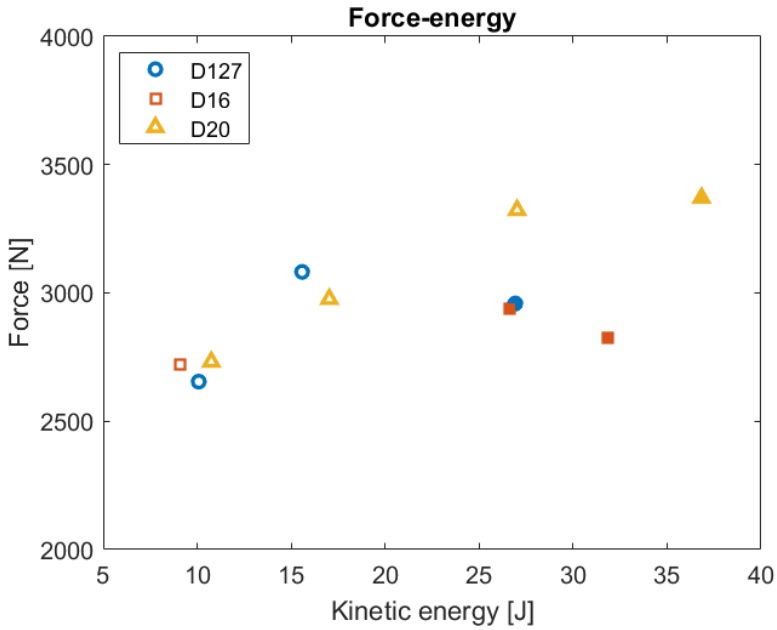

Figure 4.28: Peak force in relation to kinetic energy (filled elements represent complete failures)

The graphs 4.31, 4.30 and 4.29 show the force vs displacement curves relative to the three types of indentation tests conducted. In general, all the graphs exhibit a linear behaviour in the first part of the curve, then a limit value is reached due to the occurrence of delamination phenomena. Successively, a constant or quasi-constant region is shown: here most of the impact energy is absorbed and other failure modes start to propagate. It is worth noting that the average values for the applied force are in between 2300 N and 3500 N for all the outcomes. In particular, the best results are exhibited by the tests performed with D20 tip and the worst by the tests performed with D16 tip. In the last part of the graphs two different behaviour are shown: a linear decreasing trend and a step negative evolution. In the first case the specimen is not completely broken and the panel does not present any breach. On the contrary, in the latter case the complete failure of the panel leads to one or more steps, these represent the complete failure of the plies inside the laminate.

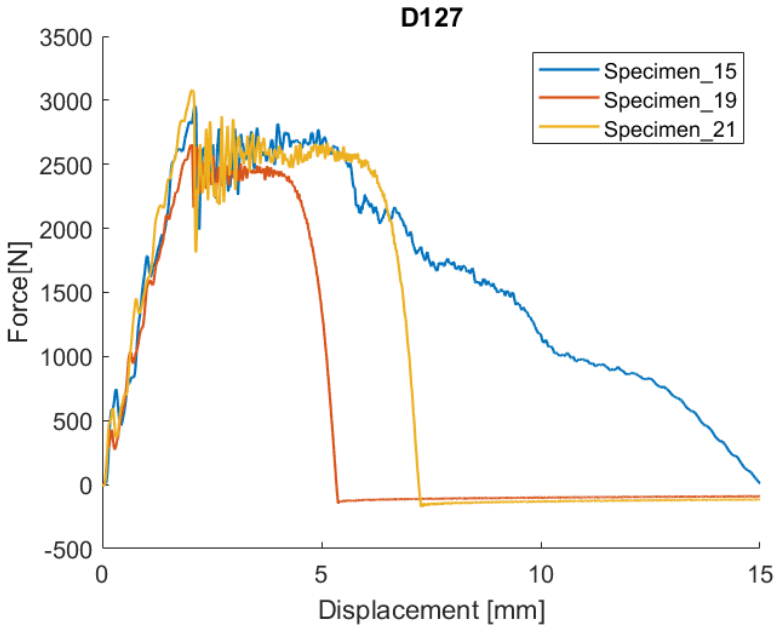

Figure 4.29: Force-displacement curve for D127

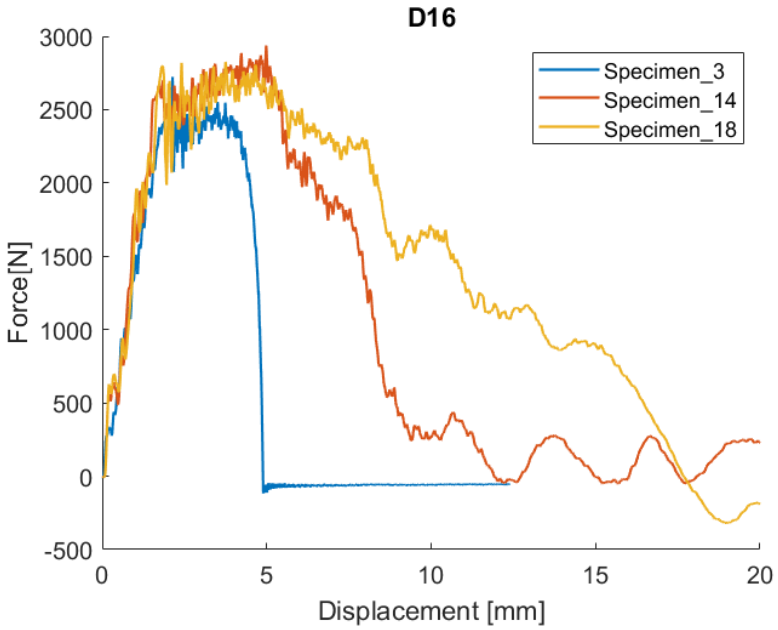

Figure 4.30: Force-displacement curve for D16

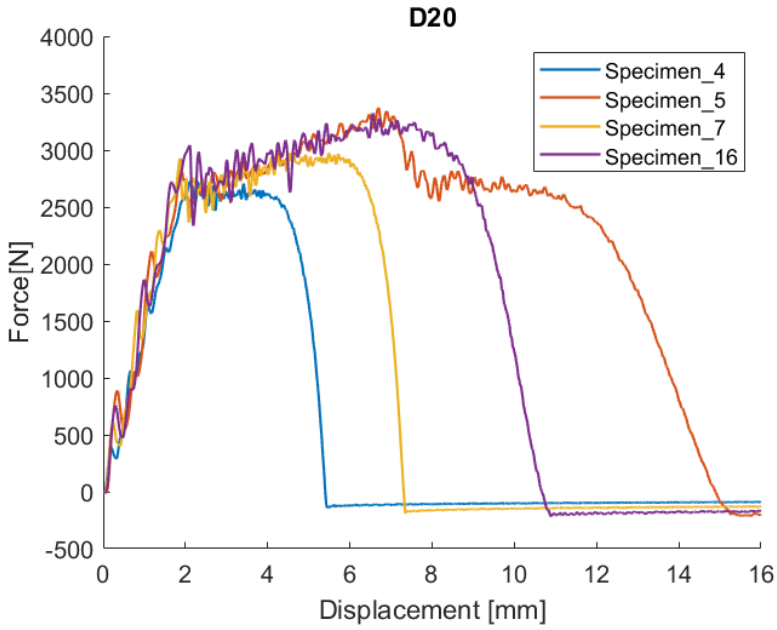

Figure 4.31: Force-displacement curve for D20

As mentioned, in order to obtain consistent evaluations both complete and incomplete failures are performed. In detail, for specimens with incomplete breakages a depression is exhibited in the upper side of the plate, with greater or lesser depth of penetration depending on the impact energy selected. The underside is characterized by the presence of splits and cracks, which are typical signs of delamination phenomena. It is worth noting that for higher impact energy tests splits occur in combined forms (see image 4.32a). Samples with complete failures are characterized by the presence of a gap in the center of the plate, in this case the most common failure modes are exhibited. With the naked eye it is possible to observe failure mechanisms such as fiber breakage, fiber pull-out, debonding and delamination phenomena. Eventually, it is important to highlight that flax composite samples do not exhibit dispersion of materials following the impact events.

(a) Underside of specimen 17 after impact (b) Underside of specimen 18 after impact

Figure 4.32: Representative failure modes indentation test

4.3.3. High-velocity impact test

Ballistic impact test is performed so as to investigate the behaviour of natural composites under high-velocity impact events. In order to execute the test a gas gun, capable of reaching 8 bar pressure, is employed (see figure 4.20). Steel spherical bullets, with a diameter of 18 mm and a weight of 23.7 g, are used to assure the failure of the samples. The latter are positioned in a suitable support called sabot, which is placed at the base of the gun barrel, immediately close to the pressure vessel. The sabots are made in teflon to guarantee a low sliding friction and the use of the components for multiple shoots. In order to ensure a proper force to the sabot a metal foil with a 0.25 mm thickness is positioned in between the pressurized vessel and the base of the barrel. In detail, once the pressure reaches the desired level, a trigger lacerates the metal foil causing an explosive thrust. Eventually, the composite panel to test is tightened on a fixture through the use of a proper mounting plate, so as to be aligned with the end of the barrel. The specimens are the same employed for indentation test, except for the length, which is 2.8 mm shorter, in table 4.13 the specimen geometry is reported.

Specimen ID	Length (mm)	Width (mm)	thickness (mm)
APX300_mix_1	122,35	100,82	4,96
APX300_mix_2	122,34	100,41	4,99
APX300_mix_6	122,44	100,57	4,95
APX300_mix_8	122,08	98,74	4,95
APX300_mix_9	122,46	100,5	4,96
APX300_mix_11	122,16	100,45	4,95

Table 4.13: Ballistic impact test specimens sizes

In order to acquire the impact velocity and the output velocity, two high-speed Phantom VEO-E 310L camera were employed. For each test at least 3 different measures are collected so as to minimize the error associated with them. In graph 4.33 and table 4.14 the most relevant results are reported.

Specimen ID	Input velocity (m/s)	output velocity (m/s)	Absorbed energy (J)	Percentage absorbed en. (%)
1	92.00	66.67	47.55	47.48
2	22.25	-	-	-
6	69.11	39.68	37.88	67.03
8	43.22	-8.22	21.31	96.38
9	126.16	100.20	69.55	36.93
11	64.51	35.47	34.35	69.76

Table 4.14: Parameters and results of ballistic impact test

With respect to indentation test the failed specimens do not exhibit a longitudinal evolution of the crack, as reported in figure 4.34, the under side of the sample n.8 shows a x-shape crack with no loss of debris. In addition, the latter specimen shows fiber breakage and fiber pull-out due to the generation of high shear and bending stresses in the non impacted side. For the same reason both n.8 and n.1 samples exhibit delamination phenomena. On the other side, the remain specimens show a complete failure and the presence of an hole after the impact. In particular, although the fragmentation of the non impacted side can be seen during impact event, a limited number of debris were generated, which is a remarkable result in the context of crashworthiness applications where the minimization of debris plays a key role. Eventually, it worth noting that the generated holes have smaller diameter compare to the bullet diameter. This aspect highlight the

elastic properties of material which is able to elastically deform during impact event.

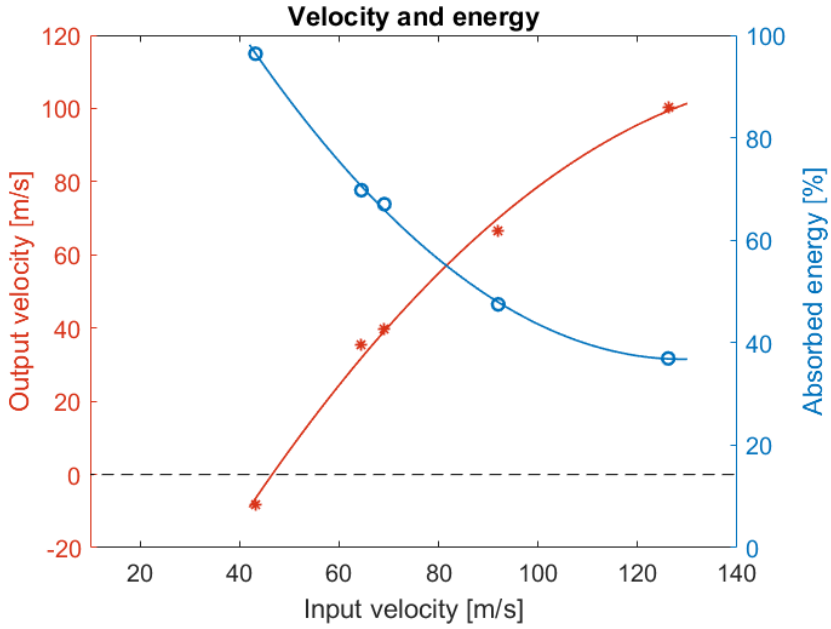

Figure 4.33: Output velocity and percentage absorbed energy in relation to input velocity

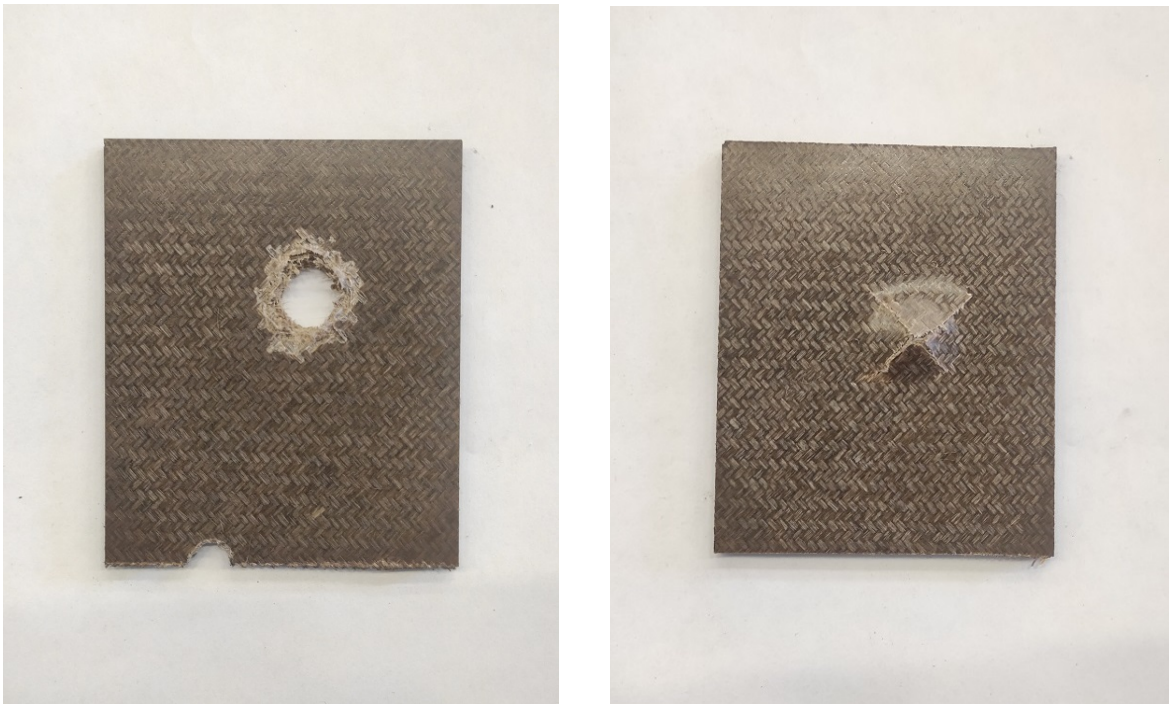

(a) Underside of specimen 1 after impact

(b) Underside of specimen 8 after impact

Figure 4.34: Representative failure modes ballistic test

5 | Numerical simulation

The last part of this project focuses on numerical modelling of the experimental tests. In detail, the static tests presented in section 4.2 will be considered so as to probe the suitability both of the material model and the model parameters choices. As previously mentioned in 2.4, finite element models are exploited to perform such analysis, the used software is LS-DYNA. Due to low thickness value with respect to length value of the employed specimens, transverse shear deformation can be neglected in the evaluation, hence the use of shell elements appears to be the most effective choice. Lastly, material card *MAT_058 is considered to model flax composite materials features.

5.1. Model set-up

As well known, static tests are performed in a quasi-static condition, where the execution time can be even in the order of the minutes. It must be highlight that the use of LS-DYNA may bring some issues. Firstly, the software employs a dynamic explicit solver which is not typically recommended for these quasi-static simulations, secondly a small integration time-step is required in order to guarantee the stability of the numerical method, which is unfeasible due to the large time simulation needed for this type of tests. Although these aspects, the final simulation outcomes can still be considered consistent and reliable, if both appropriate assumptions and investigations are made. In order to obtain reasonable computational cost, time simulation can be reduced to some tenth of a second. Despite the huge reduction of this parameter, quasi-static condition can be still guarantee through the assumption of low kinetic energy level with respect to total energy. In detail, the balance equation for a simple system without the presence of dissipation effects is: $Total\ Energy = Kinetic\ Energy + Internal\ Energy$. Where the total energy represents the whole energy introduced into the system while the internal energy is associated with the deformation energy. To ensure quasi-static condition, an upper limit value for the kinetic energy equal to 5% of the total energy is selected. This allow to prevent the achievement of poor outcomes, while guaranteeing that the majority of the introduced energy is exploited to deform the specimen.

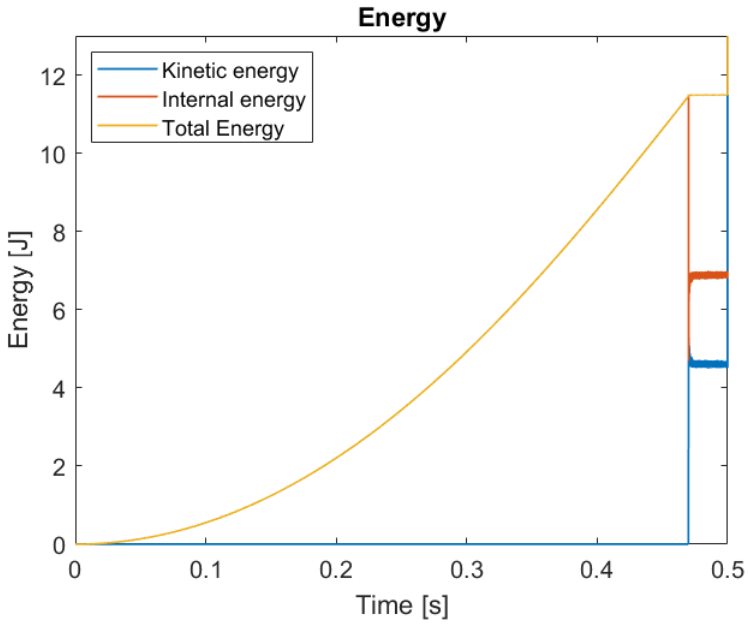

(a) Energy comparison

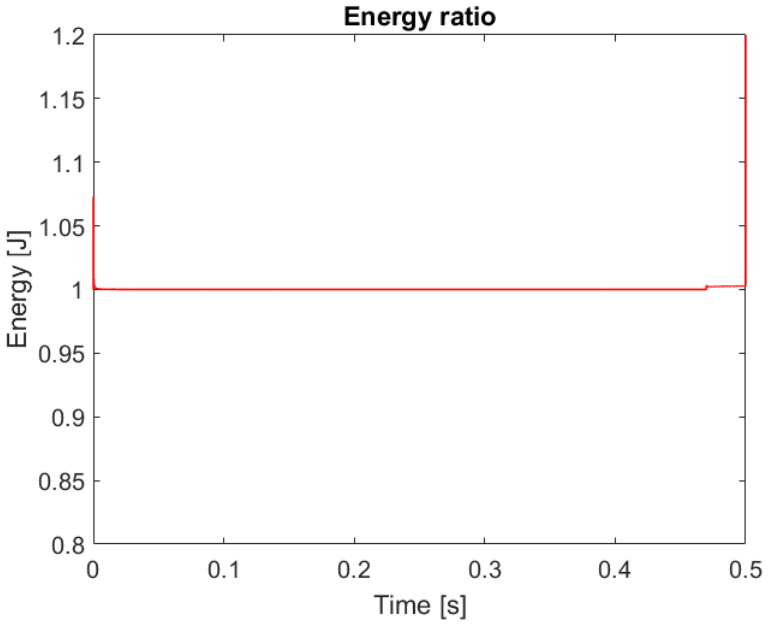

(b) Energy ratio

Figure 5.1: Energetic validation

Eventually, other energy parameters can be evaluated to assure the validation of the model. The energy ratio is defined as the ratio between the total energy and the sum of internal energy with external work applied on the system. If this parameter is close or equal to 1 consistent results are guaranteed, since energy balance is satisfied and the model is correctly working. When friction is involved in the simulation a dissipative

process takes place, the amount of energy spent in this process is measured by the energy dissipation parameter. It is worth noting that friction is not applied for most of the simulations, except for bending test model. Eventually, when high deformation occurs, hourglass energy value is fundamental in the evaluation of results. In this numerical activity the latter parameter does not represent a threat since fully integrated element are used.

In table 2.1, the material card 58 and the associated parameters are already presented. The latter can be divided in: physical and non-physical constants. In detail, the physical parameters such as ultimate stress, ultimate strain or modulus of elasticity are obtained directly from the experimental tests. On the other side, the non-physical parameters are associated with the material behaviour and must be calibrated in order to achieve reliable outcomes. This activity can be done in different ways, but the most simple and effective is the trial-and-error methodology, which is particularly suitable in the first phases of numerical modelling process. The most relevant parameters analysed are:

- Mesh size: this is not a parameter to be defined in the card, but it is essential in strain damage models, since can affect the failure threshold. Several mesh size in between 1mm and 10mm are investigated but no sensible changes can be observed. Consequently, computational time is chosen as a driver and the selected final mesh sizes are in between 3mm and 5mm.
- SLIM: this parameter controls the behaviour of the stress after which the ultimate stress value is reached. It can be assumed in between 0 and 1 and represents a percentage. Although several tests are performed with different values, no significant changes are observed in composite behaviour, unless for extreme value of 1, which resembles a perfectly plastic material. Since brittle behaviour are investigated the initial value of 0.1 is maintained.
- ERODS: it depicts the effective strain to failure parameter. Different values are tested to verify changes in failure point in the stress-strain curve. Even in this case, no sensitivity is found, which also means that localization problem can not be addressed through regularization curve process.
- SOFT: physical fidelity can be increased through this parameter. In particular, crack propagation process is controlled by reducing elements properties adjacent to failed element, so as to start the crashfront algorithm. This parameter is omitted since, also in this case, no influence in the failure process are observed.

The material card employed to perform numerical activities is depicted in table 5.1:

MID	1.334E-9	17730	17870	0	0.14	39.75	0.025
1960	980	1960	0.1	0.1	0.1	0.1	1
AOPT	1E-9	-0.3	0.9	-1	0	0	0.9
XP	YP	ZP	A1	A2	A3	0.14	0.5
V1	V2	V3	D1	D2	D3	BETA	LCDFAIL
9.412E-3	1.28E-2	9.424E-3	1.15E-2	4.7E-2			
141.57	181.39	141.53	161.69	46.21			

Table 5.1: *MAT_058 card for APX300 composite

5.2. Tensile test

As explained above, shell elements are used with a mesh size of 5mm in order to reproduce tensile test specimen with a geometry of 250x25x2.34mm. This layout allow to maintain as square as possible the elements of the model, preventing from distortion, which could be source of errors. The specimen thickness and lamination sequence are represented by means of CLT, and layers are considered perfectly bounded. As in experimental tests, a gage section of 150mm is considered and the two ends are constrained through nodal boundaries. In particular, one end is clamped whereas the other end is forced to move according to an imposed displacement law. In graphs 5.3 and 5.4 results are shown, stress value is obtained as the ratio of force over the specimen area, while the strain is simply calculated as $\Delta L/L$, where the displacement increment is known and L is the section gage of the specimen. The latter formula is capable to well represent the actual strain, since the model does not consider any slippage at the ends and exact values both of section gage and displacement variation are considered. The forces are measured through a section placed in the middle of the section gage, this measure results to be more accurate and no filter is needed to obtain final stress-strain curve.

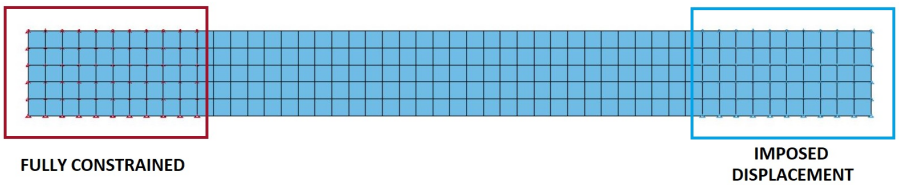

Figure 5.2: Numerical tensile test set-up

Samples with both 0° and 90° oriented warp fibers are tested. Although ultimate stress and ultimate strain values are consistent with the experimental results, the model is not able to capture the correct degradation of the elastic modulus. In detail, the transition strain point is not located at the beginning of the stress-strain curve, but at the end of it. This outcome can be consider acceptable, but improvement are needed to achieve a proper stress-strain curve so as to model a proper brittle failure.

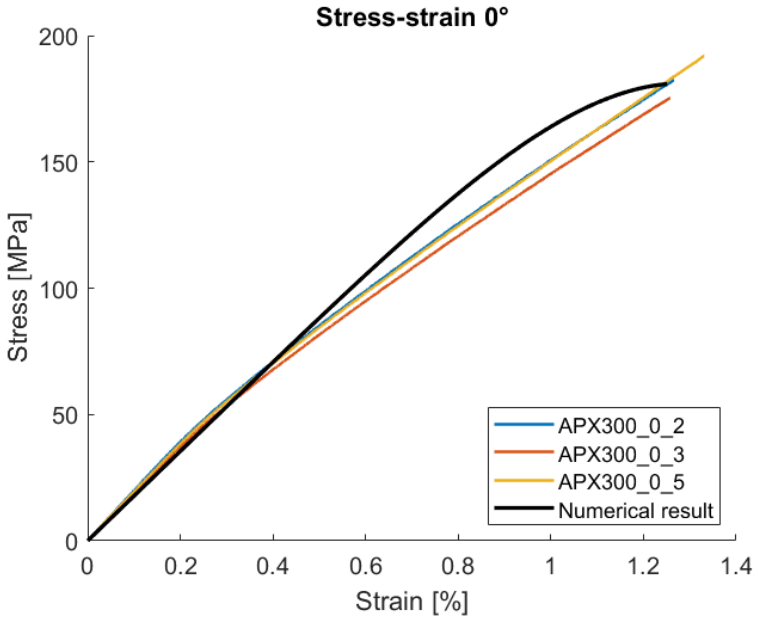

Figure 5.3: Stress-strain curves comparison for 0° specimens

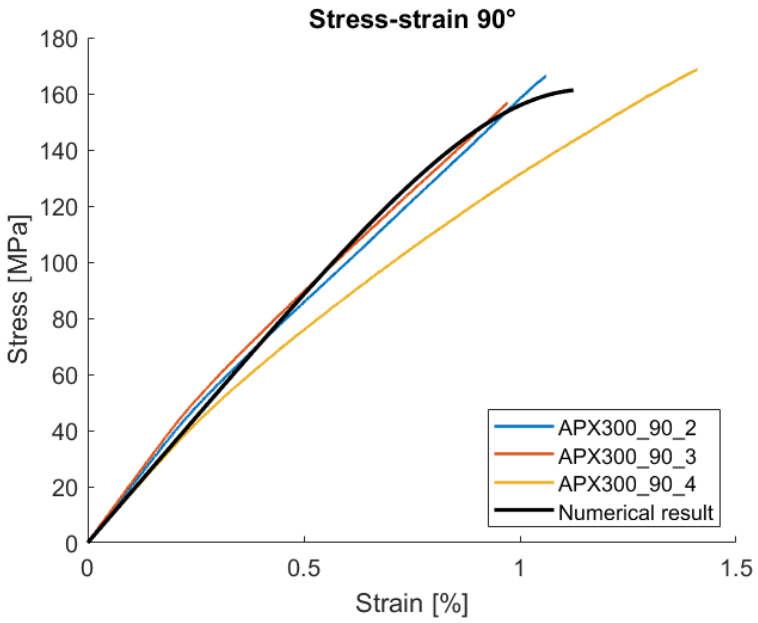

Figure 5.4: Stress-strain curves comparison for 90° specimens

5.3. Shear test

Specimen is modelled as in tensile test but in this case a geometry of 250x25x3.12mm is considered. Due to high deformation level, distortion of the element can be an issue. In general, the material rely on element coordinate system, but if the element distortion is excessively high the model can return inconsistent evaluation. In order to avoid the latter case while obtaining reliable results a global material coordinate system is defined. Moreover, a control over the accuracy of the model is set to ensure the stability of the model.

As in the tensile model the forces are measured through a section located in the middle part of the specimen. So as to achieve shear stress and shear strain, the formulas presented in section 4.2.3 are used. To calculate shear strain both transverse and axial strains are requested. As above mentioned, the latter is a known quantity, whereas transverse shear has to be achieved. In order to obtain this value the assumption of Poisson's ratio equal to 1 is employed and transverse strain can be assumed equal to axial strain. The comparison between numerical and experimental results is shown in graph 5.5 within 5% of shear strain. In detail, the bi-linear numerical curve slightly underestimates the real behaviour, especially in the last part of the graph. However, acceptable outcomes are achieved if shear modulus and maximum shear strain are considered.

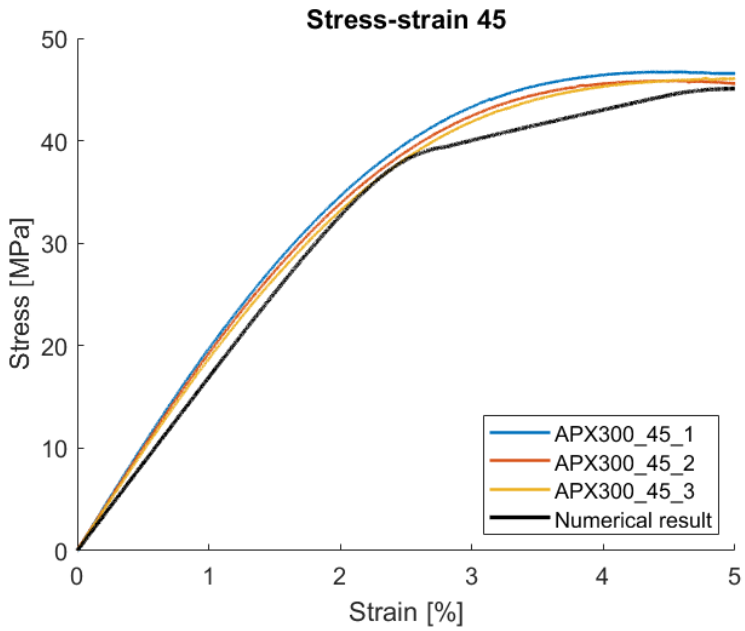

Figure 5.5: Stress-strain curves comparison for ±45° specimens

5.4. Compression test

Compression model set-up is similar to the above mentioned models, expect for the mesh size. In this case 4mm mesh is selected to best fit the specimen geometry of 140x16x2.34mm. The material card 58 does not allow for the definition of compressive Young's modulus. Consequently, a choice is made: in order to not affect the tensile response, the compressive modulus of elasticity is considered equal to the tensile one, hence, only the tensile Young's modulus is evaluated for the definition of the material (see table 5.1). Although the presence of this assumption, the obtained results in terms of compressive modulus are similar to the experimental outcomes. Test are performed both for 0° and 90° oriented warp fibers samples, and a section gage of 12mm is adopted, in compliant with standard D6641.

The achieved ultimate compressive stress values are comparable with experimental results. In detail, for specimens with 0° oriented fibers, a maximum value of 140.87Mpa is recorded, while for 90° samples a maximum value of 140.84Mpa is obtained. These outcomes are less than 1% lower with respect to experimental counterparts, hence the model can be considered suitable to numerically approximate compressive behaviour.

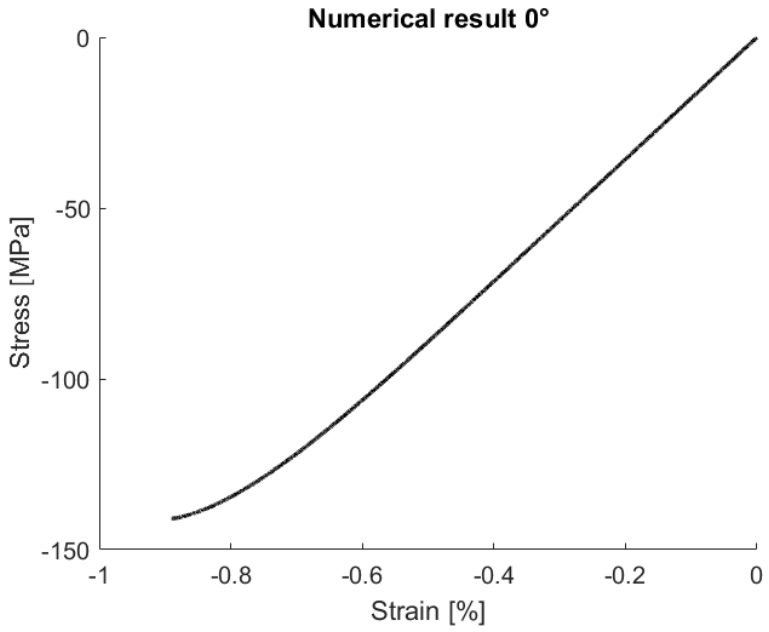

Figure 5.6: Compression test numerical outcomes for 90° specimens

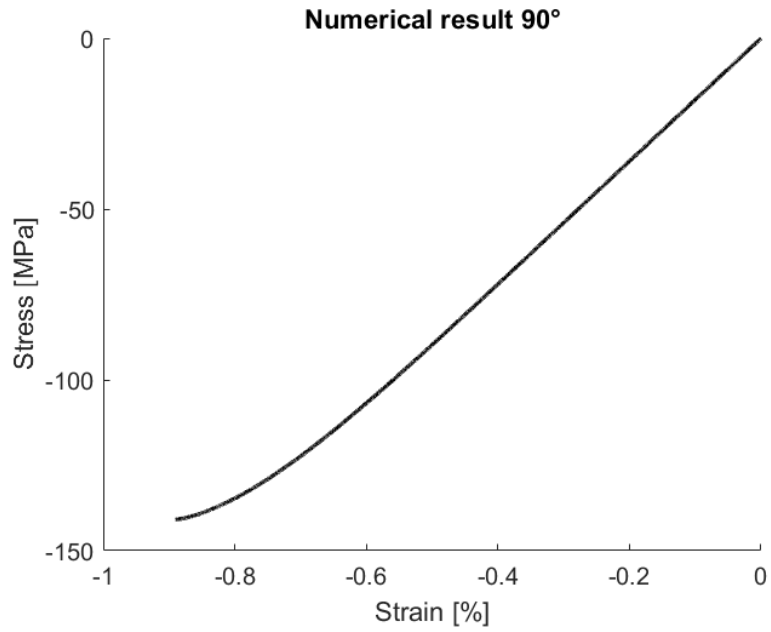

Figure 5.7: Compression test numerical outcomes for 90° specimens

5.5. Bending test

Out-of-plane bending test is modelled differently with respect to the other models. The numerical specimen is similar to the ones presented in the previous sections, but in this case the load is generated by means of three cylinders, as shown in figure 5.8.

The latter components are modelled by exploiting shell elements so as to reduce computational cost. In the experimental tests, cylinders are made by steel, thus in numerical model they can be considered as rigid body. In order to interact with the specimen an AUTOMATIC_SURFACE_TO_SURFACE contact, with a static friction coefficient of 0.5, is used so as to prevent any slippage phenomena during numerical simulation. As mentioned above, a check on the dissipative energy is conducted to ensure the consistency of the results. Eventually, a mesh size of 3mm is selected both for the specimen and the cylinders to achieve better numerical outcomes.

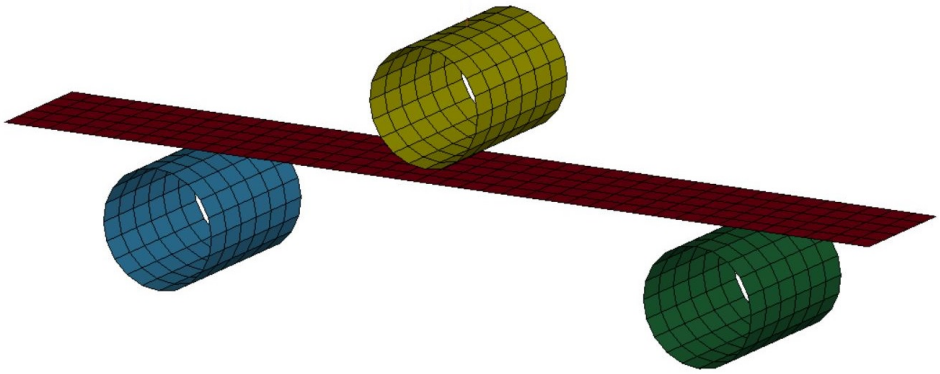

(a) Initial configuration

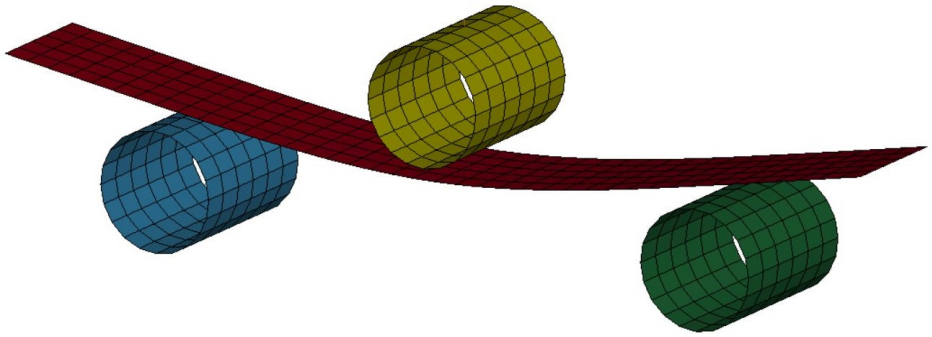

(b) Deformed configuration

Figure 5.8: Numerical bending test set-up

The set-up to perform the test is presented below: the lower cylinders are completely constrained, while an imposed vertical displacement is applied to the upper cylinder. The specimen is completely free to move, but due to the static friction no motions are recorder during the simulation. The results are shown in figure 5.9: the numerical curve is filtered using a SAE filter with cutting frequency of 180 Hz so as to reduce the contact noise. In the first half of the graph experimental and numerical results are comparable, while, with high deformation, numerical test seems to be not able to capture the real behaviour of the material. These discrepancies can be correlated with some slippage phenomena or even with imperfect alignment during the experimental test. However, the latter are not able to justify the poor result in terms of displacement, numerical improvement must be performed. Hence, more refined optimization techniques must be considered to enhance consistent numerical performances. Eventually, it worth noting that maximum numerical force is comparable with experimental results, although premature failure occurs.

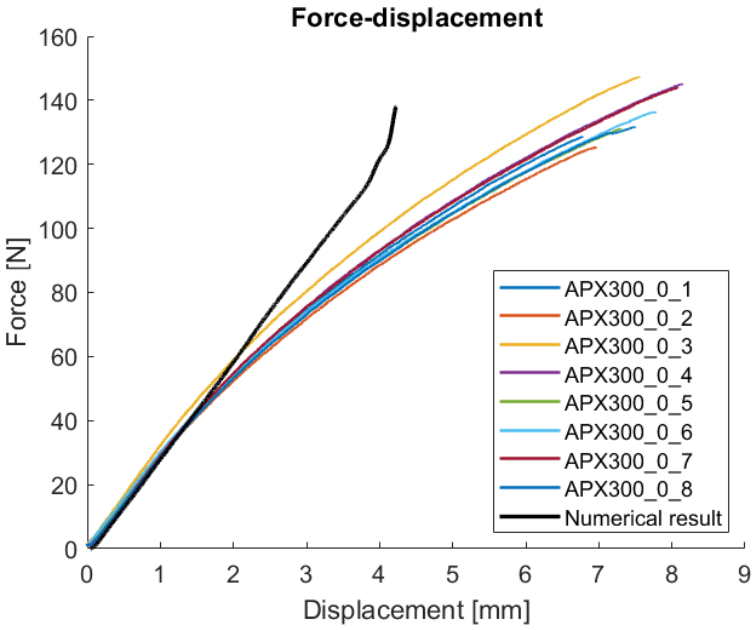

Figure 5.9: Force-displacement curves comparison for bending test

6 | Conclusions and future developments

This thesis work aims to investigate both the static and dynamic mechanical performances of flax-fiber reinforced composite material and their numerical modeling, through the development of a suitable material card. The results achieved can be considered positive and significant, since the major mechanical features of the material were analyzed and numerical outcomes shown a general consistency with respect to the experimental data.

Although the presence of flaws both in the procedure and in some specimens, experimental static tests were able to provide consistent outcomes. Hence, static mechanical performances can be considered reliable for future potential design processes. During dynamic tests, especially strain rate sensitivity tests, some procedural issue arose. In detail, the employed drop tower machine was not able to acquire the data in some attempts, leading to a consequent wasting of samples. In addition, the use of emery cloth and aluminium in place of tabs seemed to be a suitable and practical solution, though further improvement must be perform to assure the reliability of the tests in every conditions. Nevertheless, the presented dynamic outcomes can be considered consistent and dependable. In particular, both indentation and ballistic impact tests parameters were not affected by issue during test procedures, except for specimens n.20 and n.17 where the data were lost.

It worth noting that, as reported in chapter 3, the achieved specific mechanical properties can be compared to those of the fiberglass composite. In detail, from the study [6], the tensile properties of a composite material, made by woven glass fiber fabric and epoxy resin, are obtained. In order to calculate the specific mechanical properties a specific gravity equal to 2 is considered. Hence, specific ultimate stress of 129.47Mpa is obtained and a specific Young's modulus of 11.86GPa is achieved as well. These parameters are lower with respect to the values acquired during this work: a specific ultimate tensile stress of 135.98MPa and a specific elastic modulus of 13.29GPa are obtained considering the lower specific gravity parameter of flax composite material, which is equal to 1.33. Lastly, comparison of dynamic properties can be done as well, the mechanical improvement of

fiberglass/epoxy composite can be found even for flax-fiber reinforced composite. In detail, in fiberglass composite tests an increase of about 30% in maximum tensile stress can be measured, while for flax composite a maximum tensile stress improvement of more than 23% was recorded. Both the results are consistent with the excepted materials behaviour.

As mentioned above, the numerical activity presented must be considered as a preliminary stage of the entire numerical modelling phase. Different material cards were investigated and the most suitable was selected so as to model flax composite material. In detail, material card 58 exhibited, except for bending test, significant and consistent outcomes with respect to experimental data. As a consequence, this study can be considered as a starting point for further improvement.

6.1. Future developments

Experimental tests were conducted in order to achieve a well-rounded understanding of natural composite material, but improvements can be surely performed. For example, during dynamic tests, a wider range of strain rate values can be considered so as to investigate sensitivity behaviour from the quasi-static condition to the high-speed impact event. In addition, a larger amount of specimens, with different layout stacking sequences and thicknesses, can be employed to gain a full understanding of the dynamic behaviour. Data acquisition system can be improved as well, for example using accelerometer in order to have an outcome independent of the machinery. Regarding both indentation test and ballistic impact test, a more in-depth analysis about the geometry and size of the damaged area can be performed through the use of nondestructive inspection techniques, such as radiography. In addition, a detailed view of the totally failed specimens can be done so as to perform a complete failure modes analysis.

Numerical model accuracy can be improved operating on both material card and numerical elements. More complex material cards can be implemented such as MAT_262, but additional experimental tests on fracture toughness must be performed in order to achieve the required parameters. Moreover, so as to study out-of-plane behaviour of composites a different modeling approach can be adopted by employing 3D elements or by introducing a stacked-shell approach. Eventually, through the use of LS-OPT, which is an optimization tools that interfaces perfectly with LS-DYNA, an optimization process of the defined parameters can be done so as to improve the outcomes in a effective way.

Manufacturing techniques may have a great margin of improvement considering that the interest in bio-materials developed just a few years ago. Both pre-production and post-production treatments can be evaluated to solve issue such as high hygroscopicity and

poor fiber-matrix adhesion. In doing so, mechanical performances and durability could be increased significantly allowing for a wider employment of natural materials.

In conclusion, natural composite materials revealed noteworthy mechanical performances in the context of crashworthiness applications. Especially, considering the exhibited failure modes during dynamic tests: few debris were found in the impacted areas, thanks to the nature of bio-fibers, which are not prone to detach from the laminate. Lastly, bio-inspired structures such as coconut tree geometry, date palm tree structure and even bamboo multi-cell structure, can be used during design phases in order to maximize the absorbed energy while fully exploiting the potential of natural composite materials.

Bibliography

[1] B. D. Agarwal, L. J. Broutman, and C. Bert. *Analysis and performance of fiber composites*. John Wiley & Sons, 2006.

[2] A. Ali, K. Shaker, Y. Nawab, M. Jabbar, T. Hussain, J. Militky, and V. Baheti. Hydrophobic treatment of natural fibers and their composites—a review. *Journal of Industrial Textiles*, 47(8):2153–2183, 2018.

[3] M. Alkbir, S. Sapuan, A. Nuraini, and M. Ishak. Fibre properties and crashworthiness parameters of natural fibre-reinforced composite structure: A literature review. *Composite Structures*, 148:59–73, 2016.

[4] M. A. Attia, M. A. Abd El-Baky, M. A. Hassan, T. A. Sebaey, and E. Mahdi. Crashworthiness characteristics of carbon–jute–glass reinforced epoxy composite circular tubes. *Polymer Composites*, 39(S4):E2245–E2261, 2018.

[5] H. Chen. Biotechnology of lignocellulose. *Theory and Practice. China: Chemical Industry Press and Springer*, 2014.

[6] W. Chen, Q. Meng, H. Hao, J. Cui, and Y. Shi. Quasi-static and dynamic tensile properties of fiberglass/epoxy laminate sheet. *Construction and Building Materials*, 143:247–258, 2017.

[7] A. Cherniaev, C. Butcher, and J. Montesano. Predicting the axial crush response of cfrp tubes using three damage-based constitutive models. *Thin-walled structures*, 129:349–364, 2018.

[8] O. Cousigné, D. Moncayo, D. Coutellier, P. Camanho, and H. Naceur. Numerical modeling of nonlinearity, plasticity and damage in cfrp-woven composites for crash simulations. *Composite Structures*, 115:75–88, 2014.

[9] M. Deorsi and C. Ermoli. Numerical and experimental characterization of composite materials. Master's thesis, Politecnico di Milano, 2022.

[10] R. A. Eshkoor, S. A. Oshkovr, A. Sulong, R. Zulkifli, A. K. Ariffin, and C. H.

Azhari. Comparative research on the crashworthiness characteristics of woven natural silk/epoxy composite tubes. *Materials & Design*, 47:248–257, 2013.

[11] M. J. Ghoushji, R. A. Eshkoor, R. Zulkifli, A. B. Sulong, S. Abdullah, and C. H. Azhari. Energy absorption capability of axially compressed woven natural ramie/green epoxy square composite tubes. *Journal of Reinforced Plastics and Composites*, 36(14):1028–1037, 2017.

[12] *Guide to composite.* Gurit Holding AG. https://www.gurit.com/-/media/Gurit/Datasheets/guide-to-composites.pdf.

[13] C. W. Isaac and C. Ezekwem. A review of the crashworthiness performance of energy absorbing composite structure within the context of materials, manufacturing and maintenance for sustainability. *Composite Structures*, 257:113081, 2021.

[14] R. M. Jones. *Mechanics of composites materials.* Taylor & Francis, 1999.

[15] M. Kabir, H. Wang, T. Aravinthan, F. Cardona, and K.-T. Lau. Effects of natural fibre surface on composite properties: A review. In *Proceedings of the 1st International Postgraduate Conference on Engineering, Designing and Developing the Built Environment for Sustainable Wellbeing (eddBE 2011)*. University of Southern Queensland, 2011.

[16] F. La Mantia and M. Morreale. Green composites: A brief review. *Composites Part A: Applied Science and Manufacturing*, 42(6):579–588, 2011.

[17] *LS-DYNA ® KEYWORD USER'S MANUAL VOLUME II Material Models Livermore Software Technology (LST), An Ansys Company.* LSTC, 1992.

[18] A. Matzenmiller, J. Lubliner, and R. L. Taylor. A constitutive model for anisotropic damage in fiber-composites. *Mechanics of materials*, 20(2):125–152, 1995.

[19] Q. Meng and Z. Wang. Theoretical analysis of interfacial debonding and fiber pull-out in fiber-reinforced polymer-matrix composites. *Archive of Applied Mechanics*, 85 (6):745–759, 2015.

[20] J. Meredith, R. Ebsworth, S. R. Coles, B. M. Wood, and K. Kirwan. Natural fibre composite energy absorption structures. *Composites Science and Technology*, 72(2): 211–217, 2012.

[21] B. Mitra. Environment friendly composite materials: Biocomposites and green composites. *Defence science journal*, 64(3), 2014.

[22] L. Mohammed, M. N. Ansari, G. Pua, M. Jawaid, and M. S. Islam. A review on

natural fiber reinforced polymer composite and its applications. *International journal of polymer science*, 2015, 2015.

[23] T.-D. Ngo. Introduction to composite materials. *Composite and Nanocomposite Materials—From Knowledge to Industrial Applications*, 2020.

[24] S. Oshkovr, R. Eshkoor, S. Taher, A. Ariffin, and C. Azhari. Crashworthiness characteristics investigation of silk/epoxy composite square tubes. *Composite Structures*, 94(8):2337–2342, 2012.

[25] P. Peças, H. Carvalho, H. Salman, and M. Leite. Natural fibre composites and their applications: a review. *Journal of composites science*, 2(4):66, 2018.

[26] P. Petit. A simplified method of determining the inplane shear stress-strain response of unidirectional composites. In *Composite materials: Testing and design*. ASTM International, 1969.

[27] D. K. Rajak, D. D. Pagar, P. L. Menezes, and E. Linul. Fiber-reinforced polymer composites: Manufacturing, properties, and applications. *Polymers*, 11(10):1667, 2019.

[28] D. K. Rajak, P. H. Wagh, and E. Linul. A review on synthetic fibers for polymer matrix composites: performance, failure modes and applications. *Materials*, 15(14): 4790, 2022.

[29] K. Rohit and S. Dixit. A review-future aspect of natural fiber reinforced composite. *Polymers from Renewable Resources*, 7(2):43–59, 2016.

[30] B. W. Rosen. A simple procedure for experimental determination of the longitudinal shear modulus of unidirectional composites. *Journal of Composite Materials*, 6(3): 552–554, 1972.

[31] A. Rubini. Analisi del processo produttivo di componenti in fibra di carbonio con autoclave: il caso di hp composites. Master's thesis, Politecnico di Torino, 2020.

[32] K. Schweizerhof, K. Weimar, T. Munz, and T. Rottner. Crashworthiness analysis with enhanced composite material models in ls-dyna–merits and limits. In *LS-DYNA world conference*, pages 1–17, 1998.

[33] E. S. Stevens. *Green plastics: an introduction to the new science of biodegradable plastics*. Princeton University Press, 2002.

[34] H. Takagi and A. Asano. Effects of processing conditions on flexural properties of

cellulose nanofiber reinforced "green" composites. *Composites Part A: Applied Science and Manufacturing*, 39(4):685–689, 2008.

[35] K. Tanaka, T. Katsura, Y. Kinoshita, T. Katayama, and K. Uno. Mechanical properties of jute fabric reinforced thermoplastic moulded by high-speed processing using electromagnetic induction. *WIT Trans Built Environ*, 97:211–219, 2008.

[36] C. Williams, S. Grove, and J. Summerscales. The compression response of fibre-reinforced plastic plates during manufacture by the resin infusion under flexible tooling method. *Composites Part A: applied science and manufacturing*, 29(1-2):111–114, 1998.

[37] M. Zin, K. Abdan, N. Mazlan, E. Zainudin, and K. Liew. The effects of alkali treatment on the mechanical and chemical properties of pineapple leaf fibres (palf) and adhesion to epoxy resin. In *IOP Conference Series: Materials Science and Engineering*, volume 368, page 012035. IOP Publishing, 2018.

A | Appendix A

A.1. Static tests specimens

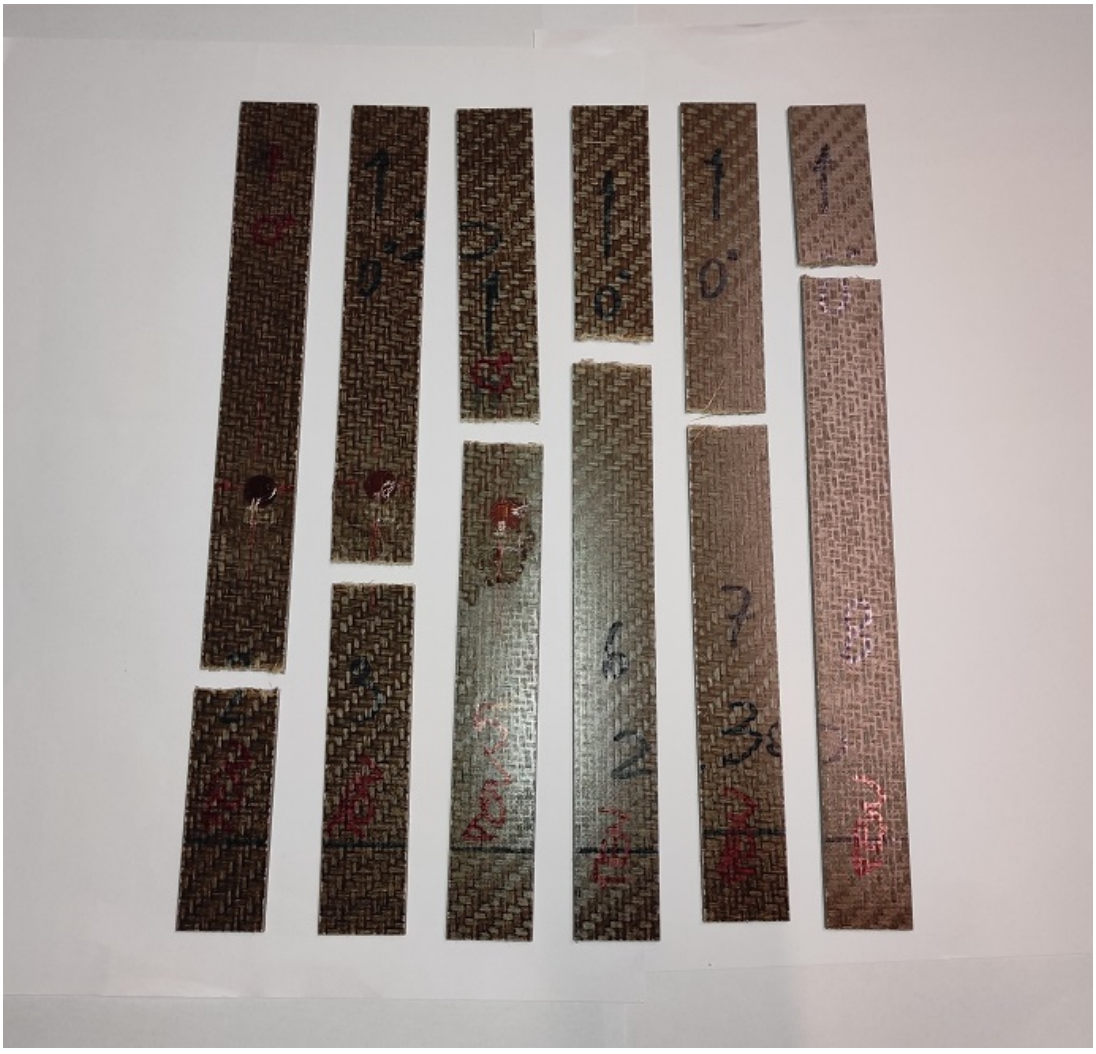

Figure A.1: Tensile test specimens with 0° oriented fibers

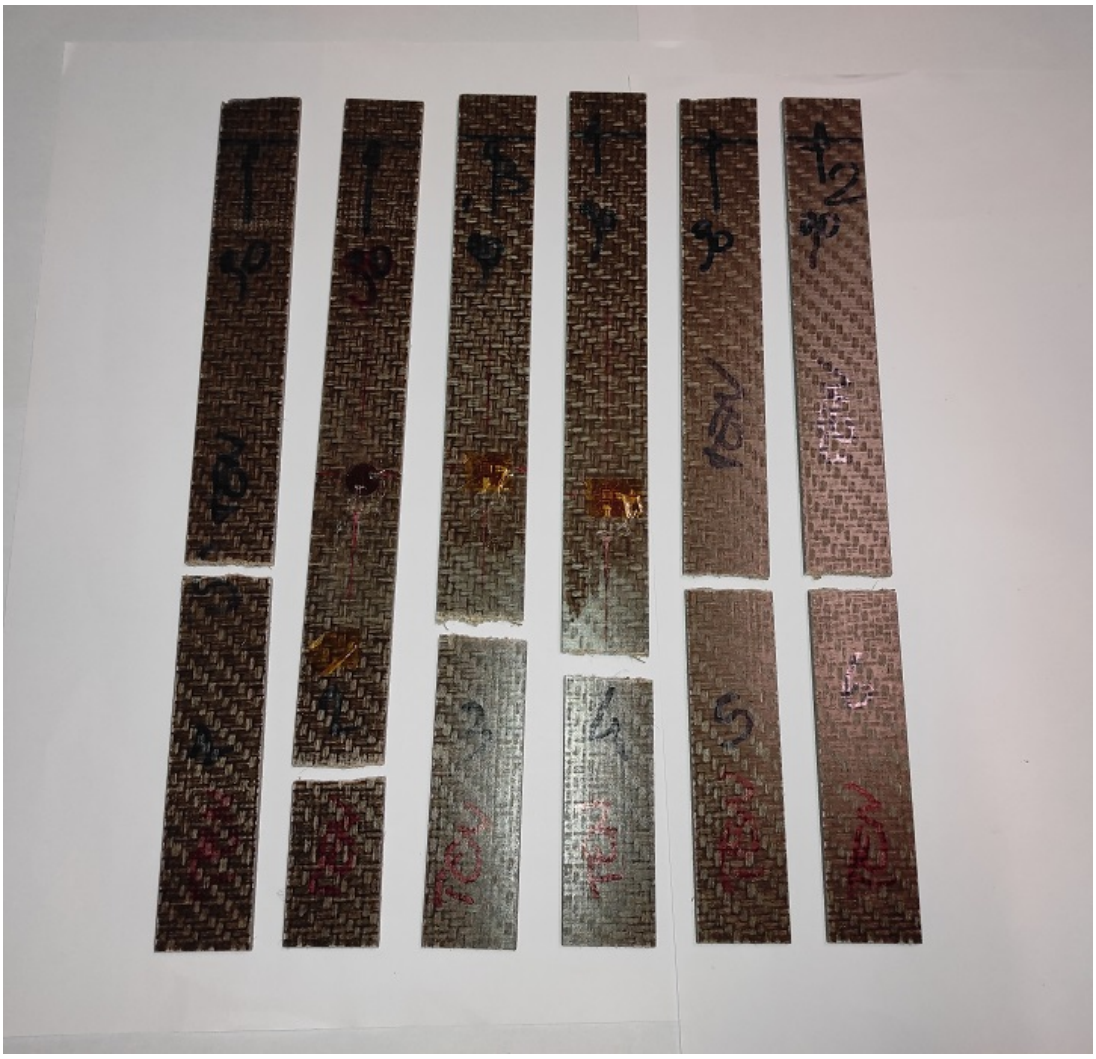

Figure A.2: Tensile test specimens with 90° oriented fibers

Figure A.3: Shear test specimens

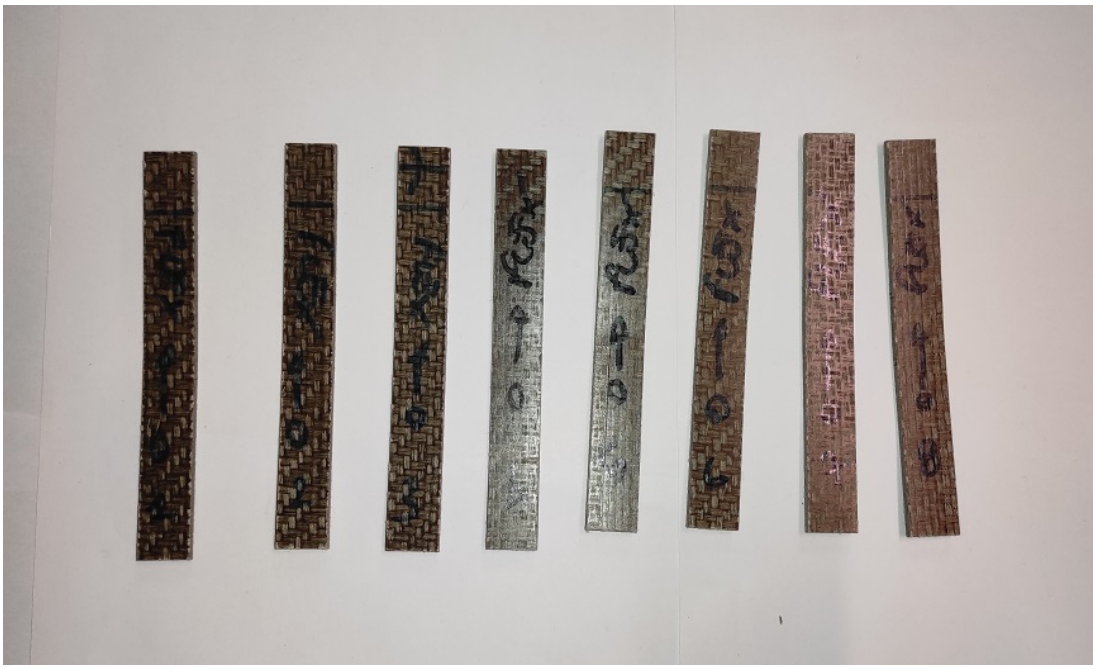

Figure A.4: Bending test specimens (top view)

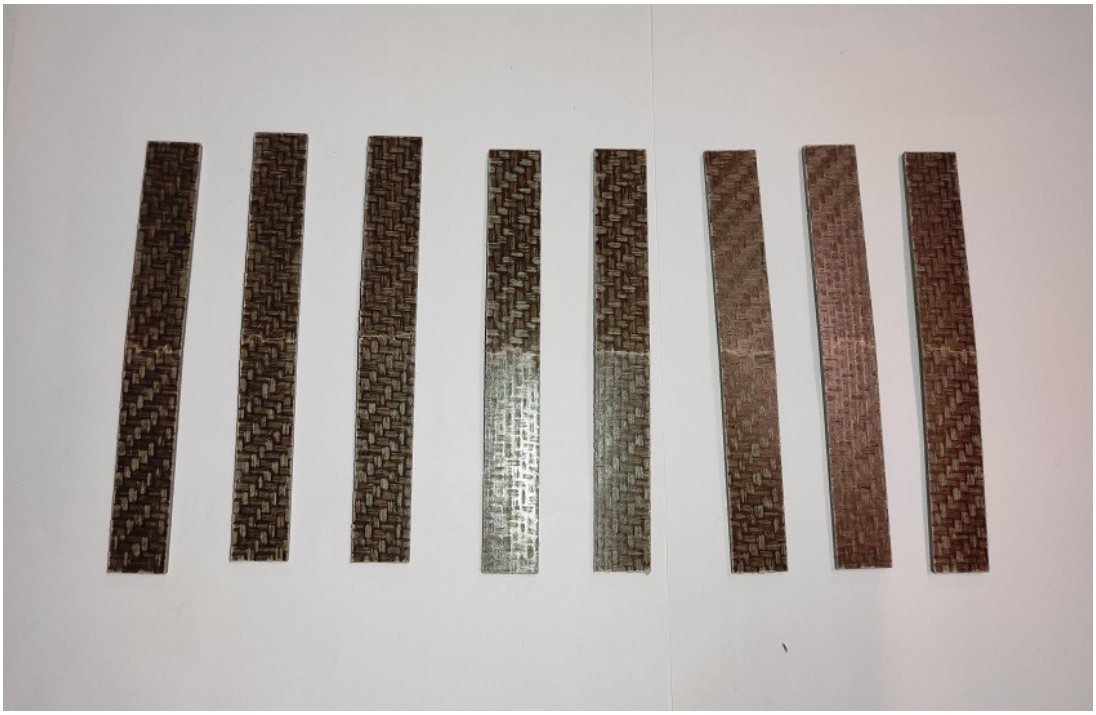

Figure A.5: Bending test specimens (bottom view)

Figure A.6: Compression test specimens with 0° oriented fibers

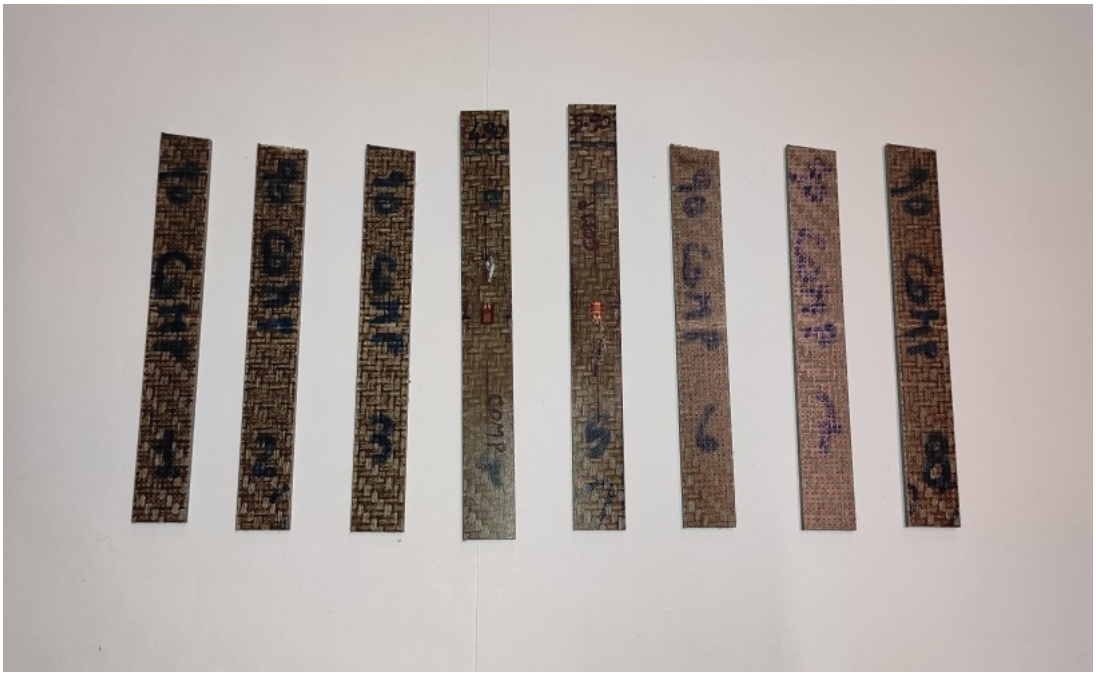

Figure A.7: Compression test specimens with 90° oriented fibers

A.2. Dynamic tests specimens

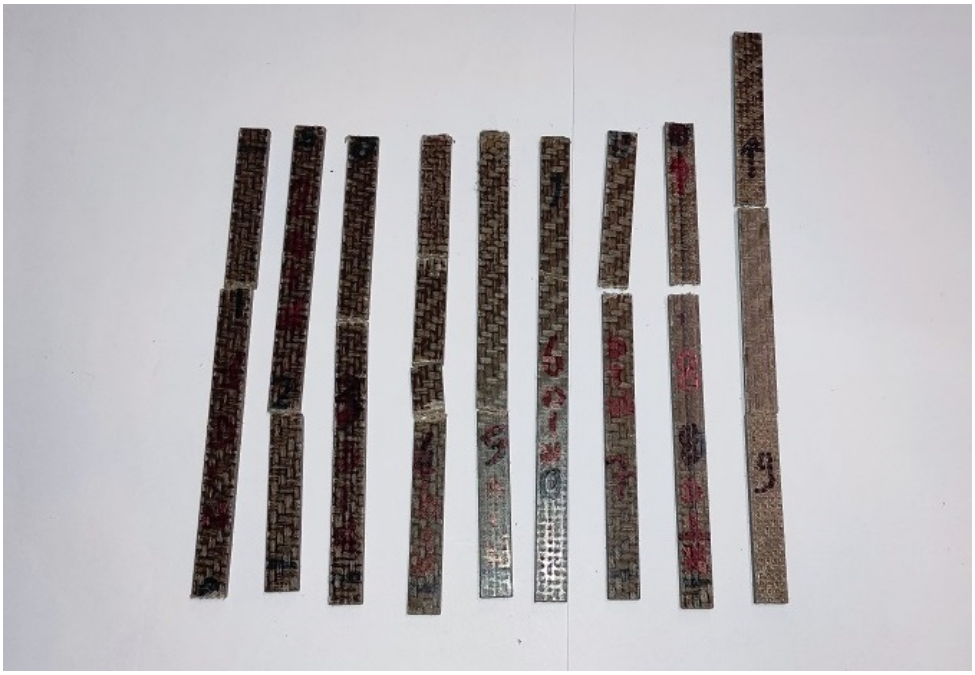

Figure A.8: Strain rate test specimens without strain gages

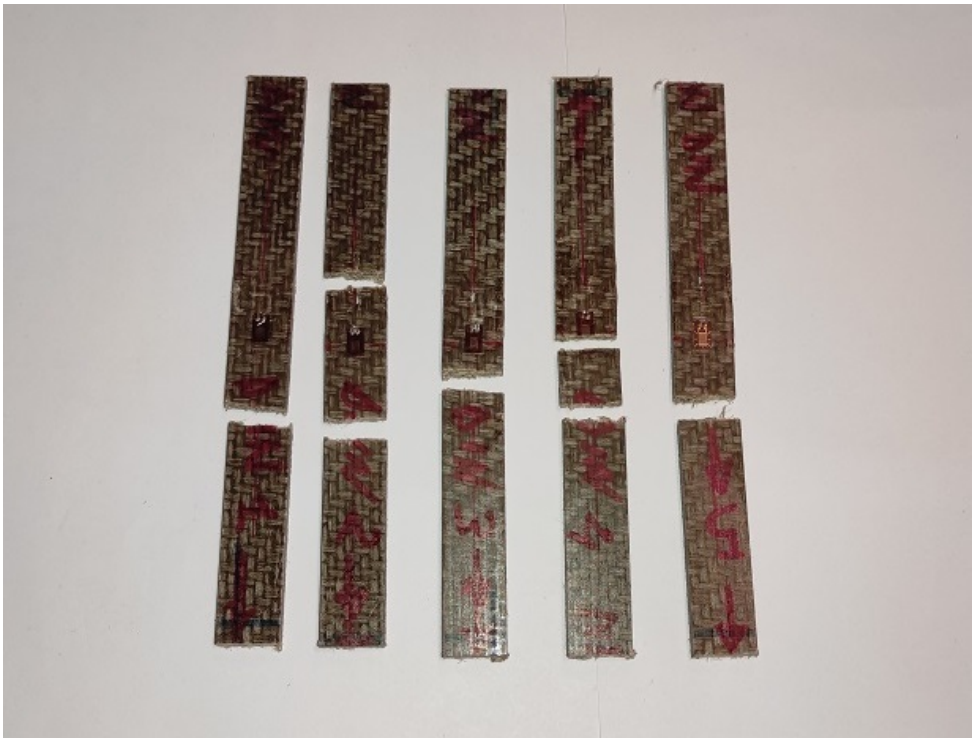

Figure A.9: Strain rate test specimens equipped with strain gages

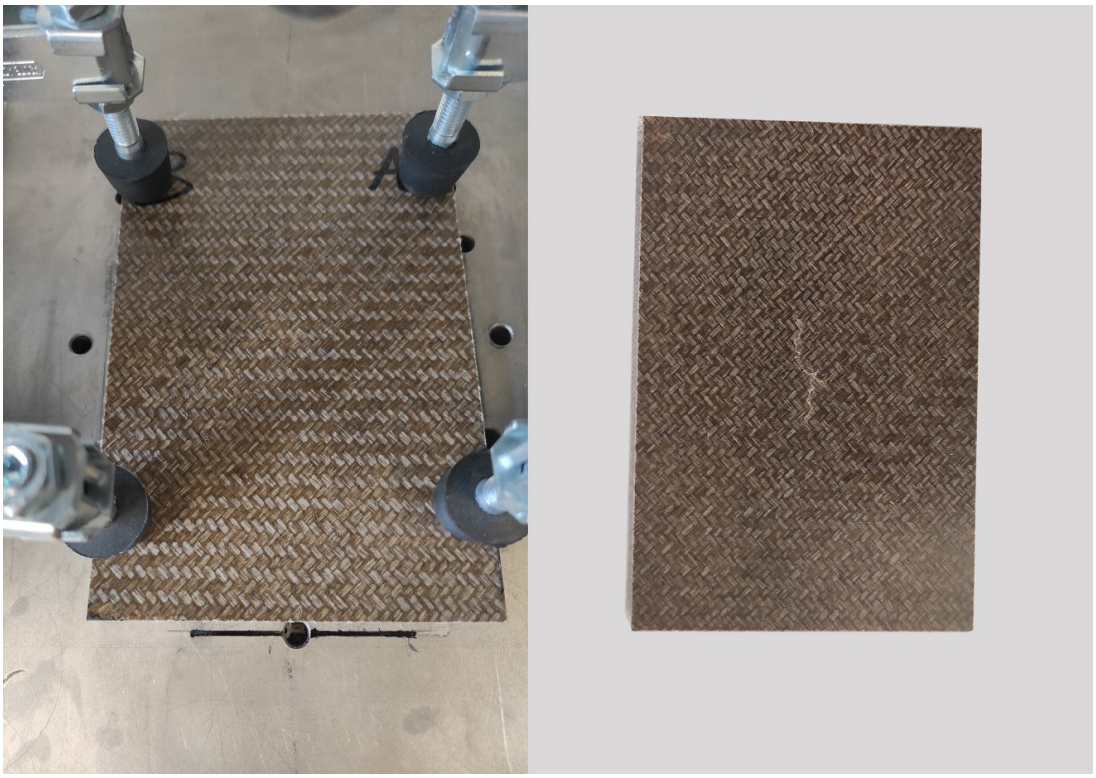

Figure A.10: Indentation test specimen 3

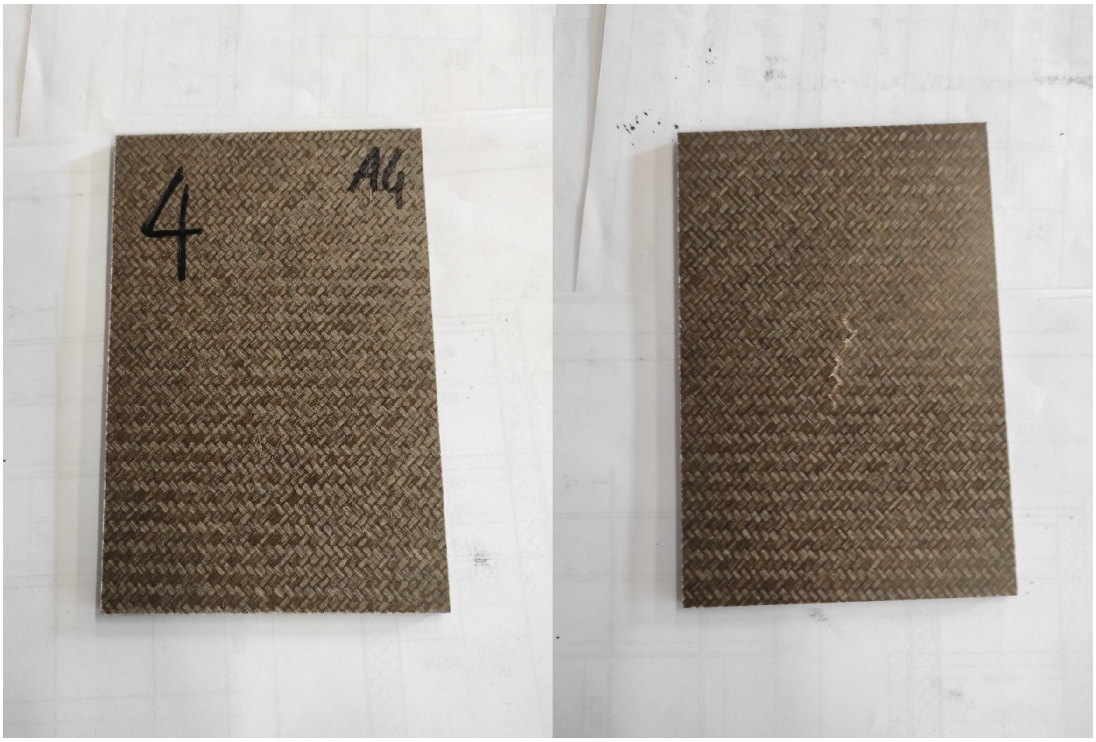

Figure A.11: Indentation test specimen 4

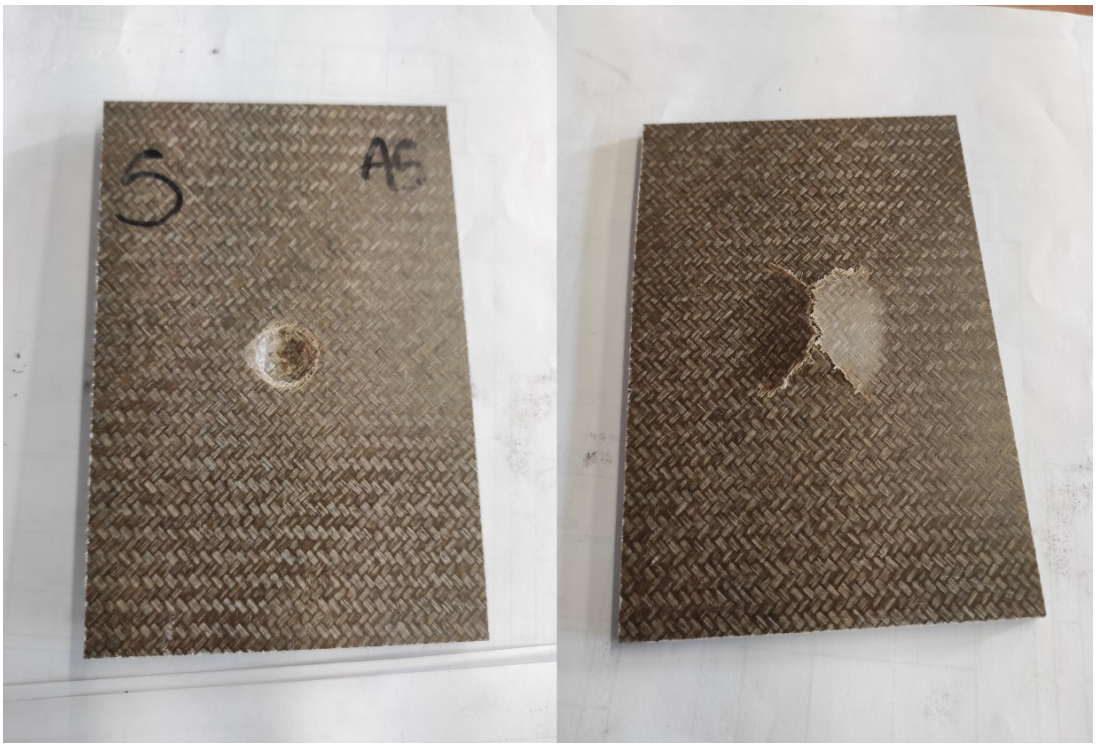

Figure A.12: Indentation test specimen 5

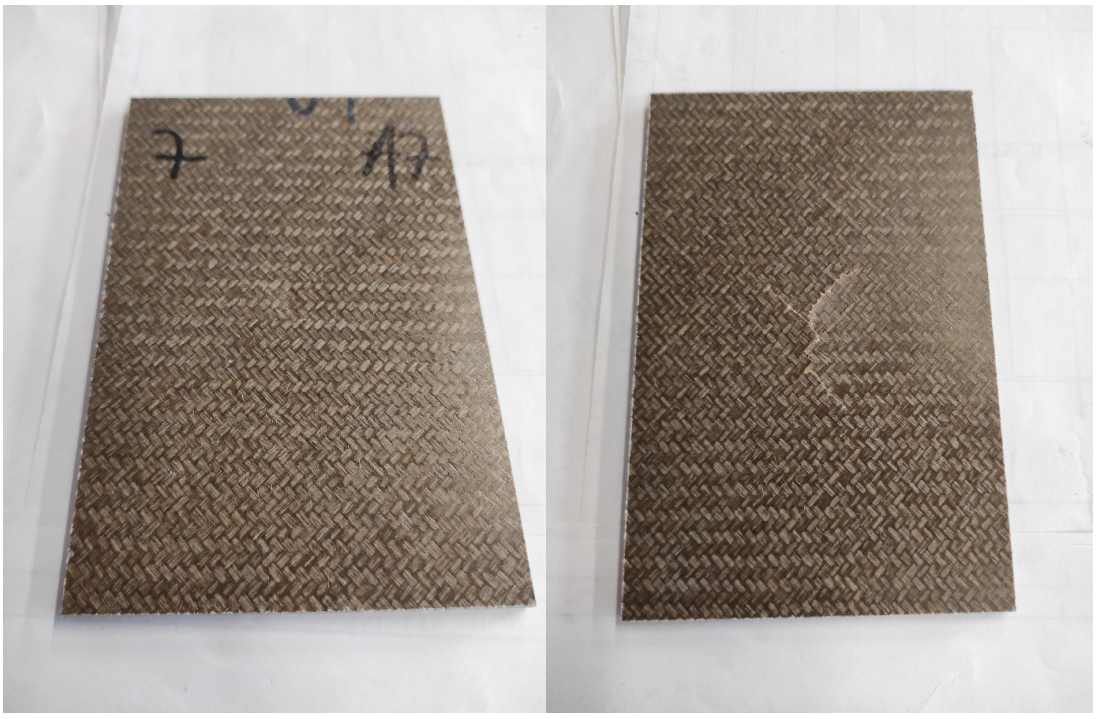

Figure A.13: Indentation test specimen 7

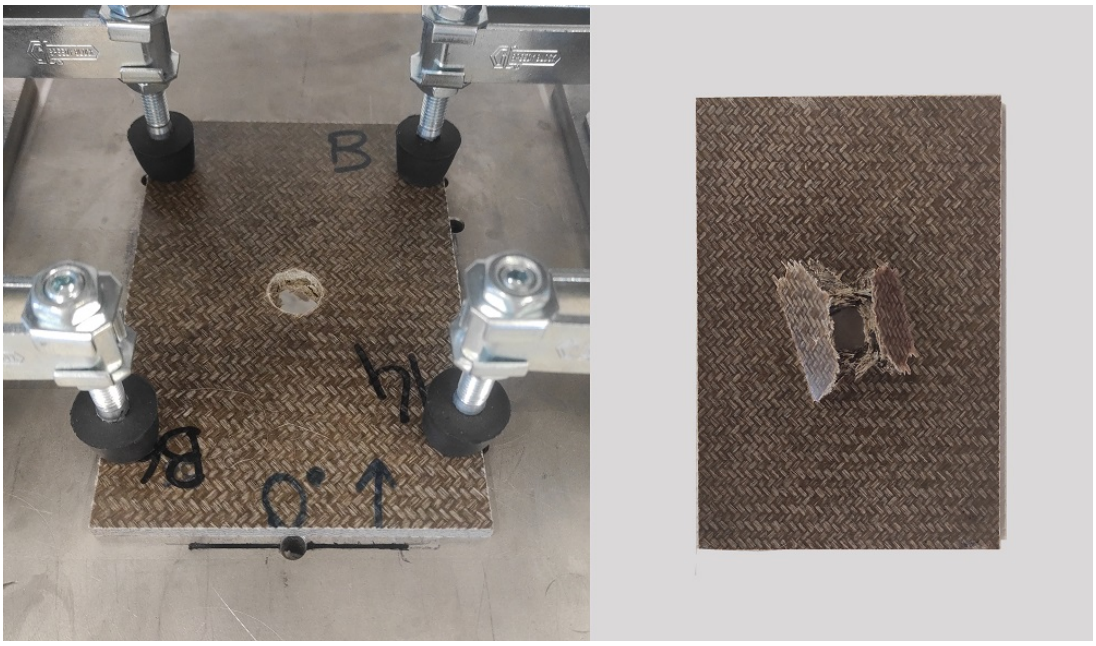

Figure A.14: Indentation test specimen 14

Figure A.15: Indentation test specimen 15

Figure A.16: Indentation test specimen 16

Figure A.17: Indentation test specimen 17

Figure A.18: Indentation test specimen 18

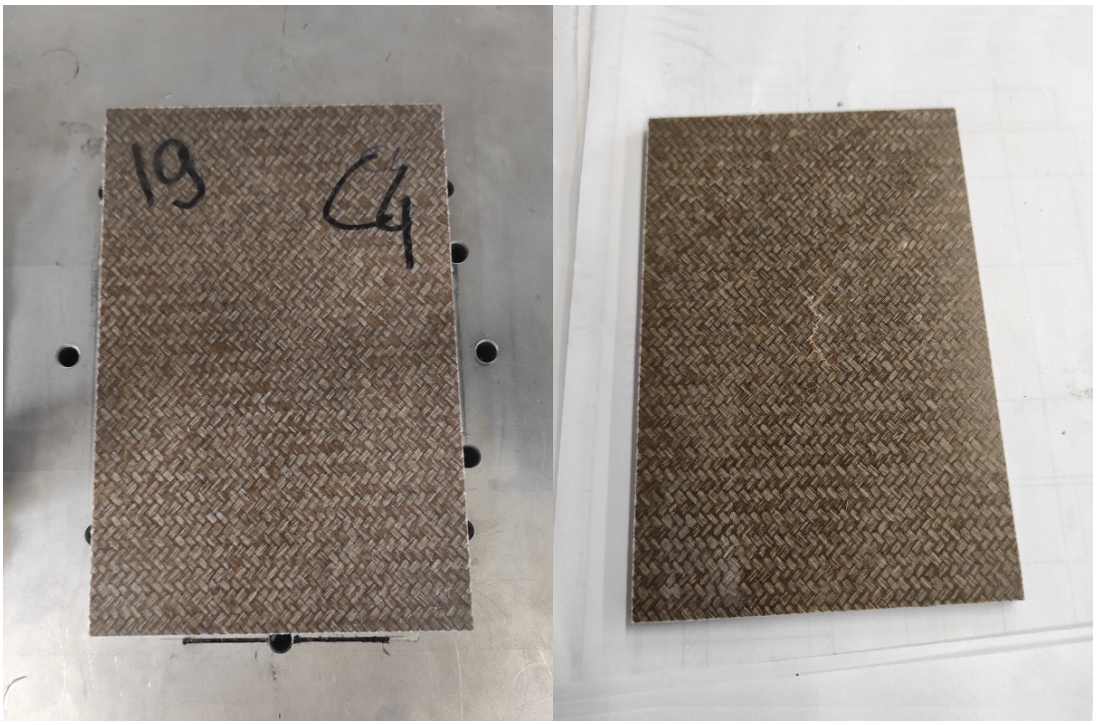

Figure A.19: Indentation test specimen 19

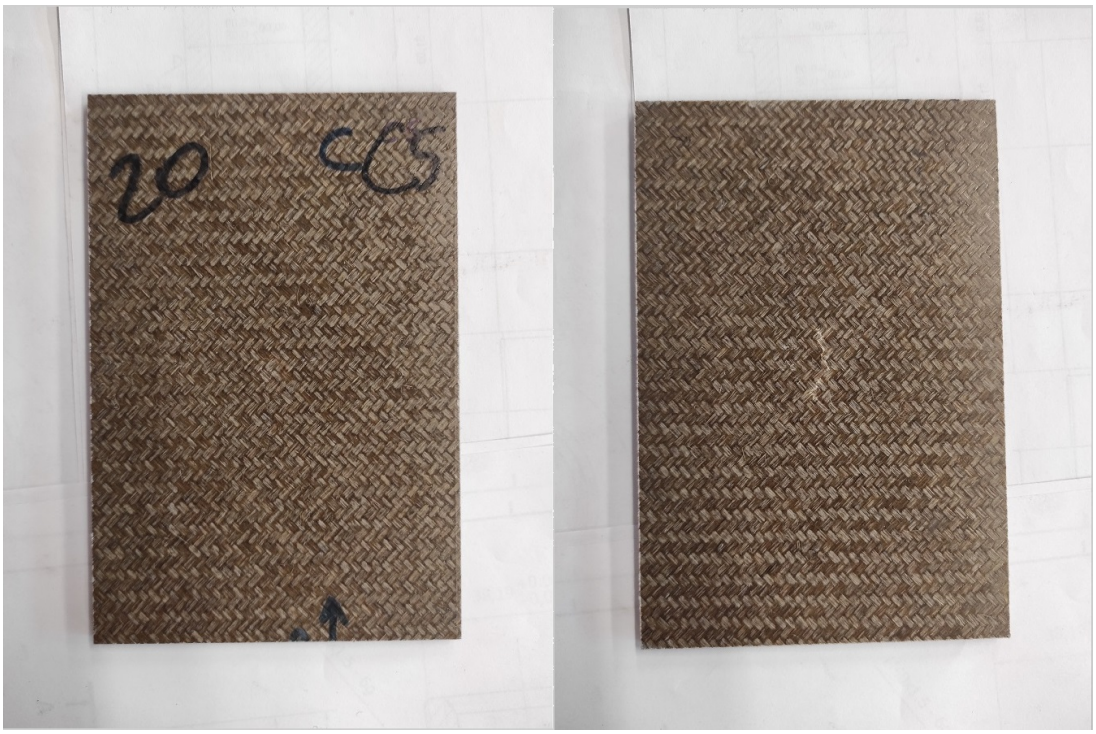

Figure A.20: Indentation test specimen 20

Figure A.21: Indentation test specimen 21

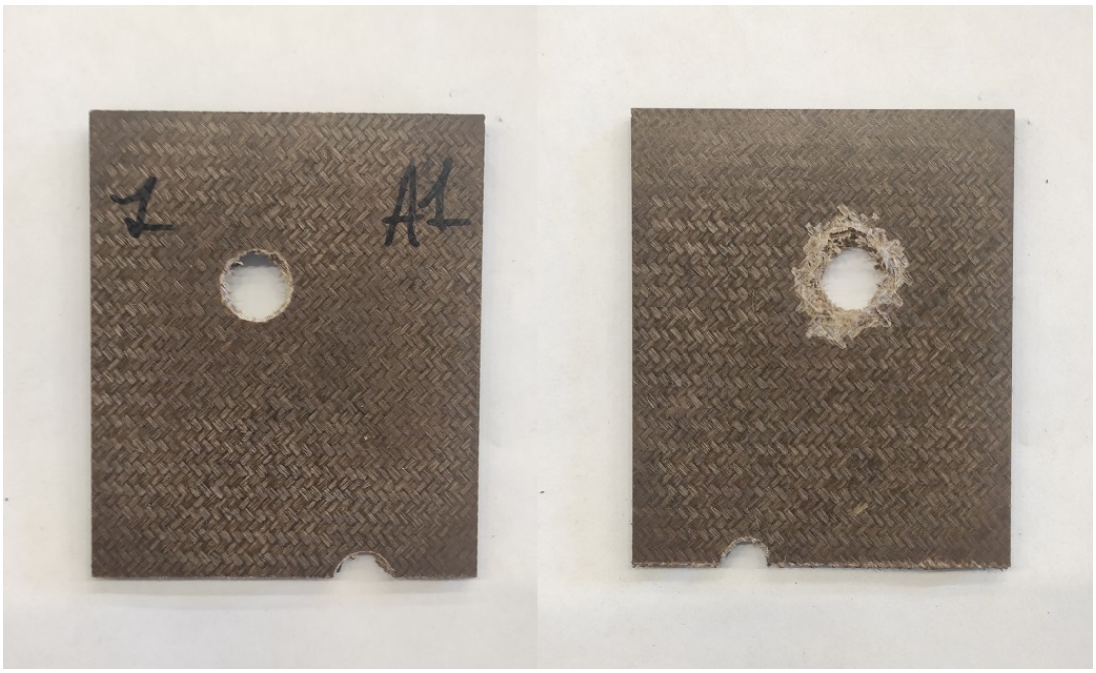

Figure A.22: Ballistic impact test specimen 1

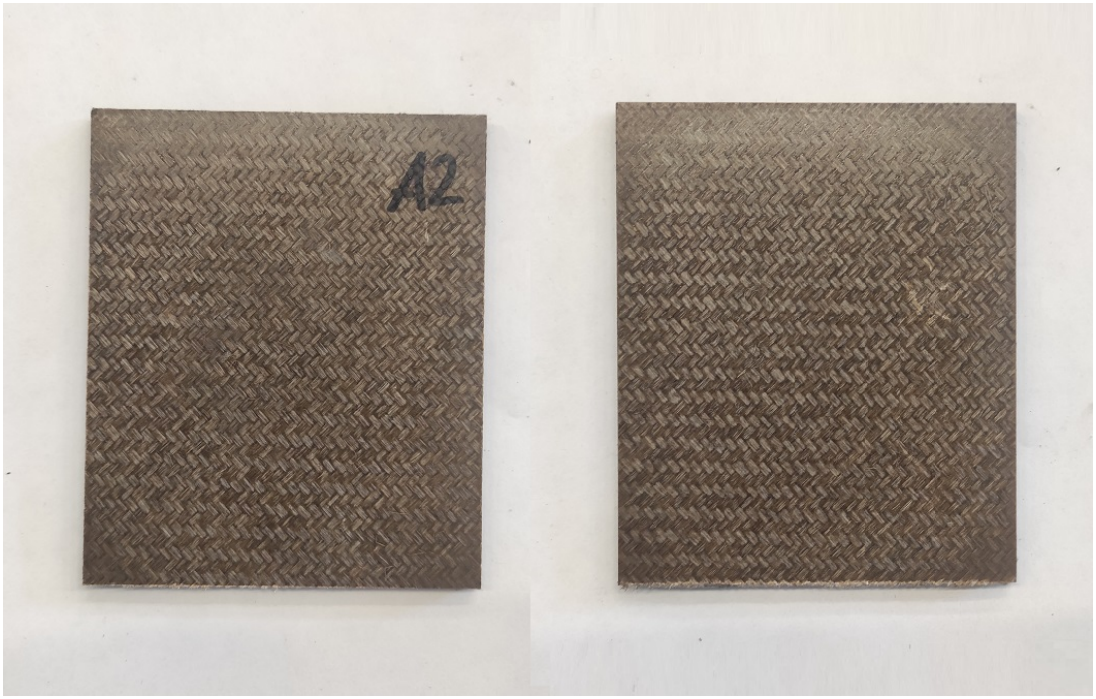

Figure A.23: Ballistic impact test specimen 2

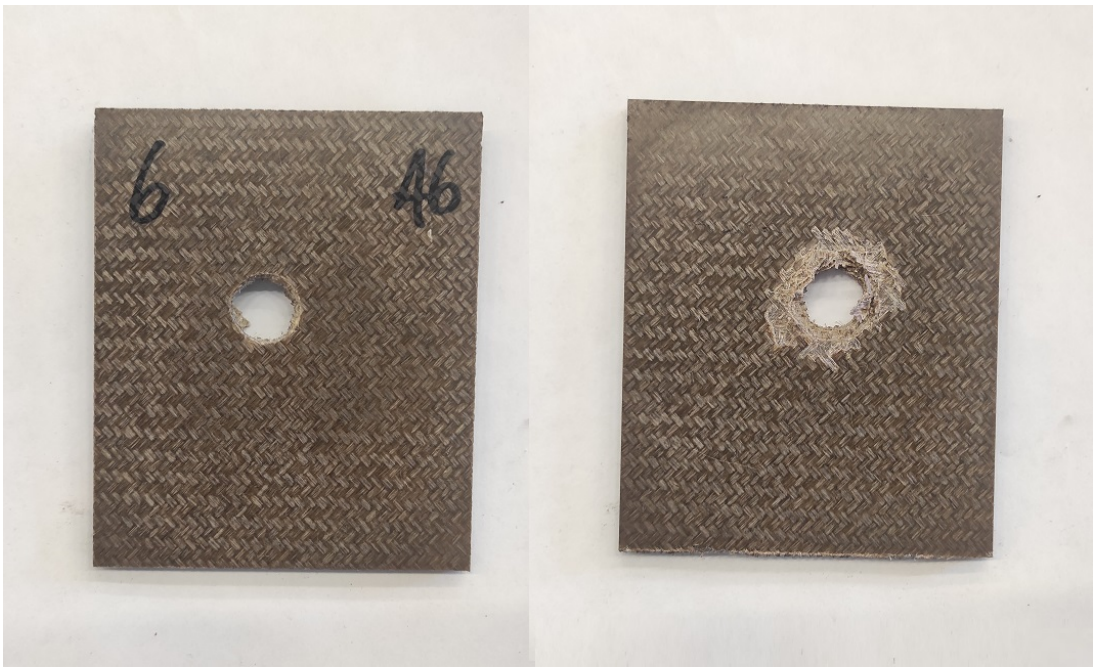

Figure A.24: Ballistic impact test specimen 6

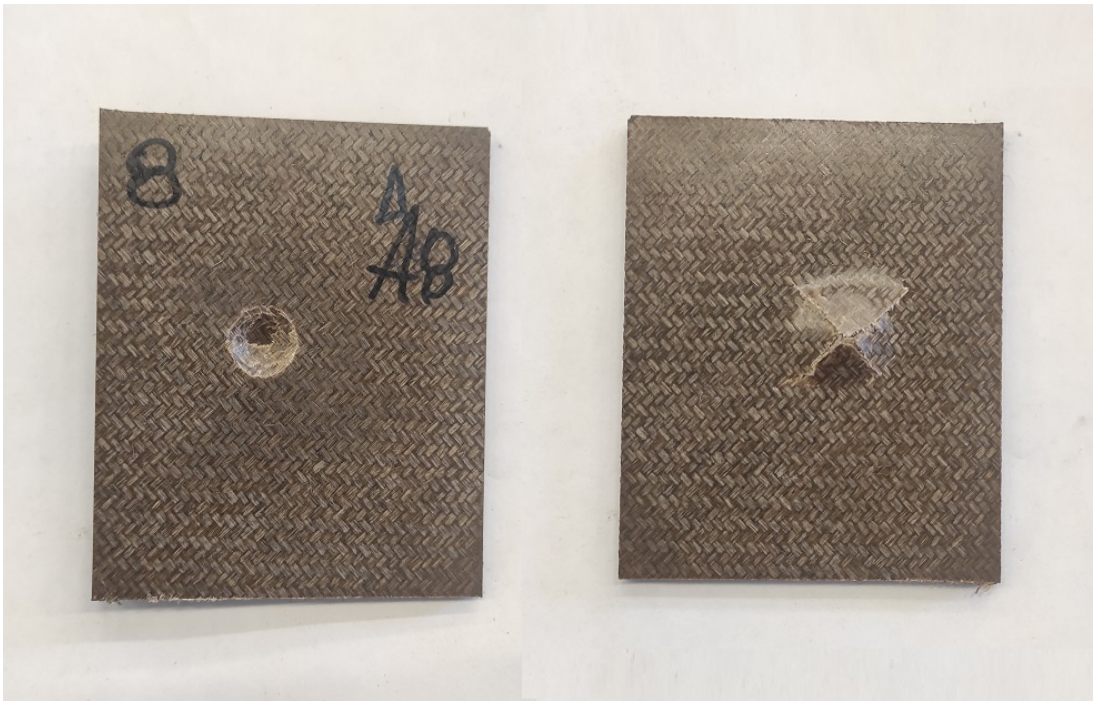

Figure A.25: Ballistic impact test specimen 8

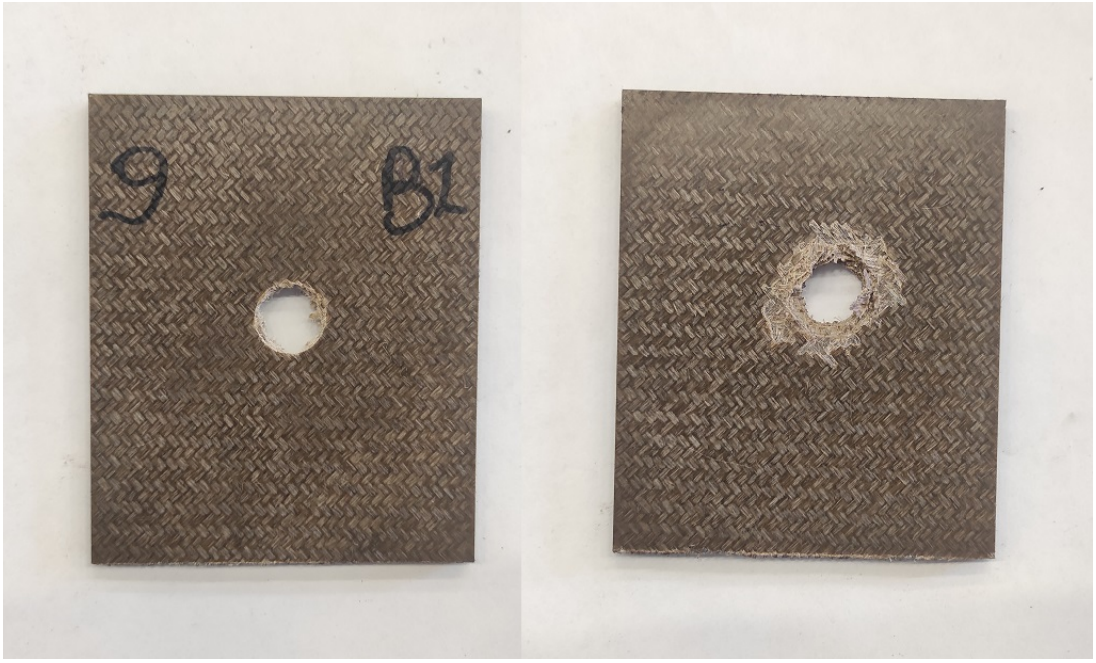

Figure A.26: Ballistic impact test specimen 9

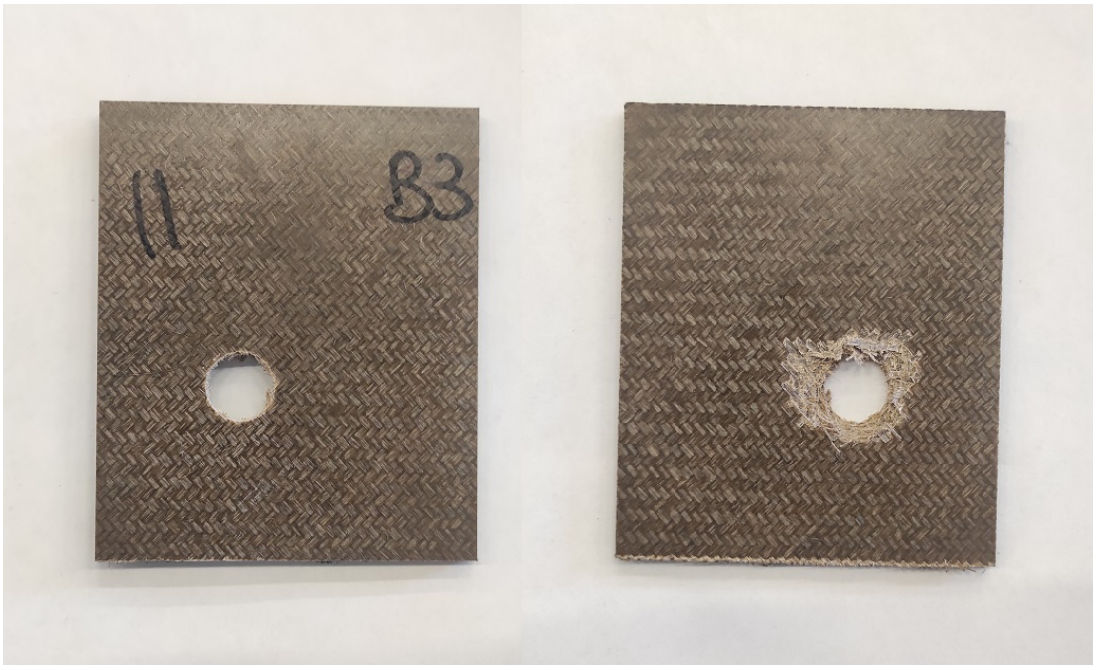

Figure A.27: Ballistic impact test specimen 11

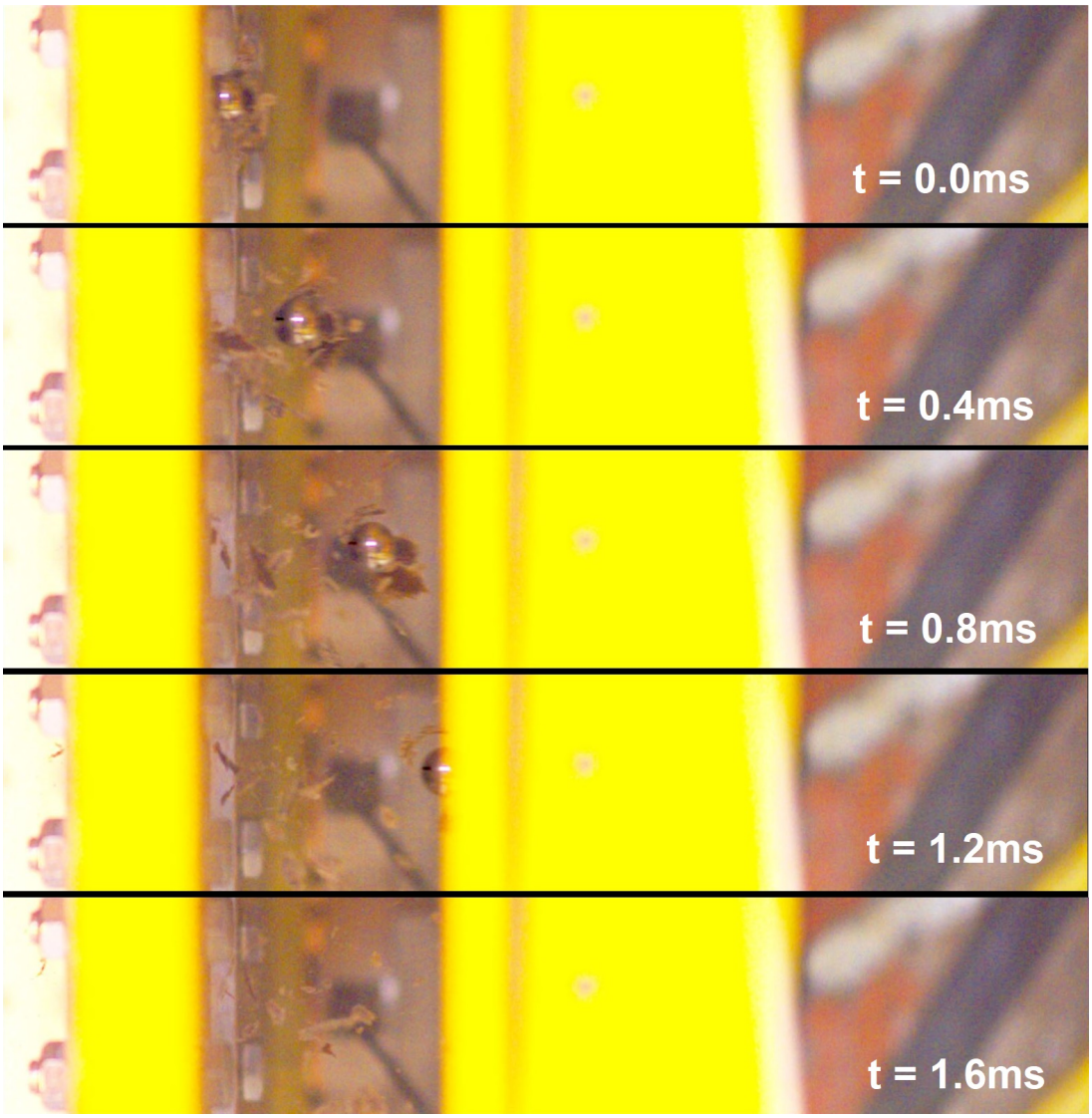

Figure A.28: Ballistic impact evolution of specimen 1

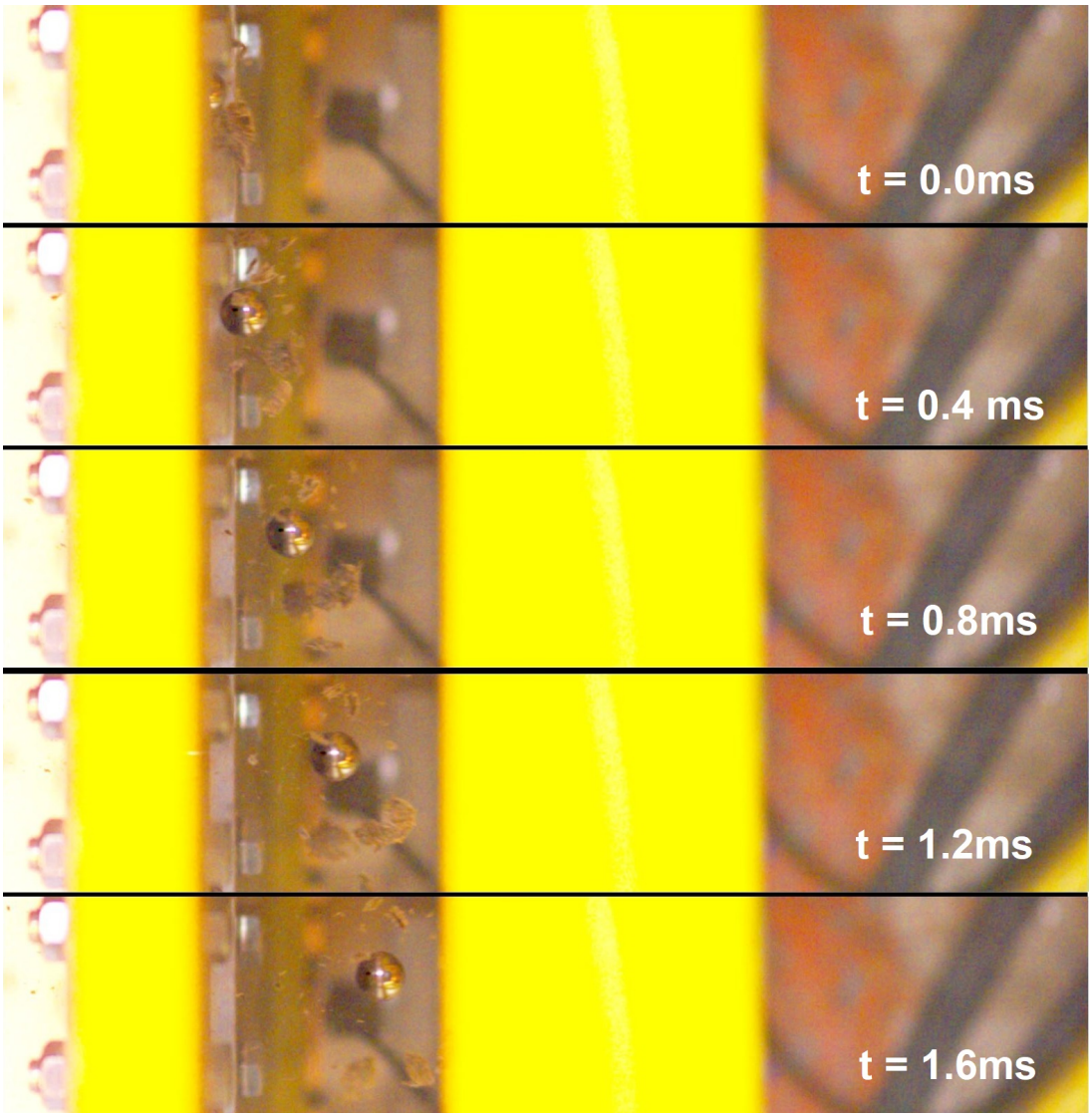

Figure A.29: Ballistic impact evolution of specimen 6

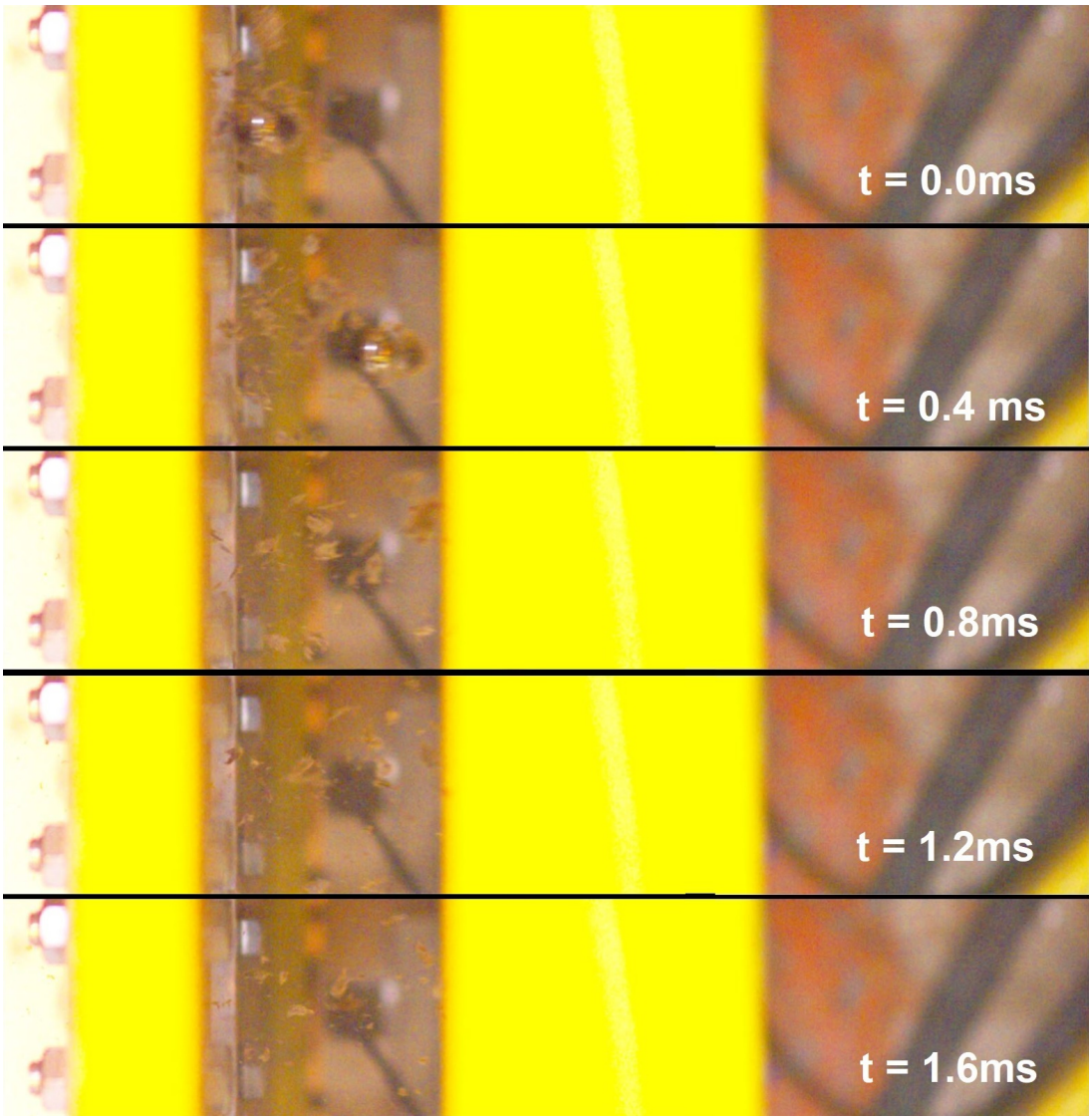

Figure A.30: Ballistic impact evolution of specimen 9

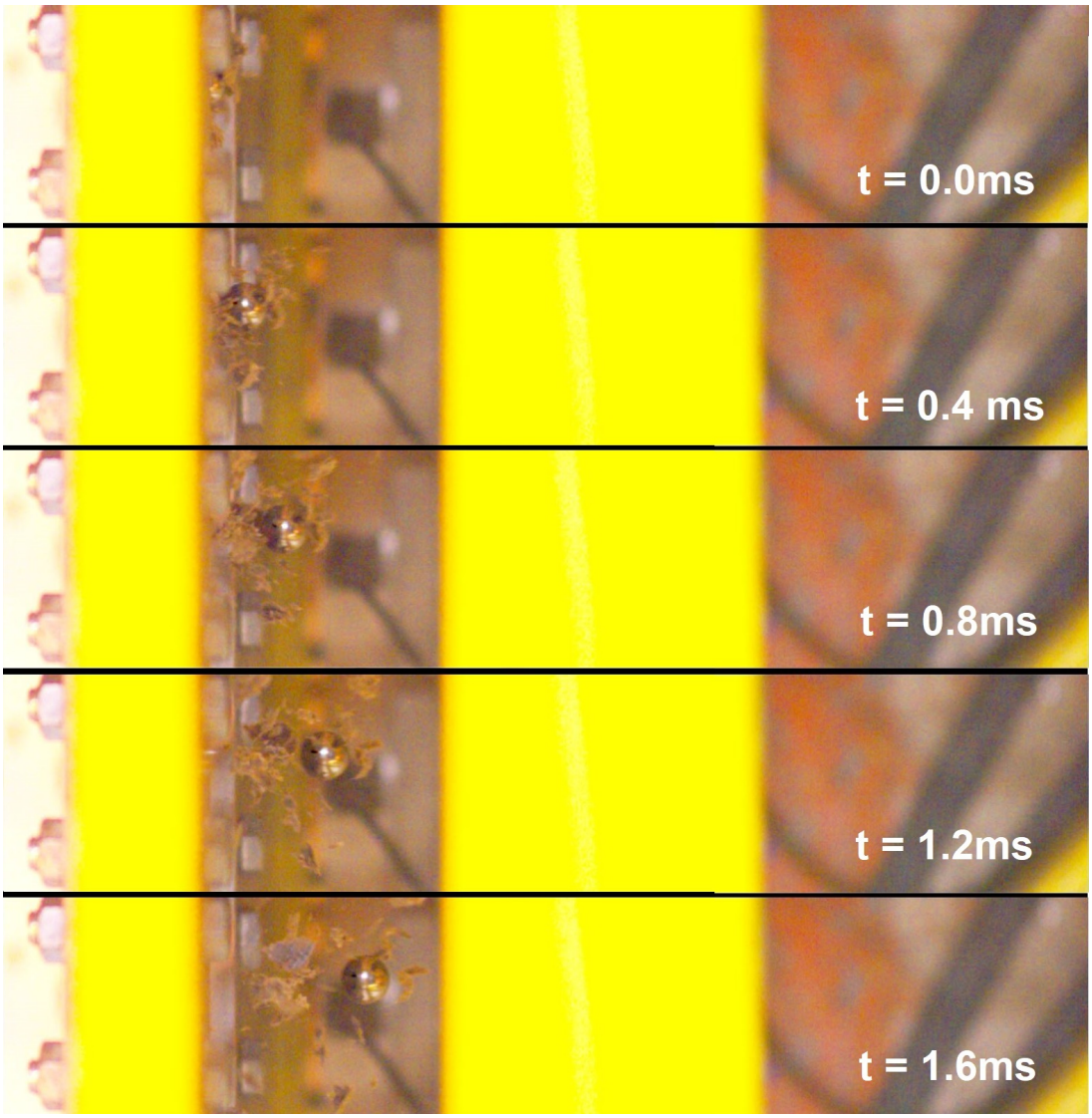

Figure A.31: Ballistic impact evolution of specimen 11

List of Figures

List of Tables